POLITECNICO
MILANO 1863

School of Industrial and Information Engineering
Department of Aerospace Science and Technology

MSc in Space Engineering

Nonlinear Control of Spacecraft Manipulator with Singularity Avoidance using Dual Quaternion

Candidates:

Giovanni Corinaldesi
ID 899770

Lorenzo Ticozzi
ID 900198

Advisor:
Prof. Mauro Massari

Co-advisor:
Prof. Panagiotis Tsiotras

Academic year 2019-2020

POLITECNICO
MILANO 1863

Georgia Institute of Technology

Giovanni Corinaldesi, Lorenzo Ticozzi: *Nonlinear Control of Spacecraft Manipulator with Singularity Avoidance using Dual Quaternion*

| Master of Science in Space Engineering, Politecnico di Milano.
| Research in collaboration with the Georgia Institute of Technology, Atlanta (GA).

To our families

Acknowledgments

The largest part of this research was carried out at the Georgia Institute of Technology. We would like to thank Prof. Mauro Massari for supporting and encouraging us in the choice of going abroad, and for being always available in the course of the work.

A big thank you to Prof. Panagiotis Tsiotras, who gave us the chance to join his lab for a wonderful six-month period, and for the "meeting Mondays" which were a great inspiration for the development of the thesis.

Thanks also to Matthew King-Smith, who supported us with patience and whose contribution was essential to move the first steps in the definition of the control, and to Francesco Cavenago for his always relevant insights on the last part of our work.

Last but not least, the friendship and lunches with Pietro "Pierpa" Pierpaoli were crucial in the successful idea of using control barrier functions to avoid singularities. Thank you, Pietro.

Thanks to my family, a gift I am never too grateful for; a special mention for my brother Francesco, who always stands by me in a unique way. I am also grateful for my classmates, it's been an honor to share life with such brilliant minds. Finally, I wouldn't be here without my friends, both the Italians and the Americans: y'all are the greatest surprise.

Milan, July 2020 L. T.

In this occasion I want to thank my family that in all these years, for better or worse, has always been by my side; I would not be here without you. Thanks to you, Ceci. I will never be grateful enough for your presence. Thanks to all my friends; life without you would not be so colorful.

Riccione, July 2020 G. C.

Abstract

As proved by the occurrence of the recent NASA Demo-2 mission, the space sector is featured by a significant push for innovation; among many other challenges, the ability to extensively exploit robots to perform in-space operations will play a key role in the next decades. The research on the on-orbit servicing requires the simultaneous processing of the dynamics of both the satellite and the manipulator, therefore demanding a unified framework to describe and solve the problem.

Within the thesis, we suggest the use of dual quaternions as an effective tool to model both the satellite and the robot kinematics and dynamics. This mathematical framework naturally keeps into account the complex coupled character of the equations, hence allowing us to propose a unique nonlinear control law to achieve coordinated pose tracking, involving both the satellite base and the end effector.

After developing the necessary nominal controllers, we advocate for the use of control barrier functions (CBFs) to achieve forward invariance of the solution with respect to a singularity-free subset of the state. This novel singularity avoidance controller proves to be robust to disturbances, as it shows enhanced tracking capability also when an unforeseen external force enters the system.

Sommario

Come dimostrato dalla recente realizzazione della missione NASA Demo-2, il settore spaziale è caratterizzato da una significativa spinta all'innovazione; tra le tante sfide, la capacità di utilizzare sistemi robotici per svolgere operazioni in orbita giocherà un ruolo chiave nei prossimi decenni. La ricerca in questo ambito richiede una trattazione simultanea della dinamica del satellite e del manipolatore, facendo quindi appello a una struttura unitaria per la descrizione e soluzione del problema.

All'interno della tesi viene proposto l'uso dei dual quaternions per modellare in modo efficiente sia la cinematica che la dinamica del sistema satellite-manipolatore. Questa cornice matematica è in grado di descrivere la natura complessa e accoppiata delle equazioni, e consente perciò di sviluppare un unico controllore al fine di tracciare in modo coordinato un input di posizione e traiettoria, sia con il satellite che con il braccio robotico.

Dopo avere sviluppato le leggi di controllo nominali, viene giustificato l'utilizzo delle control barrier functions (CBFs) per ottenere invarianza controllata della soluzione in un sottoinsieme dello stato libero da singolarità cinematiche. Questo nuovo controllore rende il sistema robusto ai disturbi, dato che esplica un migliore tracciamento del segnale di riferimento anche in presenza di sollecitazioni impreviste.

Contents

List of Figures

List of Tables

Chapter 1

Introduction

Mankind was born on Earth... It was never meant to die here.

From *Interstellar*

When we think about the future of mankind, whether we are engineers, poets or politicians, we cannot help ourselves but stare at the sky and imagine an era of space travels, planets colonization and every other sort of activities that books, movies and science fiction have been describing throughout the last century.

Leaving the imagination to the movie directors and their akin, it is still clear that the access to space has opened a wide range of commercial, military and scientific perspectives which have already had a huge impact on our everyday life - think about GPS during the daily commute or the satellite-enabled TV broadcast. In the next decades the space exploitation is expected to grow and, according to two main players in the global economy such as Morgan Stanley and Merrill Lynch, the space-based market will generate an estimated revenue between 1100 and 2700 US$bn per year within the first half of the 2040s [1, 2].

The counterpart to all this is that access to space still has high costs and technical difficulties which makes it profitable mainly for a few organizations all around the world; the NASA report in

[3] highlights how our space exploitation paradigm is based on expensive pieces of hardware which allow no room for failures and still need to bring with them everything they need. This proves to be limited both from a commercial and scientific viewpoint, whereas instead we would highly profit of more flexible platforms with an higher operational autonomy, an extended lifetime and an increased fault-tolerance.

Another major obstacle to the further development of space activities is caused by the so called *space debris* phenomenon, as postulated by Kessler [4]; its existence was already under study in the 1960s [5] and eventually led to the creation of the Inter-Agency Space Debris Coordination Committee (IADC) in 1993 to better face the global dimension of the problem.

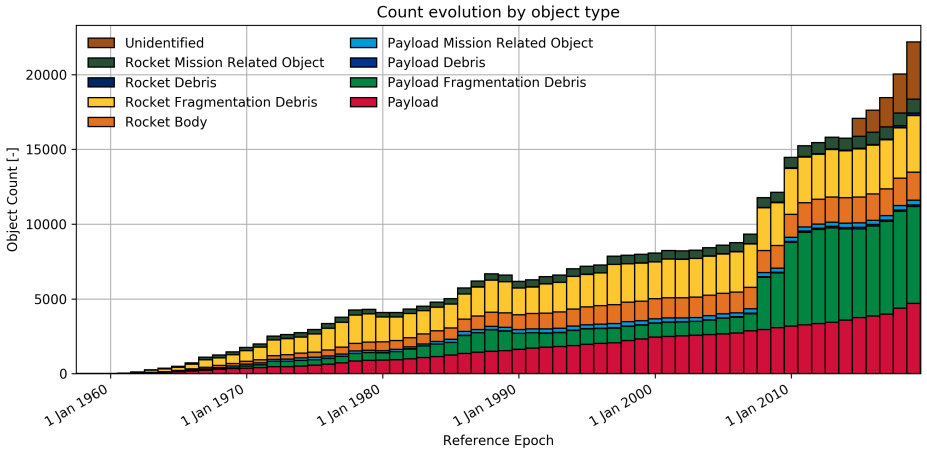

Figure 1.1: Space debris count evolution according to ESA, [6]

The already large space debris population (Fig. 1.1) increases on a daily basis whenever a collision between two orbiting objects takes place, whether they are spent upper stages, particles coming from explosions of satellites or rocket bodies, etc: all these high-speed orbiting fragments not only represent a risk for operating satellites in LEO and GEO but also a potential hazard to the future access of man to space.

From the previous considerations it is possible to argue that, even if extra-terrestrial activity is considered a promising land with almost no boundaries in terms of commercial and scientific opportunities, there are still a lot of open questions and existing problems that need to be addressed to further push the boundaries of our ventures into space.

After briefly mentioning two of the main scientific and technical challenges which space exploration science needs to take into account, it is possible to move forward and start analyzing some of the solutions that have gained growing popularity in the last years.

CubeSats, a particular branch of the *smallsat* category, are one of the most innovative elements in the spectrum of viable solutions to some aspects of the previously highlighted problems; the CubeSat program was initiated in the early 2000s as a collaboration between Stanford University and the California Polytechnic State University [7]. An early concern during the project development was to create standards that could be used to simplify a large scale production of the CubeSats and facilitate their subsequent launch into orbit: this *per se* is an element of newness in the space sector, where components and their assemblies are usually a one-of-a-kind solution to a very peculiar problem. This idea allowed several research institutes and emerging countries to gain access to space while facing relatively low development and operational costs, and still has to prove its full capabilities: in the future CubeSats will probably be deployed in swarms or constellations [8] to optimize their usage and share resources, further expanding their range of use.

If the rise of CubeSats leaves the door open to an interesting future in which a lot of small organizations will be able to afford their share of real-estate in the near-Earth space environment, still it poses the question on how such a boost in the amount of in-orbit objects could be managed from the maintenance and end-of-life standpoint. As suggested by Morris and Tamanini [9], the possible presence of an high number of small satellites also at GEO causes concerns related to the Space Situational Awareness (SSA) and to

the tracking capability of the Space Surveillance Network (SSN) for such small and far objects.

In light of these considerations, it's reasonable to highlight the role and the benefits of what will be the main character of this study, the so called *On-Orbit Servicing* (OOS).

1.1 On-Orbit Servicing: a brief overview

«The term *on-orbit servicing* refers to operations conducted on in-orbit spacecraft intended to accomplish some value-added task.» [10]

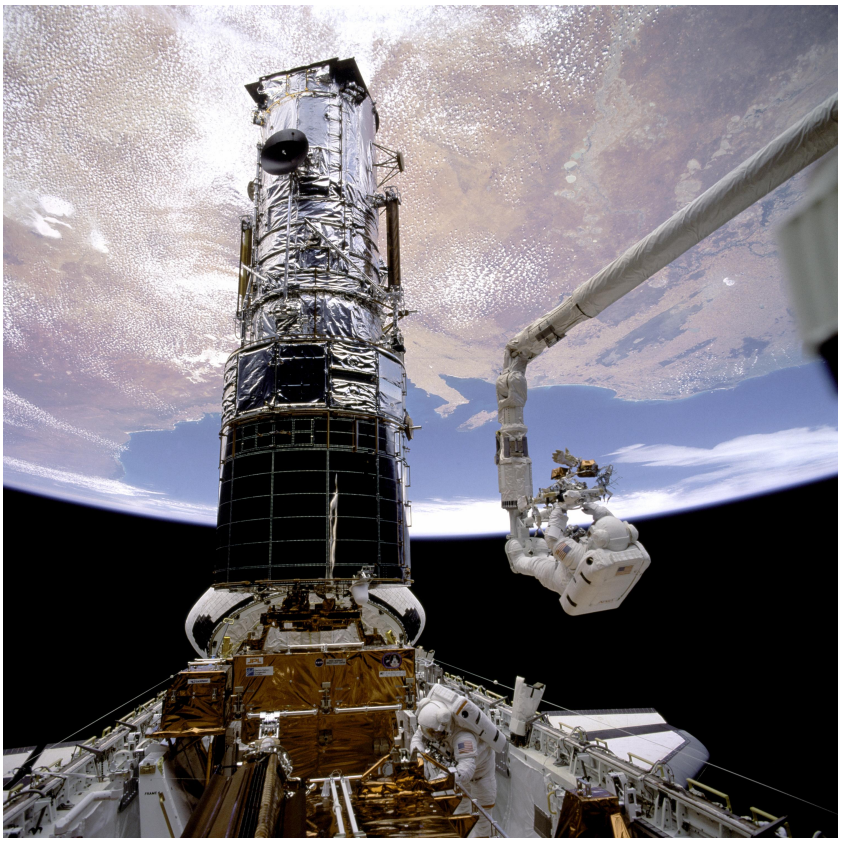

Figure 1.2: The first servicing mission to the Hubble Space Telescope saw astronauts install a set of specialized lenses to correct the flawed main mirror in the telescope. *Credits: NASA*

As of now, major space agencies and research institutions, between which ESA, NASA and DARPA [3, 11–13], have ongoing research programs and planned missions whose key idea is the one of actively exploiting an orbiting spacecraft to perform a number of different tasks, which include robotic manipulations, life extension, towing and inspections. The potential of OOS has widely been proved by the five Hubble Space Telescope (HST) servicing missions and by the extensive use of robotic manipulators in the assembly, operation and maintenance of the International Space Station - the Space Station Remote Manipulator System (SSRMS) or Canadarm2 is perhaps the most famous example. Without neglecting the heritage of successful past missions, it is worth underlining that the foreseeable future of OOS seems to differ in a lot of aspects from past experiences; each HST servicing mission had an estimated cost between 1 and 2 US$bn and was featured by intensive extra-vehicular activity (EVA) of the crew, hence being a rather not appealing example in terms of cost and risk. Recall that the astronauts during EVA are subject to an heavy physical stress both due to the effort of the cardiovascular system and to the presence of radiation; this can lead to a peak metabolic consumption of about 200 kcal/h and to significant weight losses (0.7 to 2.2 kg) [14]. Next OOS missions will likely require partnership with commercial organizations, as in the case of the NASA OSAM-1 [10]. Moreover, the express purpose of such missions is to «transfer [...] technologies to commercial entities to help jump-start a new domestic servicing industry» [12], rather than to be an outstanding scientific and technical *unicum* with few chances to be replicated. The underlying belief conveyed by these words is that OOS really has the potential to widen in a dramatic way both the commercial and scientific opportunities introduced by the space frontier.

Even though OOS missions may have very different profiles, a significant percentage of them is distinguished by the presence of a robotic subsystem which can be of help in a number of different situations (docking, refueling, rescuing, active debris removal...).

The first appearance of a manipulator in the context of a space mission can be placed back in 1981 with the second shuttle flight STS-2 [15]; from then on, space agencies and research organizations have put a lot of effort in developing dexterous space manipulators able to carry on tasks that were previously performed by astronauts in EVA. Among them the Deutsches Zentrum für Luft- und Raumfahrt (DLR) has had a long time space robotic program [16], while JAXA, NASA and DARPA realized a number of successful demonstration missions featuring space robots [17–19].

1.2 Thesis recap and goals

The content of this thesis can be summarized in the following way: first, the authors will exploit the *Dual Quaternions* (DQ) formulation of the 6 DOF dynamics and control of a rigid body [20–25], which was recently extended to the SMM case by Valverde and Tsiotras [26, 27], to build a flexible high-fidelity simulation environment designed to reproduce the dynamics of a SMM. This general framework will then be adjusted to describe the recently installed experimental platform of the *Dynamics and Control System Laboratory* (DCSL) at the Georgia Institute of Technology, consisting of a 6R Universal Robot manipulator (UR10e) attached to the wall via a prismatic joint. After numeric verification of the model, the authors will derive the control laws to perform some pose tracking maneuvers and will test them against the aforementioned simulation environment. In order to account for possible kinematic singularities in the manipulator workspace, a novel CBF based singularity avoidance method will be proposed. After dealing with the necessary theoretical background, the results of the numerical simulations will be reported and discussed to support the validity of the adopted approach.

The purpose of this work is manifold: first, the authors want to prove the effectiveness of the DQ in the description of a complex multibody spacecraft-manipulator system. Although the general problem is widely treated in the literature, the DQ formulation for a

multibody robotic system is surprisingly recent, and therefore worth using also to fill the gap in the literature. The DQ algebra stems from its quaternion counterpart, a formulation which is already familiar to the *guidance, navigation & control* (GNC) community, hence providing a tool to relate two main aspects of any OOS mission, i.e. control of the satellite and of the manipulator. A second goal of the thesis is to exploit the previously described dynamics environment to derive nonlinear torque-based control laws and to prove the pose tracking capability of the end-effector of the UR10e arm. The problem setup will be such that it will be straightforward to draw a parallel between the DCSL testbed and a possible space application of the aforementioned control laws. Also, the authors will show that the DQ framework is a particularly suitable one for a control-oriented description of the problem. After ensuring theoretical convergence of the controlled system towards the desired state, it will be shown that the nominal control strategy reveals weaknesses in the presence of kinematic singularities, which can arise, for example, in the case of disturbances or model uncertainties. Hence the work will focus on enforcing controlled forward invariance of the set of joints values, so that it will be possible to prove that the space of the feasible solutions is singularity-free. In conclusion, the purpose of the last section is to further clarify the overall framework through the introduction and discussion of practical numerical examples; moreover, the simulations will prove the suitability of the above explained approach if tested against possible different solutions.

1.3 Literature review and state of the art

The authors relied on several other previous works in order to understand and then try to give their contribution to the treatment of the topics involved in this thesis. The present section is meant to be a brief literature review and inquiry on the state of the art, i.e. the scientific foundations and developments that brought the discussion to the current state. Some of the documents involved were thoroughly

analyzed, some others are reported because of their undisputed relevance for a more general understanding of the problems and of their possible solutions. For the sake of clarity a further subdivision on the basis of the different topics is hereby made.

1.3.1 Spacecraft-mounted manipulators

Once proved that OOS can increase flexibility and provide additional opportunities to the present and future of the space infrastructure, it is necessary to point out that modeling and operating a *Spacecraft-mounted Manipulator* (SMM) remains a complex task with a lot work that still needs to be carried out.

A classic description of a SMM features the presence of a base with 6 degrees of freedom (6 DOFs) plus a N-DOFs manipulator attached to the base, hence leading to a multibody system with 6+N DOFs. The main difference between a space robot and a ground-based manipulator is that the SMM doesn't experience constraints due to the presence of the ground and is usually subject to reduced gravity force, hence resulting in the conservation of linear and angular momentum. A further distinction can be made between SMMs, depending on whether the spacecraft base is actively controlled in both its translational and rotational dynamics, only in the rotational one (i.e. no thrusters, only reaction wheels) or completely non-actuated and therefore free to move accordingly to the motion of the manipulator. The first two cases (fully or partially actuated base) are often grouped together and referred to as *free-flying* case, while the last one goes under the name of *free-floating* case [28]. As it will be clear in the following, these two cases give birth to highly different problems in the description of the systems, which need to be taken into account with a number of different mathematical tools and models.

The free-floating case has received extensive attention from scientific literature, its appeal also being due to the fact that achieving end-effector control assuming a non-actuated base means saving fuel and electric energy; path planning in this case has to compen-

sate *a priori* for the motion of the base caused by the manipulator. Sticking to this framework Vafa and Dubowsky in [29] proposed a *Virtual Manipulator* (VM), i.e. a massless kinematic chain attached to the so called *Virtual Ground*, a virtual point coinciding with the center of mass of the SMM. Due to the conservation of the system center of mass, the virtual kinematic chain originating in this point has some useful properties which allowed the authors to describe the kinematics and dynamics of the free floating robot in a much simpler way. Their idea was further developed by Liang et al. in [30] with the *Dynamically Equivalent Manipulator* (DEM), not only a useful mathematical abstraction but also a physically realizable platform which proved its utility also in a testing environment [31].

A solution of the kinematic problem in the framework of the under-actuated base was presented by Umetani and Yoshida in [32] recurring to a *Generalized Jacobian Matrix* (GJM) which takes into account inertial properties of the system and compensates the rotational movement of the base under assumptions of non-attitude control of the main satellite body. The authors proved trajectory-tracking capability under the assumption of non-singularity of the GJM. Papadopoulos and Dubowsky pointed out that such singularities may arise not only as a consequence of the kinematic properties of the system, but can depend on its masses and inertias, and therefore can be addressed to as *dynamic singularities* [33]. Unlike their kinematic counterparts, which are fixed in the inertial workspace, dynamic singularities are *path dependent*; this happens because there is not a unique mapping from the singular point in the joint space to a point in the inertial workspace, as each point in the manipulator workspace can be reached with infinite different system configurations for its redundant nature. Therefore a position in the end-effector workspace can or cannot be singular depending on the joint configuration which leads to that position. The workspace locations that may be reached in singular configurations give birth to the *Path Dependent Workspace* (PDW), while subtracting the PDW from the reachable workspace results in the *Path Independent Workspace*

(PIW), i.e. the collection of workspace points that «can be reached by any path, assuming that this path lies entirely in the PIW» [33].

The work by Papadopoulos and Dubowsky shed some light on the complex kinematic and dynamic coupling between the manipulator and its base in the free-floating case; they highlighted the fact that even if more energy-efficient, the design of a safe non-attitude controlled strategy for a SMM would come across significant issues.

The analysis of free-flying SMM is therefore resumed; this particular configuration presents criticalities related to fuel and energy consumption, while on the other hand it has some advantages that makes it a valuable tool in the field of OOS. The simultaneous control of base and manipulator (*coordinated control*) allows the end-effector to reach the desired position and attitude (in the following, *pose*) in the optimal configuration to apply a prescribed force, for example, or to couple the end-effector motion with a base motion such that also pointing requirements are fulfilled, etc. The SMM coordinated control has been attempted in a variety of different ways; Dubowsky and Papadopoulos in [34] adopted a Lagrangian approach relying on null potential energy (null gravity and null strain forces) and writing the system Lagrangian exploiting equivalence with the system kinetic energy; they also proposed a controller in the operational space. Highlighting difficulties in the hand derivation of Lagrange's equation, Stoneking [35] presented a method based on Newton-Euler equations of motion for a two-body system connected by a joint; as highlighted by the author, the approach is easily adjustable to an arbitrarily complex N-body tree-topology system. Antonello and al. in [36] expanded the existing Newton-Euler approach to coordinated control design, involving accurate treatment of the system actuators (thrusters and wheels) and achieving simultaneous station keeping of the base and end-effector trajectory tracking; the control design is carried out in the joint space, assuming that the reference trajectory is in a singularity-free space.

In conclusion, the research field on SMMs modeling has been a vivid one since the '80s, when manned missions onboard the shuttle

started to urge scientists to find more effective ways to describe and plan space manipulators activities. Even in front of the aforementioned works, it remains clear that further steps in the understanding of the problem from different perspectives can be done, along with innovative solutions to better tackle such always challenging problems.

1.3.2 Kinematic singularities avoidance

The American National Standard for Industrial Robots and Robot Systems defines singularities as «a condition caused by the collinear alignment of two or more robot axes resulting in unpredictable robot motion and velocities» [37]. Singular configurations cause difficulties in the inverse mapping from Cartesian space to joint space (*inverse kinematic*), because in correspondence of a joint space singularity inifinite inverse kinematic solutions exist, namely the Jacobian (the matrix mapping joint velocities into Cartesian ones) becomes rank deficient and its inverse cannot be found. A number of different workarounds have been investigated in the literature to restrict problems originating from singularities, providing numerical and physical robustness to the system; a main contribution to this field of research is the one from Nakamura and Hanafusa [38], who introduced a singularity robust inverse (SR-inverse) of the Jacobian matrix based on the simple but effective idea of adding an extra parameter to the pseudo-inverse of the Jacobian when the system is close to singularity. This method has been successfully applied to other cases featuring close-to-singular matrix inversion as in the case of control moment gyros steering laws [39, 40]. Another class of methods is based on the so called *null-space*, derived from redundant manipulators and adapted to the non-redundant case: the end-effector trajectory is parametrized using an additional dependent variable, which is not the time, obtaining an augmented joint space. The consequent augmented Jacobian will maintain rank also at singular points, provided that a suitable parameterization has been used (see [41, 42]).

1.3.3 Control barrier functions

The study of barrier functions and their alternative forms is tightly related to the notion of safety, in particular when safety can be described drawing a parallel with the invariance of a set, i.e. the fact that a trajectory starting from a certain "safe" set will never reach the complement of such set, i.e. the "unsafe" region. A landmark result in this sense was obtained by Nagumo, who postulated the necessary and sufficient conditions to obtain set invariance [43] for a dynamical system in the form $\dot{x} = f(x)$. This result was then adapted to prove safety of nonlinear and hybrid systems introducing the notion of *barrier certificates* [44, 45]. these works, initially valid in the context of closed dynamical systems (i.e. systems without input), were later extended to the case of open dynamical systems ($\dot{x} = f(x) + g(x)u$), earning relevance for the control theory and leading to the name *Control Barrier Functions* (CBF) [46]. The modern meaning of CBF is related to the work of Ames and al. in [47, 48], who extended the barrier function condition which was initially limited to the boundary of the set to the whole set, therefore allowing design of controllers satisfying safety requirements. The effectiveness of this approach has been proved by the wide range of its applications in different fields, including robotics (see [49] for an overview of the different applications).

1.4 Thesis structure

Chapter 2 develops the main mathematical tools of this thesis. Sec. 2.2 introduces quaternions and dual quaternions as two different groups within the Clifford algebra framework, highlighting similarities between the two cases. Sec. 2.3 relates the dual quaternions to the description of the physical model of the SMM. In Sec. 2.4 the authors derive the equations of the system, highlighting a possible solution routine for a simulation environment.

Chapter 3 is about the SMM control design strategy. After a general layout of the main ideas behind feedback linearization in Sec. 3.2, Sec. 3.3 investigates the dual quaternion form of the proposed approach. Sec. 3.4 exploits the above mentioned framework to derive and discuss validity of nolinear control laws for the UR10e manipulator.

Chapter 4 displays the approach pursued by the authors to ensure singularity robustness even in case of disturbances, uncertainties, etc. Sec. 4.2 offers a brief review of the control barrier functions theory, while Sec. 4.3 applies the tool to the above mentioned singularity avoidance scheme, with a particular focus on the manipulator of interest.

Chapter 5 gathers the simulations and results performed throughout the research to ensure feasibility, validity and suitability of the whole work. Sec. 5.2 includes the technical details and specifications of the UR10e manipulator. Sec. 5.3 collects the simulations which have been carried out to numerically verify the model of the arm. Sec. 5.4 shows the numeric generation of the reference pose trajectories in terms of dual quantities. Sec. 5.5 exploits the previously derived control laws to track the reference pose, illustrating 3 different approaches to deal with the problem. In Sec. 5.6 a number of different simulations and results are displayed to assess the performance of the proposed solution strategy.

Chapter 6 provides a final overview of the work, drawing the conclusions and making some final remarks on possible next developments of the research.

Chapter 2

Dual quaternion in robotics

2.1 Introduction

Dual quaternion (DQ) algebra provides the mathematical framework for the development of this work. To the authors' view, its most attractive feature is the inherent potential of expressing a rigid spatial motion with a representation close to the minimal one; the *special Euclidean group* $SE(3)$, which is widely used in robotics to represent rigid body motions, is the set of all 4x4 real matrices T such that

Note that the position and orientation of a rigid body expressed in some coordinate system is known as pose.

$$T = \begin{bmatrix} R & p \\ 0 & 1 \end{bmatrix}, \tag{2.1}$$

where $R \in SO(3)$ represent the orientation of the reference frame and $p \in \mathbb{R}^3$ its origin. This representation involves the use of 16 scalars, 6 of which are independent, while the dual quaternion formulation implies 8 scalars subject to two scalar constraints. A wide use of the latter has been made to parametrize a rigid body displacement within the *screw theory* [50].

Another benefit is that the DQ formulation allows 'recycling' of a great part of the quaternion-based control strategies which have been successfully applied to the spacecraft attitude control problem in the past. Possible drawbacks of the DQ approach are the

loss of physical sense with respect to a vector-matrix formulation, and the *unwinding phenomenon* leading to large (>180°) physical rotations even when smaller rotations exist to achieve the same final attitude; this problem has already been tackled in other works (see for example [25]).

Once the algebraic framework will be established, the chapter will deal with the physical and mathematical model of the problem at hand, hence leading to the representation of the spacecraft and its manipulator(s) in terms of *sketches* and *algebraic/differential equations*.

The physical model provides the "engineer's perception" of the real system, i.e. it involves abstraction and assumptions, while the mathematical model is in charge of developing equations to describe the behavior of the physical model

Sec. 2.2 will introduce some basic notions regarding Clifford algebras and then will put both quaternions and dual quaternions within this context, in order to highlight differences and similarities between the two. After the needed algebraic tools are made available to the reader, Sec. 2.3 will deal with the physical model of the real system (bodies, joints, masses, inertias...) and with the algebraic quantities needed to represent and characterize such features and the existing relationships between them. Sec. 2.4 will cover the differential and algebraic equations which describe the dynamics and kinematics of the multibody system.

2.2 Dual quaternions mathematical preliminaries

2.2.1 Clifford algebras

The common idea of Euclidean vector space can be extended to the notion of Clifford space, which is populated by more general elements, called *multivectors*. The definition of a product between multivectors (Clifford product or geometric product) generates a Clifford algebra.

These algebras are unital and associative over a vector space V with quadratic form $v^2 = Q(v)$, $v \in V$. The set of basis vectors $e_0 = 1$ (unit, or scalar) and $\{e_1, \ldots, e_n\}$ constitutes a standard basis

for V, and $e_i^2 \in \{+1, -1, 0\}$. Every Clifford algebra $\mathrm{Cl}_{(p,q,r)}(V, Q)$ is identified by the previously defined V, Q and by its *signature* elements (p, q, r) which satisfy the relationship $n = p + q + r$, where n is the dimension of V. The basis elements e_i satisfy

$$e_i^2 = \begin{cases} +1 & \text{if } i \in \{1, \ldots, p\} \\ -1 & \text{if } i \in \{p+1, \ldots, p+q\} \\ 0 & \text{if } i \in \{p+q+1, \ldots, n\} \end{cases} \tag{2.2}$$

and

$$e_i e_j + e_j e_i = 0, \text{ if } i \neq j. \tag{2.3}$$

Using Eq. (2.2) and Eq. (2.3), a product of basis vectors

$$e_{abc\ldots d} \triangleq e_a e_b e_c \ldots e_d, \quad \{a, b, c, \ldots, d\} \subseteq \{1, \ldots, n\}, \tag{2.4}$$

can always be simplified such that each e_i appears at most once. If the basis vectors appear in the form

$$e_{k_1 k_2 \ldots k_p}, \ k_i \in \{1, \ldots, n\} \tag{2.5}$$

where $k_1 < k_2 < \ldots < k_p$, then the product in Eq. (2.5) is grade-p, or $e_{k_1 k_2 \ldots k_p} \in \bigwedge^p V$, the p-th exterior algebra of V. This creates a canonical basis for the Clifford algebra expressed as

$$\mathrm{Cl}(p, q, r) = \bigoplus_{i=0}^{i=n} \bigwedge^i V. \tag{2.6}$$

The Clifford algebra in Eq. (2.6) can be decomposed as

$$\mathrm{Cl}(p, q, r) = \mathrm{Cl}^+(p, q, r) \oplus \mathrm{Cl}^-(p, q, r), \tag{2.7}$$

where the even terms and e_0 form a sub-algebra closed under mul-

tiplication

$$Cl^{+}(p,q,r) = \bigoplus_{\substack{i=0 \\ i \text{ even}}}^{i=n} \bigwedge {}^{i}V. \tag{2.8}$$

2.2.2 Quaternions

The relationship between quaternions and Clifford algebras is straightforward if the algebra $Cl_{(0,2,0)}\left(\mathbb{R}^2, Q(v)\right)$ is considered, where $Q(v) = -v_1^2 - v_2^2$ given $v = v_1 e_1 + v_2 e_2$. The canonical basis for this algebra is $\{1, e_1, e_2, e_{12}\}$, and reminding Eq. (2.2) it is immediate to write

$$\begin{aligned} e_1^2 &= e_2^2 = -1 \\ e_{12}^2 &= e_{12}e_{12} = e_1e_2e_1e_2 = -e_1e_1e_2e_2 = -(-1)(-1) = -1 \\ e_1e_2e_{12} &= e_1e_2e_1e_2 = -e_1e_1e_2e_2 = -e_1^2e_2^2 = -(-1)(-1) = -1 \end{aligned} \tag{2.9}$$

Recalling the definition of quaternions by Lord Hamilton (1843), $\mathbb{H} \triangleq \{q = q_0 + q_1 i + q_2 j + q_3 k : i^2 = j^2 = k^2 = ijk = -1, q_0, q_1, q_2, q_3 \in \mathbb{R}\}$ defines a four-dimensions associative algebra over the real numbers field. It is straightforward to see that $Cl_{(0,2,0)} \simeq \mathbb{H}$. In detail,

$Cl_{(0,2,0)}$	$\mathbb{H}$
e_0	1
e_1	i
e_2	j
e_{12}	k

Table 2.1: Comparison between $Cl_{(0,2,0)}$ and $\mathbb{H}$

Operation	**Definition**
Addition	$a + b = (a_0 + b_0, \bar{a} + \bar{b})$
Multiplication by scalar	$\lambda a = (\lambda a_0, \lambda \bar{a})$
Multiplication	$ab = (a_0 b_0 - \bar{a} \cdot \bar{b}, a_0 \bar{b} + b_0 \bar{a} + \bar{a} \times \bar{b})$
Conjugate	$a^* = (a_0, -\bar{a})$
Dot product	$a \cdot b = (a_0 b_0 + \bar{a} \cdot \bar{b}, 0_{3\times1}) = \frac{1}{2}(a^* b + b^* a)$
Cross product	$a \times b = (0, a_0 \bar{b} + b_0 \bar{a} + \bar{a} \times \bar{b}) = \frac{1}{2}(ab - b^* a^*)$
Norm	$\|a\| = \sqrt{a \cdot a}$

Table 2.2: Quaternion operations

Quaternions are often decomposed in a scalar and a vector part hence becoming $q = [q_0, \bar{q}]^T$ where $q_0 \in \mathbb{R}$, $\bar{q} = [q_1, q_2, q_3] \in \mathbb{R}^3$.

The quaternion formulation is particularly suitable to display rotations, but since these are described by three independent parameters the unit norm constraint is enforced; hence, each quaternion representing rotations is part of the set defined as $\mathbb{H}^u = \{q \in \mathbb{H} : q^* q = q q^* = 1\}$, $1 = [1, 0, 0, 0]^T$. The quaternion expression of a rotation is related to the Euler's rotation theorem; every rotation quaternion can be built accordingly as $q = [\cos(\theta/2), \bar{n} \sin(\theta/2)]^T$, being $\bar{n}$ the Euler axis and θ the corresponding angle.

The orientation of a frame Y with respect to a frame X is expressed as $q_{Y/X}$, and $q^*_{Y/X} q_{Y/X} = q_{Y/X} q^*_{Y/X} = 1$. Given three different reference frames X, Y, Z,

$$q_{Z/X} = q_{Y/X} q_{Z/Y}. \tag{2.10}$$

Any 3-dimensional vector $\bar{s}$, expressed in a reference frame X such that $\bar{s}^X \in \mathbb{R}^3$, can be expressed as a quaternion $s^X = [0, \bar{s}^X]^T$ belonging to the vector quaternion set $\mathbb{H}^v = \{q \in \mathbb{H} : q_0 = 0\}$; this formulation allows to exploit the quaternion formulation to express a change of reference frame, as in

$$s^Y = q^*_{Y/X} s^X q_{Y/X} = q_{X/Y} s^X q^*_{X/Y}. \tag{2.11}$$

In addition, given $s \in \mathbb{H}^v$ it is possible to define an operator $[\cdot]^\times : \mathbb{H}^v \mapsto \mathbb{R}^{4\times4}$ as

$$[s]^\times = \begin{bmatrix} 0 & 0_{1\times3} \\ 0_{3\times1} & [\bar{s}]^\times \end{bmatrix}, \quad \text{where } [\bar{s}]^\times = \begin{bmatrix} 0 & -s_3 & s_2 \\ s_3 & 0 & -s_1 \\ -s_2 & s_1 & 0 \end{bmatrix}. \tag{2.12}$$

The quaternion product can be represented in the matrix-vector product form by suitably defining the left and right quaternion multiplication operators $[\![\cdot]\!]_L, [\![\cdot]\!]_R : \mathbb{H} \mapsto \mathbb{R}^{4\times4}$; if $a = [a_0, \bar{a}]^T, b = [b_0, \bar{b}]^T \in \mathbb{H}$, then

$$ab \triangleq [\![a]\!]_L * b \triangleq a * [\![b]\!]_R, \tag{2.13}$$

with

$$[\![a]\!]_L = \begin{bmatrix} a_0 & -\bar{a} \\ \bar{a}^T & a_0 I_3 + [\bar{a}]^\times \end{bmatrix} \quad \text{and} \quad [\![b]\!]_R = \begin{bmatrix} b_0 & -\bar{b} \\ \bar{b}^T & b_0 I_3 - [\bar{b}]^\times \end{bmatrix}. \tag{2.14}$$

As a last remark, the spatial attitude kinematics of a reference frame Y expressed with respect to a frame X evolves according to

$$\dot{q}_{Y/X} = \frac{1}{2} q_{Y/X} \omega^Y_{Y/X} = \frac{1}{2} \omega^X_{Y/X} q_{Y/X}, \tag{2.15}$$

where $\omega^Z_{Y/X} = [0, \bar{\omega}^Z_{Y/X}]^T \in \mathbb{H}^v$, and $\bar{\omega}^Z_{Y/X}$ is the angular velocity of frame Y with respect to frame X expressed in Z−frame coordinates.

2.2.3 Dual quaternions

Exploiting the very same framework of the previous two sections, we first consider a Clifford algebra $Cl^{+}_{(0,3,1)}\left(\mathbb{R}^4, Q(v)\right)$ whose standard basis $\{e_1, e_2, e_3, e_4\}$ fulfill Eq. (2.2), leading to $e_1^2 = e_2^2 = e_3^2 = -1,\ e_4^2 = 0$. Given an element $v = v_1 e_1 + v_2 e_2 + v_3 e_3 + v_4 e_4$, $Q(v) = -v_1^2 - v_2^2 - v_3^2$; the canonical basis for this algebra can be expressed as in Eq. (2.6), therefore leading to $\{e_0, e_{12}, e_{13}, e_{14}, e_{23}, e_{24}, e_{34}, e_{1234}\}$.

Two of the most relevant properties arising from Clifford algebra vectors are hereby reported:

$$\begin{aligned} e_{12}^2 = e_{13}^2 = e_{23}^2 = e_{12}e_{13}e_{23} = -1, \\ e_{1234}^2 = -e_{123}e_4^2e_{123} = 0. \end{aligned} \tag{2.16}$$

The dual quaternion group is defined as

$$\begin{aligned} \mathbb{Q}_d = \{-1, i, j, k, \epsilon, \epsilon i, \epsilon j, \epsilon k : i^2 = j^2 = k^2 = ijk = -1, \\ \epsilon i = i\epsilon, \epsilon j = j\epsilon, \epsilon k = k\epsilon, \epsilon \neq 0, \epsilon^2 = 0\}. \end{aligned} \tag{2.17}$$

$Cl^{+}_{(0,3,1)}$	$\mathbb{H}_d$
e_0	1
e_{12}	i
e_{13}	j
e_{23}	k
e_{34}	ϵi
e_{24}	$-\epsilon j$
e_{14}	ϵk
e_{1234}	$-\epsilon$

Table 2.3: Comparison between $Cl^{+}_{(0,3,1)}$ and $\mathbb{H}_d$

As for the quaternion case, it is interesting to match the algebra $Cl^{+}_{(0,3,1)}$ with the dual quaternion algebra in Eq. (2.17) (see Table 2.3).

The vector dual quaternion set will be extensively used in this work; in a similar fashion to what already done for quaternions it is

defined as $\mathbb{H}_d^v \triangleq \{\mathbf{q} = q_r + \epsilon q_d : q_r, q_d \in \mathbb{H}^v\}$, where q_r, q_d will be referred to as *real* and *dual part* of the dual quaternion and ϵ is the dual unity. The definition of the dual quaternion operations will closely follow the one by Filipe and Tsiotras in [25]; a table featuring the different operations is hereby reported.

Operation	**Definition**
Addition	$\mathbf{a} + \mathbf{b} = (a_r + b_r) + \epsilon(a_d + b_d)$
Multiplication by scalar	$\lambda\mathbf{a} = (\lambda a_r) + \epsilon(\lambda a_d)$
Multiplication	$\mathbf{ab} = (a_r b_r) + \epsilon(a_d b_r + a_r b_d)$
Conjugate	$\mathbf{a}^* = (a_r^*) + \epsilon(a_d^*)$
Dot product	$\mathbf{a} \cdot \mathbf{b} = (a_r \cdot b_r) + \epsilon(a_d \cdot b_r + a_r \cdot b_d) = \frac{1}{2}(\mathbf{a}^*\mathbf{b} + \mathbf{b}^*\mathbf{a})$
Cross product	$\mathbf{a} \times \mathbf{b} = (a_r \times b_r) + \epsilon(a_d \times b_r + a_r \times b_d) = \frac{1}{2}(\mathbf{ab} - \mathbf{b}^*\mathbf{a}^*)$
Circle product	$\mathbf{a} \circ \mathbf{b} = (a_r \cdot b_r + a_d \cdot b_d) + \epsilon 0$
Swap	$\mathbf{a}^S = a_d + \epsilon a_r$
Norm	$\|\mathbf{a}\| = \sqrt{\mathbf{a} \circ \mathbf{a}}$
Vector part	$\mathrm{vec}(\mathbf{a}) = (0, \bar{a}_r) + \epsilon(0, \bar{a}_d)$

Table 2.4: Dual quaternion operations

It is also useful to define the unit dual quaternion which will often be mentioned in the following of the discussion, namely $\mathbf{1} = 1 + \epsilon 0$.

Recall that $0 = [0, \bar{0}]^T$ is the null quaternion, while $\mathbf{0} = 0 + \epsilon 0$.

Similarly to what was done in Eq. (2.12), the operator $[\cdot]^\times : \mathbb{H}_d^v \mapsto \mathbb{R}^{8\times 8}$ can be created, where

$$[\mathbf{s}]^\times = \begin{bmatrix} [s_r]^\times & 0_{4\times 4} \\ [s_d]^\times & [s_r]^\times \end{bmatrix}. \tag{2.18}$$

In order to express dual quaternion multiplication in the more familiar matrix-vector form, two other operators $[\![\cdot]\!]_L, [\![\cdot]\!]_R : \mathbb{H}_d \mapsto \mathbb{R}^{8\times 8}$ are defined; if $\mathbf{a} = a_r + \epsilon a_d$, $\mathbf{b} = b_r + \epsilon b_d$ and $\star$ is the operator representing dual quaternion product as a matrix-vector product, then

$$\mathbf{ab} \triangleq [\![a]\!]_L \star \mathbf{b} \triangleq [\![b]\!]_R \star \mathbf{a}, \tag{2.19}$$

where

$$[\![a]\!]_L = \begin{bmatrix} [\![a_r]\!]_L & 0_{4\times 4} \\ [\![a_d]\!]_L & [\![a_r]\!]_L \end{bmatrix} \quad \text{and} \quad [\![b]\!]_R = \begin{bmatrix} [\![b_r]\!]_R & 0_{4\times 4} \\ [\![b_d]\!]_R & [\![b_r]\!]_R \end{bmatrix}. \tag{2.20}$$

Two properties descending from Table 2.4 and Eq. (2.19) are worth mentioning as they will be used in the following of this work; the first shows that dual quaternion cross product is invariant to frame transformation, i.e.

$$\mathbf{a}^Y \times \mathbf{b}^Y = (q_{Y/X}^* \mathbf{a}^X q_{Y/X}) \times (q_{Y/X}^* \mathbf{b}^X q_{Y/X}) = q_{Y/X}^* (\mathbf{a}^X \times \mathbf{b}^X) q_{Y/X}. \tag{2.21}$$

Eq. (2.21) can be easily proved:

$$\begin{aligned} q_{Y/X}^* (\mathbf{a}^X \times \mathbf{b}^X) q_{Y/X} &= q_{Y/X}^* (\mathbf{a}^X \mathbf{b}^X - (\mathbf{b}^X)^* (\mathbf{a}^X)^*) q_{Y/X} \\ &= q_{Y/X}^* \mathbf{a}^X \mathbf{b}^X q_{Y/X} - q_{Y/X}^* (\mathbf{b}^X)^* (\mathbf{a}^X)^* q_{Y/X} \\ &= q_{Y/X}^* \mathbf{a}^X q_{Y/X} q_{Y/X}^* \mathbf{b}^X q_{Y/X} \\ &\quad - q_{Y/X}^* (\mathbf{b}^X)^* q_{Y/X} q_{Y/X}^* (\mathbf{a}^X)^* q_{Y/X} \\ &= (q_{Y/X}^* \mathbf{a}^X q_{Y/X}) \times (q_{Y/X}^* \mathbf{b}^X q_{Y/X}) \\ &= \mathbf{a}^Y \times \mathbf{b}^Y \end{aligned} \tag{2.22}$$

The second property is about the left and right dual quaternion multiplication operators defined in Eq. (2.19):

$$\begin{aligned} [\![q]\!]_L [\![q^*]\!]_R [\![q^*]\!]_L [\![q]\!]_R &= I_{8\times 8}, \\ [\![q^*]\!]_L [\![q]\!]_R [\![q]\!]_L [\![q^*]\!]_R &= I_{8\times 8}. \end{aligned} \tag{2.23}$$

A simple proof is hereby reported:

$$\begin{aligned} [\![q]\!]_L [\![q^*]\!]_R [\![q^*]\!]_L [\![q]\!]_R \star \mathbf{a} &= [\![q]\!]_L [\![q^*]\!]_R [\![q^*]\!]_L \star \mathbf{aq} \\ &= [\![q]\!]_L [\![q^*]\!]_R \star (\mathbf{q}^* \mathbf{aq}) \\ &= [\![q]\!]_L \star (\mathbf{q}^* \mathbf{aq}) \mathbf{q}^* \\ &= \mathbf{q}(\mathbf{q}^* \mathbf{aq}) \mathbf{q}^* \\ &= \underbrace{\mathbf{qq}^*}_{1} \mathbf{a} \underbrace{\mathbf{qq}^*}_{1}. \end{aligned} \tag{2.24}$$

Note that spatial rigid body motions are uniquely defined by six independent parameters, corresponding to three rotations and three translations. As a dual quaternion encompasses eight scalars, there must be two scalar constraints such that two scalars can be recovered from the other six independent elements. The relation

$$\mathbf{q}_{B/I} = q_{B/I,r} + \epsilon q_{B/I,d} = q_{B/I} + \epsilon \frac{1}{2} q_{B/I} r^B_{B/I} \tag{2.25}$$

describes the pose of the reference frame B with respect to the frame I, where $r^B_{B/I}$ is the vector quaternion position expressing the distance from the origin of frame I to the origin of frame B, expressed in frame B; the two necessary constraints are expressed as $q_{B/I,r} \cdot q_{B/I,r} = 1$ and $q_{B/I,r} \cdot q_{B/I,d} = 0$. Moreover, a dual quaternion $\mathbf{q}$ expressing a pose transformation is a unit dual quaternion, $\mathbf{q} \in \mathbb{H}^u_d$, i.e. it satisfies the relation $\mathbf{q} \cdot \mathbf{q} = \mathbf{q}^* \mathbf{q} = \mathbf{1}$.

Drawing a parallel with Eq. (2.10), having two pose transformations $\mathbf{q}_{Y/X}$ and $\mathbf{q}_{Y/Z}$, the pose transformation leading from X to Z is

the composition of the previous two through the product

$$q_{Z/X} = q_{Y/X} q_{Z/Y}. \tag{2.26}$$

Another key quantity in the description of a spatial rigid body motion is the dual velocity, a dual quantity collecting both the linear and angular velocity components. Its expression is

$$\omega^{Z}_{Y/X} = q^{*}_{Z/Y} \omega^{Y}_{Y/X} q_{Z/Y}, \tag{2.27}$$

where $\omega^{Z}_{Y/X} = \omega^{Z}_{Y/X} + \epsilon(v^{Z}_{Y/X} + \omega^{Z}_{Y/X} \times r^{Z}_{Y/X}) \in \mathbb{H}^{v}_{d}$ describes the dual velocity of the frame Y with respect to a frame X written in a Z coordinate system. Both $\omega^{Z}_{Y/X}, v^{Z}_{Y/X} \in \mathbb{H}^{v}$, $\omega^{Z}_{Y/X} = [0, \bar{\omega}^{Z}_{Y/X}]^{T}$, $v^{Z}_{Y/X} = [0, \bar{v}^{Z}_{Y/X}]^{T}$ and $\bar{\omega}^{Z}_{Y/X}, \bar{v}^{Z}_{Y/X} \in \mathbb{R}^{3}$ are the usual Cartesian velocities.

The kinematic equation describing the time evolution of the pose

$$\dot{q}_{Y/X} = \frac{1}{2} q_{Y/X} \omega^{Y}_{Y/X} = \frac{1}{2} \omega^{X}_{Y/X} q_{Y/X} \tag{2.28}$$

is the dual counterpart of Eq. (2.15), but it also includes an information on the position of the origin of Y with respect to X.

Since the overall model has to be completely written in the dual quaternion formulation to fully take advantage of it, also forces and torques have to be encoded in a dual vector as already done for kinematic quantities; by doing this the *dual wrench* (force and torque) applied to a certain point of a multibody system can be shifted to another point of the same system by simply applying the dual quaternion pose transformation rules. The wrench $W^{Z}(O_p) \in \mathbb{H}^{v}_{d}$, i.e. the force-torque pair applied to a point O_p and expressed in Z−frame coordinates, is written as

$$W^{Z}(O_p) = f^{Z} + \epsilon \tau^{Z}, \tag{2.29}$$

and $f^{Z} = [0, \bar{f}^{Z}]^{T}$, $\tau^{Z} = [0, \bar{\tau}^{Z}]^{T}$. In order to express the dynamical equivalent of Eq. (2.29) if reported to another point O_q, the transport

theorem yields to

$$\boldsymbol{W}^{Z}(O_q) = f^{Z} + \epsilon(\tau^{Z} + r^{Z}_{p/q} \times f^{Z}), \tag{2.30}$$

where $r^{Z}_{p/q}$ is the distance from O_q to O_p in frame Z. If instead one wants to study the effect of the wrench $\boldsymbol{W}^{X}(O_X) = f^{X} + \epsilon\tau^{X}$ on another point O_Y expressed in a different reference frame Y, i.e. $\boldsymbol{W}^{Y}(O_Y)$, the following holds:

$$\begin{aligned}
\boldsymbol{W}^{Y}(O_Y) &= q^{*}_{Y/X}\boldsymbol{W}^{X}(O_X)q_{Y/X} \\
&= (q_{Y/X} + \epsilon\frac{1}{2}r^{X}_{Y/X}q_{Y/X})^{*}(f^{X} + \epsilon\tau^{X})(q_{Y/X} + \epsilon\frac{1}{2}r^{X}_{Y/X}q_{Y/X}) \\
&= (q^{*}_{Y/X} + \epsilon\frac{1}{2}q^{*}_{Y/X}r^{X*}_{Y/X})(f^{X} + \epsilon\tau^{X})(q_{Y/X} + \epsilon\frac{1}{2}r^{X}_{Y/X}q_{Y/X}) \\
&= (q^{*}_{Y/X} - \epsilon\frac{1}{2}q^{*}_{Y/X}r^{X}_{Y/X})(f^{X} + \epsilon\tau^{X})(q_{Y/X} + \epsilon\frac{1}{2}r^{X}_{Y/X}q_{Y/X}) \\
&= (q^{*}_{Y/X} - \epsilon\frac{1}{2}q^{*}_{Y/X}r^{X}_{Y/X})\Big(f^{X}q_{Y/X} + \epsilon(\tau^{X}q_{Y/X} + \\
&\quad + f^{X}\frac{1}{2}r^{X}_{Y/X}q_{Y/X})\Big) \\
&= q^{*}_{Y/X}f^{X}q_{Y/X} - \epsilon(\frac{1}{2}q^{*}_{Y/X}r^{X}_{Y/X}f^{X}q_{Y/X}) \\
&\quad + \epsilon(q^{*}_{Y/X}\tau^{X}q_{Y/X} + q^{*}_{Y/X}f^{X}\frac{1}{2}r^{X}_{Y/X}q_{Y/X}) \\
&= f^{Y} + \epsilon(\tau^{Y} + \frac{1}{2}q^{*}_{Y/X}f^{X}q_{Y/X}q^{*}_{Y/X}r^{X}_{Y/X}q_{Y/X} \\
&\quad - \frac{1}{2}q^{*}_{Y/X}r^{X}_{Y/X}q_{Y/X}q^{*}_{Y/X}f^{X}q_{Y/X}) \\
&= f^{Y} + \epsilon(\tau^{Y} + \frac{1}{2}f^{Y}r^{Y}_{Y/X} - \frac{1}{2}r^{Y}_{Y/X}f^{Y}) \\
&= f^{Y} + \epsilon\Big(\tau^{Y} + \frac{1}{2}f^{Y}r^{Y}_{Y/X} - \frac{1}{2}(r^{Y}_{Y/X})^{*}(f^{Y})^{*}\Big).
\end{aligned} \tag{2.31}$$

Applying the quaternion cross product as defined in Table 2.2, the

expression becomes

$$\begin{aligned} \mathcal{W}^{Y}(O_Y) &= q^{*}_{Y/X}\mathcal{W}^{X}(O_X)q_{Y/X} \\ &= f^{Y} + \epsilon(\tau^{Y} + f^{Y} \times r^{Y}_{Y/X}) \\ &= f^{Y} + \epsilon(\tau^{Y} + r^{Y}_{X/Y} \times f^{Y}) \end{aligned} \tag{2.32}$$

As expected, Eq. (2.32) shows that in order to express a wrench in a different reference frame it is not enough to rotate its components, but a transport term has to be added to obtain a dynamically equivalent condition.

As a recap, Table 2.5 collects some quantities of interest expressed with the previously explained tools.

	$\mathbb{R}^3$	$\mathbb{H}$	$\mathbb{H}_d$
Position	$\bar{r}^{Y}_{Y/X}$	$r^{Y}_{Y/X} = [0, \bar{r}^{Y}_{Y/X}]^{T}$	$q_{Y/X} = q_{Y/X} + \epsilon\frac{1}{2}q_{Y/X}r^{Y}_{Y/X}$
Attitude	—	$q_{Y/X}$	
Linear velocity	$\bar{v}^{Y}_{Y/X}$	$v^{Y}_{Y/X} = [0, \bar{v}^{Y}_{Y/X}]^{T}$	$\omega^{Y}_{Y/X} = \omega^{Y}_{Y/X} + \epsilon(v^{Y}_{Y/X} + \omega^{Y}_{Y/X} \times r^{Y}_{Y/X})$
Angular velocity	$\bar{\omega}^{Y}_{Y/X}$	$\omega^{Y}_{Y/X} = [0, \bar{\omega}^{Y}_{Y/X}]^{T}$	
Force	$\bar{f}^{Y}$	$f^{Y} = [0, \bar{f}^{Y}]^{T}$	$\mathcal{W}^{Y} = f^{Y} + \epsilon\tau^{Y}$
Torque	$\bar{\tau}^{Y}$	$\tau^{Y} = [0, \bar{\tau}^{Y}]^{T}$	

Table 2.5: Variable construcion in the different frameworks

2.3 Physical model of a spacecraft multibody robotic system

2.3.1 Assumptions

As a first step, we highlight the main assumptions that were made in the transition from the real system to the physical one:

- All the bodies constituting the overall system are considered rigid. This is reasonable since there is no interest in studying possible structural effects; possible deformations are considered negligible when compared to rigid body motion for what concerns computations of the system position/orientation.
- The masses of some elements of the manipulator (joints, motors, ...) are lumped into the link masses; similarly, all the components attached to the satellite base (instruments, solar panels, ...) are neglected and their mass is part of the base mass. All the rigid bodies have uniform and constant density; this means that, for example, no fuel consumption is considered when it comes to mass properties of the base.
- No friction force due to the interaction between different bodies has been taken into account; every degree of freedom is either completely blocked by reaction forces (e.g. translational motions for a revolute joint) or subject to null force if not constrained. This assumption has indeed some significant effects on the overall modeling and simulation framework; thinking of friction as a velocity-dependent force, it is however reasonable to neglect it whenever mechanical parts in contact are moving at low relative velocities, which may be the case for a spacecraft mounted manipulator and in particular for the problem of interest. On the other hand, involving a non-conservative force into the model means that the mechanical energy is not conserved, thus changing the system's behavior

in a number of different situations. Dissipative effects, which must be carefully considered in the design of a space mission, are however out of the scope of this discussion; it would be interesting to consider them in a further development of this work to get an idea of their impact on the system.

- When dealing with the generation of a control input, no actuator dynamics will be considered; the control forces and torques introduced in the system will therefore correspond to the ideal ones computed with the different control strategies. Given the performances of the modern actuators, especially when it comes to the field of robotics, it is assumed that they will accurately reproduce the ideal control profile.

2.3.2 System topology

Intuitively, it is straightforward to imagine a SMM as a multibody system made up by the combination of a base (the satellite itself) and one or more multibody subsidiary structures, the manipulators, attached to the base through some kind of connections. This idea, although basic, is nonetheless able to capture the core of the problem, and it is the starting point of the proposed analysis. The connections between the manipulators and the base and between the manipulator links themselves are described by different joint types, which define the constraint imposed by the connection to its adjacent bodies; the possible joint types for the model at hand will be

- Revolute (R)
- Prismatic (P)
- Spherical (S)
- Cylindrical (C)
- Cartesian (U).

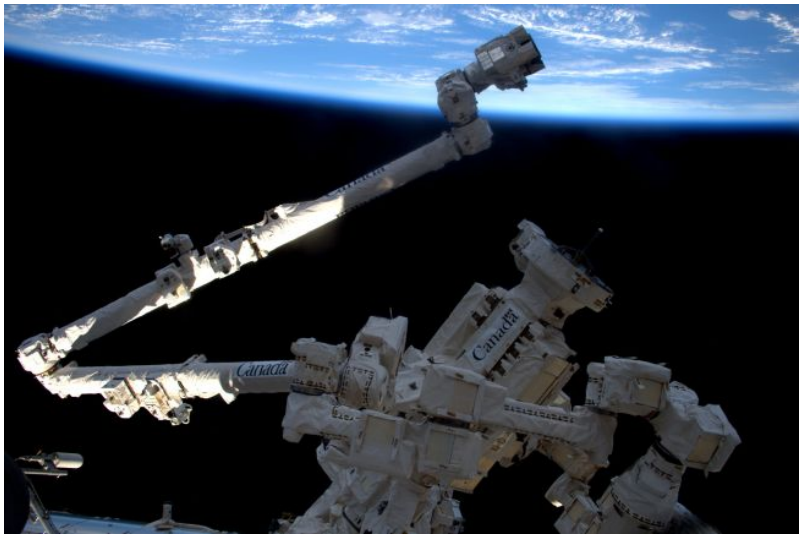

Figure 2.1: Canadarm2 and Dextre, the Special Purpose Dexterous Manipulator. *Credits: ESA/NASA*

Given this main framework, which is supported by the generic layout of a space manipulator (see an example in Fig. 2.1), the SMM can be thought of as a *Directed Acyclic Graph* $\mathcal{G}(v, e)$, where v is the number of vertices and e the number of edges; this graph corresponds to a directed and rooted tree structure where direction of the edges matters. The rigid bodies composing the system will be the nodes (vertices), while the joints will act as the edges (Fig. 2.2).

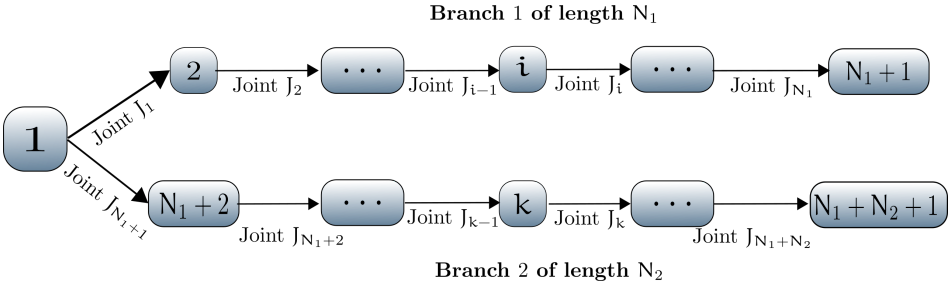

Figure 2.2: Graph representation of a spacecraft mounted manipulator with two branches.

In order to render relationships between elements at the graph level, i.e. to describe the system's topology, two different matrices

are used, namely C and T. The first is the incidence matrix, which highlights the type of connection between the elements of the graph; each row in C will represent the i^{th} joint, while every column gathers information about the j^{th} body. Thus, the element c_{ij} returns the relationship between joint i and body j in the form

$$c_{ij} \triangleq \begin{cases} 1 & \text{if joint } i \text{ is proximal, body } j \text{ is distal} \\ 0 & \text{if joint } i \text{ is not connected to body } j \\ -1 & \text{if joint } i \text{ is distal, body } j \text{ is proximal.} \end{cases} \tag{2.33}$$

T is instead the branch termination vector and it defines whether a body j terminates a branch, according to

$$t_j \triangleq \begin{cases} 1 & \text{if body } j \text{ terminates a branch,} \\ 0 & \text{otherwise.} \end{cases} \tag{2.34}$$

As a last remark, two operators $P[\cdot]$ and $N[\cdot]$ are defined to extract information from C, T; given either the incidence matrix or the branch termination vector, or a single row/column of one of them, $P[\cdot]$ returns the indices of the "1" entries while $N[\cdot]$ does the same for "-1" values.

Once the system's configuration is known in terms of number of branches, number of bodies per branch and types of joints, these information uniquely define some meaningful quantities. If B is the number of branches, then $i \in \{1, \dots, B\}$ identifies a particular branch and N_i is the number of bodies in that branch, while N is the total number of bodies; similarly, if the system has J joints, d_i is the number of degrees of freedom of the i^{th} joint, $i \in \{1, \dots, J\}$. Hence, $N = 1 + J$ where $J = \sum_{i=1}^{B} N_i$, cause the first and last element of the manipulator chain is always a rigid body; the previous expressions of C and T can be specialized, becoming $C \in \mathbb{R}^{J \times N}$ and $T \in \mathbb{R}^{N}$. $D = \sum_{i=1}^{J} d_i$ will be the number of degrees of freedom allowed by the joints (e.g., the number of degrees of freedom of the manipulator), and conversely $R = \sum_{i=1}^{J} r_i = \sum_{i=1}^{J} (6 - d_i)$ will be the number of

reaction forces exerted by all the joints.

A vector $\mathcal{y} \in \mathbb{R}^{8N}$ collecting the dual velocities of all the bodies can be defined as

$$\mathcal{y} \triangleq \begin{bmatrix} \boldsymbol{\omega}^{\mathcal{B}_1}_{\mathcal{B}_1/I} \\ \vdots \\ \boldsymbol{\omega}^{\mathcal{B}_i}_{\mathcal{B}_i/I} \\ \vdots \\ \boldsymbol{\omega}^{\mathcal{B}_N}_{\mathcal{B}_N/I} \end{bmatrix}, \tag{2.35}$$

where $\boldsymbol{\omega}^{\mathcal{B}_1}_{\mathcal{B}_1/I}$ is the velocity of the base, i.e. the satellite. The collection of all the joints generalized coordinates $\Gamma \in \mathbb{R}^D$ can be found as

$$\Gamma \triangleq \begin{bmatrix} \Gamma_{J_1} \\ \vdots \\ \Gamma_{J_i} \\ \vdots \\ \Gamma_{J_J} \end{bmatrix}. \tag{2.36}$$

Note that the size and parametrization of each Γ_{J_i} varies upon the type of joint J_i, according to Table 2.6 (see [27]).

The generalized coordinates of each joint are always written in the reference frame of the joint itself

A three-axial rotation due to a spherical (S) joint is modeled with a 3-2-1 ($\psi - \theta - \phi$) Eulerian rotation

Joint type	**Generalized joint coordinates Γ_{J_i}**	**d_i (DOF)**
R	$\theta_{i/\mathcal{B}_k} \in \mathbb{R}^1$	1
P	$z_{i/\mathcal{B}_k} \in \mathbb{R}^1$	1
S	$[\phi_{i/\mathcal{B}_k}, \theta_{i/\mathcal{B}_k}, \psi_{i/\mathcal{B}_k}]^T \in \mathbb{R}^3$	3
C	$[\theta_{i/\mathcal{B}_k}, z_{i/\mathcal{B}_k}]^T \in \mathbb{R}^2$	2
U	$[x_{i/\mathcal{B}_k}, y_{i/\mathcal{B}_k}, z_{i/\mathcal{B}_k}]^T \in \mathbb{R}^3$	3
	$k = N[C(i,:)]$	

Table 2.6: Generalized joint coordinates Γ_{J_i} for the different joint types.

The $N[\cdot]$ operator has been used in Table 2.6 to define the k subscript, since the generalized coordinates of each joint J_i express a motion with respect to its proximal body; the joint coordinates have to be interpreted as the parametrization of the motion of an i reference frame attached to the i^{th} joint.

Although in principle a joint frame can be oriented in a number of different ways, some conventions are adopted to make the process more intuitive. When dealing with a joint featuring a single degree of freedom (R or P), this will act along the joint's Z axis, so for example the local Z axis of a prismatic joint will be parallel to its linear translation with respect to the parent body, and the same holds for the rotation of a revolute joint; the orientation of the other two axes can be chosen arbitrarily. In the cylindrical joint case, two joints R and P are joined, leading to a rotation and translation on the local Z axis; when a joint displays three degrees of freedom, the axes will be aligned to the directions of the physical motion for a Cartesian joint, while in the case of a spherical one it is common to define the local X pointing towards the next body in the manipulator chain.

2.3.3 Frames and variables definition

Before going on with the discussion it is necessary to thoroughly explain the characterization of the physical system from a practical standpoint; Fig. 2.3 will act as a reference for the next remarks. In the first place, the general configuration is assessed by visual inspection of the system; this step is necessary to model the SMM as a graph (Fig. 2.2), i.e. to define the previously mentioned quantities C, T, N, B, J. Once this is done the designer shall make a distinction between the joints according to their features and pick a particular type for each one of them, choosing between the proposed ones. Once every joint is associated to a specific joint type, D and R are known and therefore the size of both $\mathcal{Y}, \Gamma$ (Eqs. (2.35) and (2.36)) is defined. Since the system's physical features (masses, inertias, dimensions, ...) are assumed to be perfectly known, it is possible

to iteratively define a frame of reference for both the bodies and the joints, moving outwards from the inertial I reference frame.

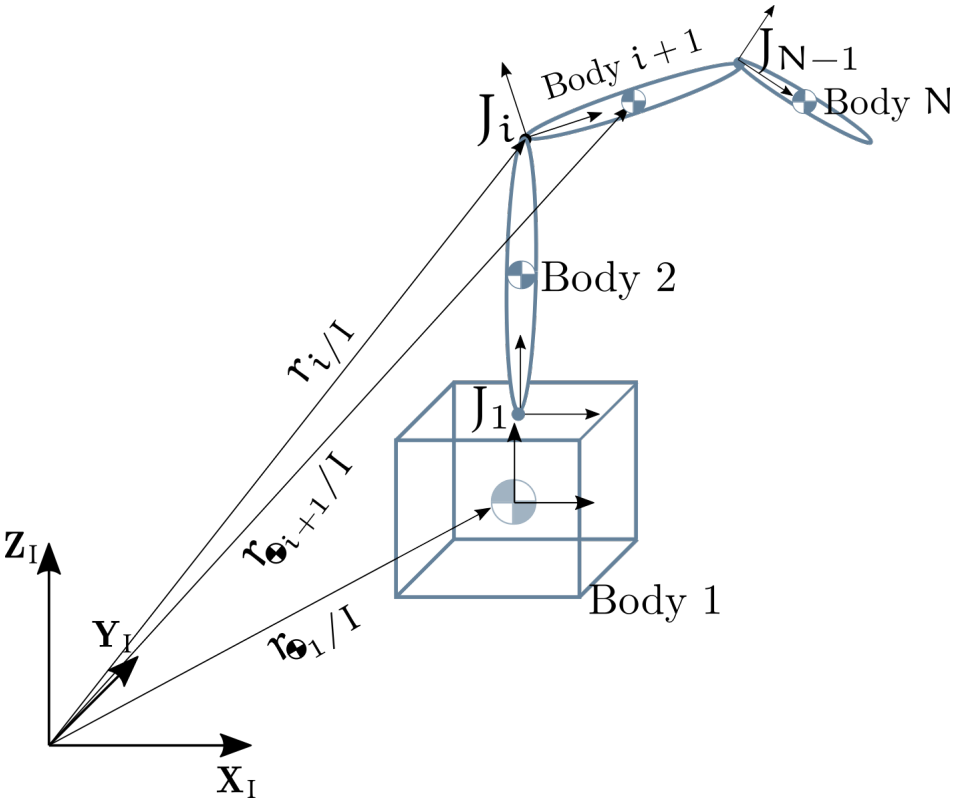

Figure 2.3: Frames and distances labeling for the physical model; the coordinate systems attached to the centers of mass of the links are not reported for brevity.

Each body frame will originate at a center of mass, while the joint frames will be defined according to the previous considerations; this procedure will lead to the creation of an inertial I frame, N body frames and J joint frames. Note that the orientation of each frame with respect to the inertial one is known by construction, and so are the quaternions $q_{i/I}, q_{\mathfrak{o}_k/I}$, where $k = N[C(i,:)]$. Hence, it is straightforward to find the relative orientation of each frame with respect to its parent one; for example, using the result of Eq. (2.10), $q_{i/I} = q_{\mathfrak{o}_k/I} q_{i/\mathfrak{o}_k}$, where $q_{i/\mathfrak{o}_k}$ is the only unknown. Applying the

conjugate $q^*_{\mathfrak{o}_k/I}$ and recalling the conjugate properties, the relative orientation can be expressed as

$$q_{i/\mathfrak{o}_k} = q^*_{\mathfrak{o}_k/I} q_{i/I}, \quad k = N[C(i,:)]. \tag{2.37}$$

The same holds when the parent frame is a joint frame, as in

$$q_{\mathfrak{o}_{i+1}/i} = q^*_{i/I} q_{\mathfrak{o}_{i+1}/I}. \tag{2.38}$$

By suitably rearranging quaternion rotations as in Eqs. (2.37) and (2.38), any relative orientation between different frames can be easily obtained; to the purpose of this work, the link frames will always be oriented as their parent joint frame, so $q_{\mathfrak{o}_{i+1}/i} = 1, i = \{1, \dots, J\}$. This is justified because the links are rigid, so no relative rotation will ever take place between a joint and its child body. On the other hand, the $q_{i/\mathfrak{o}_k}$ will play a major role in the discussion as they encompass the information on the displacement of each joint.

A similar methodology has to be exploited when dealing with the position vectors, which are necessary to fully define the geometry of the system. The spatial configuration of the system is known (CAD measurements, inspection, ...), so as long as the I frame is defined, the designer also knows the quaternion positions $r^I_{\mathfrak{o}_i/I}, r^I_{i/I} \in \mathbb{H}^v$. Once more, the relative distance vectors can be computed in a quaternion form through simple subtractions, as in

$$r^I_{i/\mathfrak{o}_k} = r^I_{i/I} - r^I_{\mathfrak{o}_k/I}, \tag{2.39}$$

and then expressed in another frame $r^i_{i/\mathfrak{o}_k} = q^*_{i/I} r^I_{i/\mathfrak{o}_k} q_{i/I}$ at the occurrence. The relative orientations and positions can be blended together to get the *relative dual pose*, i.e. the relative rigid displacement between different frames expressed in dual quaternions, such

as

$$\begin{aligned} \mathbf{q}_{\mathfrak{i}/\mathfrak{o}_k} &\triangleq q_{\mathfrak{i}/\mathfrak{o}_k} + \epsilon \frac{1}{2} q_{\mathfrak{i}/\mathfrak{o}_k} r^{\mathfrak{i}}_{\mathfrak{i}/\mathfrak{o}_k}, \\ \mathbf{q}_{\mathfrak{o}_{i+1}/\mathfrak{i}} &\triangleq q_{\mathfrak{o}_{i+1}/\mathfrak{i}} + \epsilon \frac{1}{2} q_{\mathfrak{o}_{i+1}/\mathfrak{i}} r^{\mathfrak{o}_{i+1}}_{\mathfrak{o}_{i+1}/\mathfrak{i}}. \end{aligned} \tag{2.40}$$

The forward kinematics formulas expressed in Eq. (2.40), which were introduced in Eq. (2.25) in a more general form, encase two different information, one about a translation and the second about a rotation; this is made evident if we rewrite $\mathbf{q}_{\mathfrak{o}_{i+1}/\mathfrak{i}}$ as a dual quaternion product by separating the translation from the rotation in the form

$$\mathbf{q}_{\mathfrak{o}_{i+1}/\mathfrak{i}} = \underbrace{(q_{\mathfrak{o}_{i+1}/\mathfrak{i}} + \epsilon 0)}_{\text{rotation}} \underbrace{(1 + \epsilon \frac{1}{2} r^{\mathfrak{o}_{i+1}}_{\mathfrak{o}_{i+1}/\mathfrak{i}})}_{\text{translation}}, \tag{2.41}$$

or, equivalently,

$$\mathbf{q}_{\mathfrak{o}_{i+1}/\mathfrak{i}} = \underbrace{(1 + \epsilon \frac{1}{2} r^{\mathfrak{i}}_{\mathfrak{o}_{i+1}/\mathfrak{i}})}_{\text{translation}} \underbrace{(q_{\mathfrak{o}_{i+1}/\mathfrak{i}} + \epsilon 0)}_{\text{rotation}}. \tag{2.42}$$

Even though the two expressions give the same result, they have different physical meaning: Eq. (2.41) first carries out the rotation and then the translation, Eq. (2.42) does the opposite. The example case illustrated in Fig. 2.3 still misses wrenches as defined in Eq. (2.29). Taking Fig. 2.4 as reference, it is possible to distinguish different kinds of wrenches; as a first remark, wrenches enter the system acting either on a center of mass (body wrenches) or on a joint (joint wrenches). Body wrenches $\boldsymbol{W}^{\mathfrak{o}_i}_{\mathfrak{o}_i}(O_{\mathfrak{o}_i})$ arise as a consequence of both natural phenomena (gravity, atmospheric drag, ...) and control inputs (base actuation); they are always expressed in the body frame. Joint wrenches instead are divided into two different types; they may describe the control input itself, in which case they are referred to as actuation wrenches $\boldsymbol{W}^{\mathfrak{i}}_{\text{act},i}(O_i)$, or represent the reaction forces/torques due to the physical constraint imposed by the joint on its two adjoining bodies, hence being reaction wrenches

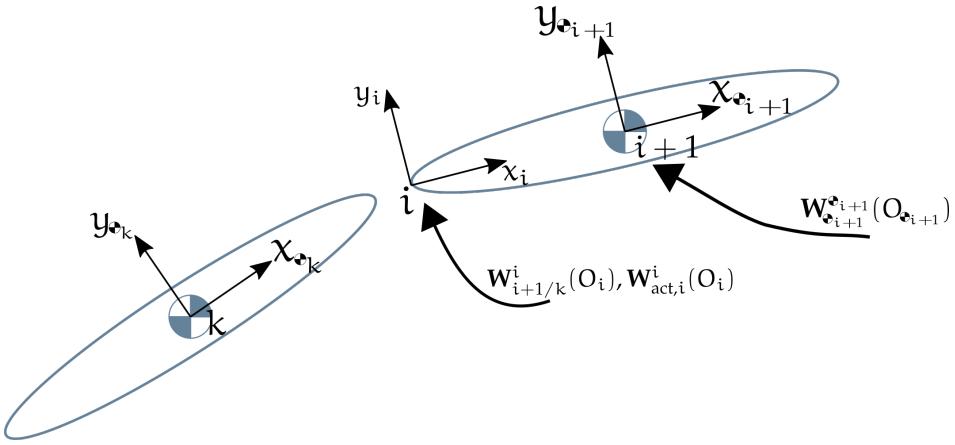

Figure 2.4: Definition and labeling of the different kinds of wrenches. Note that k = N[C(i, :)].

$\boldsymbol{W}^{i}_{\mathfrak{o}_{i+1}/\mathfrak{o}_k}(O_i)$. The notation here is meaningful as it shows that a reaction wrench acts on the origin of the joint frame O_i and is caused by the presence of the joint itself acting on the k^{th} and $(i+1)^{th}$ body.

2.3.4 Kinematics and mapping matrices

Position and velocity kinematics

Starting from the ideas of Secs. 2.3.2 and 2.3.3, we now focus on the assembly of the previous information, building the kinematic tools and relations that will enable the solution of the problem at hand. Given the SMM configuration, its kinematics is fully defined if and only if the base linear and angular coordinates and the joint generalized coordinates (see Eq. (2.36) and Table 2.6) are known; this provides a set of 6 + D scalars which has to be updated at each step of the solution process.

Labeling the base as the first body, its kinematics will be expressed using the result in Eq. (2.28), therefore leading to

$$\dot{q}_{\mathfrak{o}_1/I} = \frac{1}{2} q_{\mathfrak{o}_1/I} \omega^{\mathfrak{o}_1}_{\mathfrak{o}_1/I}. \tag{2.43}$$

The manipulator kinematics instead depend on the kind of joints; for an N−bodies SMM the general forward kinematics has the form

$$\mathbf{q}_{\mathfrak{o}_N/I} = \mathbf{q}_{\mathfrak{o}_1/I}\mathbf{q}_{1/\mathfrak{o}_1}\left(\prod_{i=2}^{N-1}\mathbf{q}_{i/i-1}\right)\mathbf{q}_{\mathfrak{o}_N/N-1}, \tag{2.44}$$

where $\mathbf{q}_{i/i-1} = \mathbf{q}_{\mathfrak{o}_k/i-1}\mathbf{q}_{i/\mathfrak{o}_k}$. For $N = 4$ (see Fig. 2.3) the product operator $\prod$ takes the form

$$\prod_{i=2}^{3} = \mathbf{q}_{2/1}\mathbf{q}_{3/2}. \tag{2.45}$$

Note also that once the generic pose $\mathbf{q}_{J/I}$ is known, the quaternion position of the origin of frame J with respect to frame I ($r^J_{J/I}$) can be easily reconstructed; recalling that $\mathbf{q}_{J/I} = q_{J/I,r} + \epsilon q_{J/I,d} = q_{J/I} + \epsilon\frac{1}{2}q_{J/I}r^J_{J/I}$, if we pre-multiply the dual part by $2q^*_{J/I}$,

$$\begin{aligned} 2q^*_{J/I}q_{J/I,d} &= \underbrace{2q^*_{J/I}\frac{1}{2}q_{J/I}}_{1}r^J_{J/I} \\ &= r^J_{J/I}. \end{aligned} \tag{2.46}$$

The velocity is instead obtained deriving Eq. (2.44) and applying the product rule to the right hand side of the equality, recalling that $\mathbf{q}_{\mathfrak{o}_N/N-1}$ is constant:

$$\begin{aligned} \dot{\mathbf{q}}_{\mathfrak{o}_N/I} = {} & \dot{\mathbf{q}}_{\mathfrak{o}_1/I}\mathbf{q}_{1/\mathfrak{o}_1}\left(\prod_{i=2}^{N-1}\mathbf{q}_{i/i-1}\right)\mathbf{q}_{\mathfrak{o}_N/N-1} + \\ & + \mathbf{q}_{\mathfrak{o}_1/I}\dot{\mathbf{q}}_{1/\mathfrak{o}_1}\left(\prod_{i=2}^{N-1}\mathbf{q}_{i/i-1}\right)\mathbf{q}_{\mathfrak{o}_N/N-1} + \\ & + \mathbf{q}_{\mathfrak{o}_1/I}\mathbf{q}_{1/\mathfrak{o}_1}\sum_{k=2}^{N-1}\left(\mathbf{q}_{k-1/1}\dot{\mathbf{q}}_{k/k-1}\mathbf{q}_{N-1/k}\right)\mathbf{q}_{\mathfrak{o}_N/N-1} \end{aligned} \tag{2.47}$$

$$
\begin{aligned}
&= \frac{1}{2}\mathbf{q}_{\mathfrak{o}_1/I}\boldsymbol{\omega}^{\mathfrak{o}_1}_{\mathfrak{o}_1/I}\mathbf{q}_{1/\mathfrak{o}_1}\left(\prod_{i=2}^{N-1}\mathbf{q}_{i/i-1}\right)\mathbf{q}_{\mathfrak{o}_N/N-1}+\\
&+\mathbf{q}_{\mathfrak{o}_1/I}\frac{1}{2}\mathbf{q}_{1/\mathfrak{o}_1}\boldsymbol{\omega}^{1}_{1/\mathfrak{o}_1}\left(\prod_{i=2}^{N-1}\mathbf{q}_{i/i-1}\right)\mathbf{q}_{\mathfrak{o}_N/N-1}+\\
&+\mathbf{q}_{\mathfrak{o}_1/I}\mathbf{q}_{1/\mathfrak{o}_1}\sum_{k=2}^{N-1}\left(\mathbf{q}_{k-1/1}\frac{1}{2}\mathbf{q}_{k/k-1}\boldsymbol{\omega}^{k}_{k/k-1}\mathbf{q}_{N-1/k}\right)\mathbf{q}_{\mathfrak{o}_N/N-1}.
\end{aligned}
$$

The end-effector dual velocity (the dual velocity of the N^{th} body) can be put into evidence multiplying each side by $2\mathbf{q}^*_{\mathfrak{o}_N/I}$, which is obtained from Eq. (2.44):

$$
\begin{aligned}
\boldsymbol{\omega}^{\mathfrak{o}_N}_{\mathfrak{o}_N/I} &= \mathbf{q}^*_{\mathfrak{o}_N/I}\mathbf{q}_{\mathfrak{o}_1/I}\boldsymbol{\omega}^{\mathfrak{o}_1}_{\mathfrak{o}_1/I}\mathbf{q}_{1/\mathfrak{o}_1}\left(\prod_{i=2}^{N-1}\mathbf{q}_{i/i-1}\right)\mathbf{q}_{\mathfrak{o}_N/N-1}+\\
&+\mathbf{q}^*_{\mathfrak{o}_N/I}\mathbf{q}_{\mathfrak{o}_1/I}\mathbf{q}_{1/\mathfrak{o}_1}\boldsymbol{\omega}^{1}_{1/\mathfrak{o}_1}\left(\prod_{i=2}^{N-1}\mathbf{q}_{i/i-1}\right)\mathbf{q}_{\mathfrak{o}_N/N-1}+\\
&+\mathbf{q}^*_{\mathfrak{o}_N/I}\mathbf{q}_{\mathfrak{o}_1/I}\mathbf{q}_{1/\mathfrak{o}_1}\sum_{k=2}^{N-1}\left(\mathbf{q}_{k-1/1}\mathbf{q}_{k/k-1}\boldsymbol{\omega}^{k}_{k/k-1}\mathbf{q}_{N-1/k}\right)\mathbf{q}_{\mathfrak{o}_N/N-1}.
\end{aligned}
\tag{2.48}
$$

Using that

$$
\mathbf{q}^*_{\mathfrak{o}_N/I}\mathbf{q}_{\mathfrak{o}_1/I} = \mathbf{q}^*_{\mathfrak{o}_N/\mathfrak{o}_1}\underbrace{\mathbf{q}^*_{\mathfrak{o}_1/I}\mathbf{q}_{\mathfrak{o}_1/I}}_{\mathbf{1}} \quad \text{and} \quad \mathbf{q}^*_{\mathfrak{o}_N/\mathfrak{o}_1}\mathbf{q}_{1/\mathfrak{o}_1} = \mathbf{q}^*_{\mathfrak{o}_N/1}\underbrace{\mathbf{q}^*_{1/\mathfrak{o}_1}\mathbf{q}_{1/\mathfrak{o}_1}}_{\mathbf{1}},
\tag{2.49}
$$

and carrying out the dual quaternion products, Eq. (2.48) becomes

$$
\boldsymbol{\omega}^{\mathfrak{o}_N}_{\mathfrak{o}_N/I} = \mathbf{q}^*_{\mathfrak{o}_N/\mathfrak{o}_1}\boldsymbol{\omega}^{\mathfrak{o}_1}_{\mathfrak{o}_1/I}\mathbf{q}_{\mathfrak{o}_N/\mathfrak{o}_1}+\mathbf{q}^*_{\mathfrak{o}_N/1}\boldsymbol{\omega}^{1}_{1/\mathfrak{o}_1}\mathbf{q}_{\mathfrak{o}_N/1}+\sum_{k=2}^{N-1}\mathbf{q}^*_{\mathfrak{o}_N/k}\boldsymbol{\omega}^{k}_{k/k-1}\mathbf{q}_{\mathfrak{o}_N/k}.
\tag{2.50}
$$

This expression of $\boldsymbol{\omega}^{\mathfrak{o}_N}_{\mathfrak{o}_N/I}$ has a straightforward physical interpretation: the dual velocity of the N^{th} body with respect to an inertial

frame is obtained summing a first term due to the velocity of the base to a series of terms descending from the joint velocities; all the different terms are rightfully expressed in the N^{th} body frame.

Keeping in mind the general result obtained in Eq. (2.50), we want to further specialize the dual velocities for different joint types and introduce some quantities that will allow a more familiar way to express end-effector velocity. Recalling that the manipulator may involve different types of joint, it is possible to draw a parallel with Table 2.6 and characterize the $\boldsymbol{\omega}^{i}_{i/\mathfrak{o}_k}$ according to a joint type-based criterion (Table 2.7).

Joint type	**Dual velocity,** $\boldsymbol{\omega}^{i}_{i/\mathfrak{o}_k}$
R	$\left(0, [0, 0, \dot{\theta}_{i/\mathfrak{o}_k}]^T\right) + \epsilon 0$
P	$0 + \epsilon \left(0, [0, 0, \dot{z}_{i/\mathfrak{o}_k}]^T\right)$
S	$\left(0, M(\phi_{i/\mathfrak{o}_k}, \theta_{i/\mathfrak{o}_k}, \psi_{i/\mathfrak{o}_k})[\dot{\phi}_{i/\mathfrak{o}_k}, \dot{\theta}_{i/\mathfrak{o}_k}, \dot{\psi}_{i/\mathfrak{o}_k}]^T\right) + \epsilon 0$
C	$\left(0, [0, 0, \dot{\theta}_{i/\mathfrak{o}_k}]^T\right) + \epsilon \left(0, [0, 0, \dot{z}_{i/\mathfrak{o}_k}]^T\right)$
U	$0 + \epsilon \left(0, [\dot{x}_{i/\mathfrak{o}_k}, \dot{y}_{i/\mathfrak{o}_k}, \dot{z}_{i/\mathfrak{o}_k}]^T\right)$
	$k = N[C(i, :)]$

Table 2.7: Dual velocities for different joint types.

Table 2.7 is built following the conventions suggested in Sec. 2.3.2 regarding the axis of translation and/or rotation for R, P, C joints; $M(\phi_{i/\mathfrak{o}_k}, \theta_{i/\mathfrak{o}_k}, \psi_{i/\mathfrak{o}_k})$ must be defined coherently with the Eulerian sequence chosen for the spherical rotation, and in our case is equal

to

$$M(\phi_{i/\mathfrak{o}_k}, \theta_{i/\mathfrak{o}_k}, \psi_{i/\mathfrak{o}_k}) = \begin{bmatrix} 1 & 0 & -\sin(\theta_{i/\mathfrak{o}_k}) \\ 0 & \cos(\phi_{i/\mathfrak{o}_k}) & \cos(\theta_{i/\mathfrak{o}_k})\sin(\phi_{i/\mathfrak{o}_k}) \\ 0 & -\sin(\phi_{i/\mathfrak{o}_k}) & \cos(\theta_{i/\mathfrak{o}_k})\cos(\phi_{i/\mathfrak{o}_k}) \end{bmatrix}. \tag{2.51}$$

Before further rearrangement of Eq. (2.50), we also need to introduce *screw matrices* $\zeta_i \in \mathbb{R}^{8\times d_i}$ for every type of joint; they are assembled so that $\omega^i_{i/\mathfrak{o}_k} = \zeta_i \dot{\Gamma}_{J_i}$.

Joint type	**Screw matrix,** $\zeta_i = \partial\omega^i_{i/\mathfrak{o}_k}/\partial\dot{\Gamma}_{J_i}$
R	$[0,0,0,1,0,0,0,0]^T$
P	$[0,0,0,0,0,0,0,1]^T$
S	$\begin{bmatrix} 0_{1\times3} \\ M(\phi_{i/\mathfrak{o}_k}, \theta_{i/\mathfrak{o}_k}, \psi_{i/\mathfrak{o}_k}) \\ 0_{4\times3} \end{bmatrix}$
C	$\begin{bmatrix} 0 & 0 & 0 & 1 & 0 & 0 & 0 & 0 \\ 0 & 0 & 0 & 0 & 0 & 0 & 0 & 1 \end{bmatrix}^T$
U	$\begin{bmatrix} 0_{5\times3} \\ I_3 \end{bmatrix}$

Table 2.8: Screw matrices for different joint types.

Going back to Eq. (2.50), the result can now be rewritten in a more familiar form; using Eq. (2.19) yields

$$\omega^{\mathfrak{e}_N}_{\mathfrak{e}_N/I} = [\![q^*_{\mathfrak{e}_N/\mathfrak{e}_1}]\!]_L [\![q_{\mathfrak{e}_N/\mathfrak{e}_1}]\!]_R \star \omega^{\mathfrak{e}_1}_{\mathfrak{e}_1/I} + [\![q^*_{\mathfrak{e}_N/1}]\!]_L [\![q_{\mathfrak{e}_N/1}]\!]_R \star \omega^1_{1/\mathfrak{e}_1} + \\ + \sum_{k=2}^{N-1} [\![q^*_{\mathfrak{e}_N/k}]\!]_L [\![q_{\mathfrak{e}_N/k}]\!]_R \star \omega^k_{k/k-1}. \tag{2.52}$$

Substituting the dual velocities with the screw matrices and the joint-level velocities results in

$$\begin{aligned} \omega^{\mathfrak{e}_N}_{\mathfrak{e}_N/I} &= [\![q^*_{\mathfrak{e}_N/\mathfrak{e}_1}]\!]_L [\![q_{\mathfrak{e}_N/\mathfrak{e}_1}]\!]_R \star \omega^{\mathfrak{e}_1}_{\mathfrak{e}_1/I} + [\![q^*_{\mathfrak{e}_N/1}]\!]_L [\![q_{\mathfrak{e}_N/1}]\!]_R \zeta_1 \dot{\Gamma}_{J_1} + \\ &\quad + \sum_{k=2}^{N-1} [\![q^*_{\mathfrak{e}_N/k}]\!]_L [\![q_{\mathfrak{e}_N/k}]\!]_R \zeta_k \dot{\Gamma}_{J_k} \\ &= [\![q^*_{\mathfrak{e}_N/\mathfrak{e}_1}]\!]_L [\![q_{\mathfrak{e}_N/\mathfrak{e}_1}]\!]_R \star \omega^{\mathfrak{e}_1}_{\mathfrak{e}_1/I} + J(q,\zeta)\,\dot{\Gamma}, \end{aligned} \tag{2.53}$$

where $J(q,\zeta) \in \mathbb{R}^{8\times D}$ is the body-frame Jacobian which has been defined as

$$J(q,\zeta) \triangleq \Big[[\![q^*_{\mathfrak{e}_N/1}]\!]_L [\![q_{\mathfrak{e}_N/1}]\!]_R \zeta_1, \ldots, [\![q^*_{\mathfrak{e}_N/i}]\!]_L [\![q_{\mathfrak{e}_N/i}]\!]_R \zeta_i, \ldots, \\ [\![q^*_{\mathfrak{e}_N/N-1}]\!]_L [\![q_{\mathfrak{e}_N/N-1}]\!]_R \zeta_{N-1} \Big]. \tag{2.54}$$

If we express the end-effector velocity with respect to the satellite base, Eq. (2.53) is brought back to the well known velocity kinematics result obtained for a fixed-base manipulator, i.e.

$$\underbrace{\omega^{\mathfrak{e}_N}_{\mathfrak{e}_N/I} - [\![q^*_{\mathfrak{e}_N/\mathfrak{e}_1}]\!]_L [\![q_{\mathfrak{e}_N/\mathfrak{e}_1}]\!]_R \star \omega^{\mathfrak{e}_1}_{\mathfrak{e}_1/I}}_{\omega^{\mathfrak{e}_N}_{\mathfrak{e}_N/\mathfrak{e}_1}} = J(q,\zeta)\,\dot{\Gamma}. \tag{2.55}$$

Mapping matrices

Screw matrices are necessary when it comes to rearranging the time derivative of the joint coordinates into a dual quaternion velocity,

i.e. they provide a map $\zeta_i : \mathbb{R}^{d_i} \mapsto \mathbb{H}_d^\nu$. Other similar mappings are worth defining as they provide a fast way to switch from/to a real quantity to/from its dual quaternion counterpart; in order to do that, we define the matrix $E_{\pi(\cdot)}$, which is built removing the rows returned by function $\pi(\cdot)$ from the 8×8 identity matrix I_8. The function $\pi(\cdot)$ selects an ordered subset of $\{1,2,3,4,5,6,7,8\}$ upon necessity; for example, if $\pi(\cdot)$ returns values $1, 5$:

$$E_{15} = \begin{bmatrix} 0 & 1 & 0 & 0 & 0 & 0 & 0 & 0 \\ 0 & 0 & 1 & 0 & 0 & 0 & 0 & 0 \\ 0 & 0 & 0 & 1 & 0 & 0 & 0 & 0 \\ 0 & 0 & 0 & 0 & 0 & 1 & 0 & 0 \\ 0 & 0 & 0 & 0 & 0 & 0 & 1 & 0 \\ 0 & 0 & 0 & 0 & 0 & 0 & 0 & 1 \end{bmatrix}. \tag{2.56}$$

Such matrices can be exploited for example when dealing with wrenches, in order to build two kinds of reduced vectors for different joint types, namely the reduced reaction wrenches $\tilde{\boldsymbol{W}}^i_{\mathfrak{o}_{i+1}/\mathfrak{o}_i}(O_i) \in \mathbb{R}^{r_i}$ (collection of reaction forces/torques applied by the i^{th} joint) and the reduced actuation wrenches $\tilde{\boldsymbol{W}}^i_{\text{act},i}(O_i) \in \mathbb{R}^{d_i}$ (actuation forces/torques displayed by the i^{th} joint). Using the definitions in Tables 2.10 and 2.11, where $V_i : \mathbb{R}^{r_i} \mapsto \mathbb{H}_d^\nu$ and $V_{\text{act},i} : \mathbb{R}^{d_i} \mapsto \mathbb{H}_d^\nu$, we obtain $\boldsymbol{W}^i_{\mathfrak{o}_{i+1}/\mathfrak{o}_i} = V_i \tilde{\boldsymbol{W}}^i_{\mathfrak{o}_{i+1}/\mathfrak{o}_i}$ and $\boldsymbol{W}^i_{\text{act},i} = V_{\text{act},i} \tilde{\boldsymbol{W}}^i_{\text{act},i}$. The reduced reaction wrenches $\tilde{\boldsymbol{W}}^i_{\mathfrak{o}_{i+1}/\mathfrak{o}_i}$ can be stacked in a vector $\mathcal{T} \in \mathbb{R}^R$ defined as

$$\mathcal{T} \triangleq \begin{bmatrix} \tilde{\boldsymbol{W}}^1_{\mathfrak{o}_2/\mathfrak{o}_1}(O_1) \\ \vdots \\ \tilde{\boldsymbol{W}}^i_{\mathfrak{o}_{i+1}/\mathfrak{o}_i}(O_i) \\ \vdots \\ \tilde{\boldsymbol{W}}^J_{\mathfrak{o}_N/\mathfrak{o}_{N-1}}(O_J) \end{bmatrix}. \tag{2.57}$$

A similar result can be obtained for velocities by using two mappings $\Lambda_i : \mathbb{H}_d^\nu \mapsto \mathbb{R}^{r_i}$ and $L_{J_i} : \mathbb{H}_d^\nu \mapsto \mathbb{R}^{d_i}$ (see Table 2.9); the first extracts

the null entries of a joint dual velocity in the form $\mathbf{0} = \Lambda_i \boldsymbol{\omega}^i_{i/\mathfrak{o}_k}$, while the latter performs the operation opposite to ζ_i, hence leading to

$$\begin{aligned}\dot{\Gamma}_{J_i} &= L_{J_i} \boldsymbol{\omega}^i_{i/\mathfrak{o}_k} \\ &= L_{J_i} \left(q_{\mathfrak{o}_{i+1}/i} \boldsymbol{\omega}^{\mathfrak{o}_{i+1}}_{\mathfrak{o}_{i+1}/I} q^*_{\mathfrak{o}_{i+1}/i} - q^*_{i/\mathfrak{o}_k} \boldsymbol{\omega}^{\mathfrak{o}_k}_{\mathfrak{o}_k/I} q_{i/\mathfrak{o}_k} \right), \quad k = N[C(i,:)].\end{aligned} \tag{2.58}$$

Note that matrix $L(\phi_{i/\mathfrak{o}_k}, \theta_{i/\mathfrak{o}_k}, \psi_{i/\mathfrak{o}_k})$ in Table 2.9 depends on the Euler sequence used to parametrize the spherical joint, as in

$$\begin{aligned}L\left(\phi_{i/\mathfrak{o}_k}, \theta_{i/\mathfrak{o}_k}, \psi_{i/\mathfrak{o}_k}\right) &= M^{-1}\left(\phi_{i/\mathfrak{o}_k}, \theta_{i/\mathfrak{o}_k}, \psi_{i/\mathfrak{o}_k}\right) \\ &= \begin{bmatrix} 1 & \tan(\theta_{i/\mathfrak{o}_k})\sin(\phi_{i/\mathfrak{o}_k}) & \cos(\phi_{i/\mathfrak{o}_k})\tan(\theta_{i/\mathfrak{o}_k}) \\ 0 & \cos(\phi_{i/\mathfrak{o}_k}) & -\sin(\phi_{i/\mathfrak{o}_k}) \\ 0 & \sin(\phi_{i/\mathfrak{o}_k})/\cos(\theta_{i/\mathfrak{o}_k}) & \cos(\phi_{i/\mathfrak{o}_k})/\cos(\theta_{i/\mathfrak{o}_k}) \end{bmatrix}.\end{aligned} \tag{2.59}$$

Joint type	L_{J_i}	Λ_i
R	$[0,0,0,1,0,0,0,0]$	E_{145}
P	$[0,0,0,0,0,0,0,1]$	E_{158}
S	$\begin{bmatrix} 0_{3\times1} & L(\phi_{i/\mathfrak{o}_k}, \theta_{i/\mathfrak{o}_k}, \psi_{i/\mathfrak{o}_k}) & 0_{3\times4} \end{bmatrix}$	E_{12345}
C	$\begin{bmatrix} 0,0,0,1,0,0,0,0 \\ 0,0,0,0,0,0,0,1 \end{bmatrix}$	E_{1458}
U	$\begin{bmatrix} 0,0,0,0,0,1,0,0 \\ 0,0,0,0,0,0,1,0 \\ 0,0,0,0,0,0,0,1 \end{bmatrix}$	E_{15678}

Table 2.9: Velocity mapping matrices.

Joint type	$\boldsymbol{W}^{i}_{\mathbf{e}_{i+1}/\mathbf{e}_i}$	$\tilde{\boldsymbol{W}}^{i}_{\mathbf{e}_{i+1}/\mathbf{e}_i}$	V_i
R	$\left(0,[f_x,f_y,f_z]^T\right)+$ $\epsilon\left(0,[\tau_x,\tau_y,0]^T\right)$	$[f_x,f_y,f_z,\tau_x,\tau_y]^T$	E^T_{158}
P	$\left(0,[f_x,f_y,0]^T\right)+$ $\epsilon\left(0,[\tau_x,\tau_y,\tau_z]^T\right)$	$[f_x,f_y,\tau_x,\tau_y,\tau_z]^T$	E^T_{145}
S	$\left(0,[f_x,f_y,f_z]^T\right)+$ $\epsilon\left(0,[0,0,0]^T\right)$	$[f_x,f_y,f_z]^T$	E^T_{15678}
C	$\left(0,[f_x,f_y,0]^T\right)+$ $\epsilon\left(0,[\tau_x,\tau_y,0]^T\right)$	$[f_x,f_y,\tau_x,\tau_y]^T$	E^T_{1458}
U	$\left(0,[0,0,0]^T\right)+$ $\epsilon\left(0,[\tau_x,\tau_y,\tau_z]^T\right)$	$[\tau_x,\tau_y,\tau_z]^T$	E^T_{12345}

Table 2.10: Full and reduced reaction wrenches.

Joint type	$W^i_{act,i}$	$\tilde{W}^i_{act,i}$	$V_{act,i}$
R	$\left(0,[0,0,0]^T\right) + \epsilon\left(0,[0,0,\tau_z]^T\right)$	τ_z	$E^T_{1234567}$
P	$\left(0,[0,0,f_z]^T\right) + \epsilon\left(0,[0,0,0]^T\right)$	f_z	$E^T_{1235678}$
S	$\left(0,[0,0,0]^T\right) + \epsilon\left(0,[\tau_x,\tau_y,\tau_z]^T\right)$	$[\tau_x,\tau_y,\tau_z]^T$	E^T_{12345}
C	$\left(0,[0,0,f_z]^T\right) + \epsilon\left(0,[0,0,\tau_z]^T\right)$	$[f_z,\tau_z]^T$	E^T_{123567}
U	$\left(0,[f_x,f_y,f_z]^T\right) + \epsilon\left(0,[0,0,0]^T\right)$	$[f_x,f_y,f_z]^T$	E^T_{15678}

Table 2.11: Full and reduced actuation wrenches.

2.4 Robot dynamics

2.4.1 Dual form of dynamic quantities

Using the formulation introduced by [51], the mass and inertia matrices computed about a rigid body's center of mass can be rearranged into a dual inertia matrix

$$M_{\bullet_i} \triangleq \begin{bmatrix} 1 & 0_{1\times3} & 0 & 0_{1\times3} \\ 0_{3\times1} & m_{\bullet_i} I_3 & 0_{3\times1} & 0_{3\times3} \\ 0 & 0_{1\times3} & 1 & 0_{1\times3} \\ 0_{3\times1} & 0_{3\times3} & 0_{3\times1} & \bar{I}_{\bullet_i} \end{bmatrix}, \tag{2.60}$$

where $m_{\bullet_i} \in \mathbb{R}$ is the mass of the i^{th} rigid body, $\bar{I}_{\bullet_i} \in \mathbb{R}^{3\times3}$ is the inertia matrix of the same body and I_3 is the 3x3 identity matrix.

$M_{\textcircled{\scriptsize i}}$ can be exploited to compute the dual momentum of the i^{th} body about its center of mass and expressed in local body frame $\textcircled{\scriptsize i}$ as

$$\mathbf{H}^{\textcircled{\scriptsize i}}_{\textcircled{\scriptsize i}}(O_{\textcircled{\scriptsize i}}) = \mathbf{H}^{\textcircled{\scriptsize i}}_{\textcircled{\scriptsize i}/I} \triangleq M_{\textcircled{\scriptsize i}} \star (\boldsymbol{\omega}^{\textcircled{\scriptsize i}}_{\textcircled{\scriptsize i}/I})^S. \tag{2.61}$$

Recalling Newton's second principle,

$$\frac{d\mathbf{H}^{\textcircled{\scriptsize i}}_{\textcircled{\scriptsize i}/I}}{dt} = \boldsymbol{W}^{\textcircled{\scriptsize i}}_i(O_{\textcircled{\scriptsize i}}), \tag{2.62}$$

where $\boldsymbol{W}^{\textcircled{\scriptsize i}}_i(O_{\textcircled{\scriptsize i}}) = f^{\textcircled{\scriptsize i}} + \epsilon\tau^{\textcircled{\scriptsize i}}$ is the net force applied on the i^{th} body; as $\mathbf{H}^{\textcircled{\scriptsize i}}_{\textcircled{\scriptsize i}/I}$ is expressed in a rotating frame $\textcircled{\scriptsize i}$, Eq. (2.62) is equivalent to

$$\dot{\mathbf{H}}^{\textcircled{\scriptsize i}}_{\textcircled{\scriptsize i}/I} + \boldsymbol{\omega}^{\textcircled{\scriptsize i}}_{\textcircled{\scriptsize i}/I} \times \mathbf{H}^{\textcircled{\scriptsize i}}_{\textcircled{\scriptsize i}/I} = \boldsymbol{W}^{\textcircled{\scriptsize i}}_i(O_{\textcircled{\scriptsize i}}). \tag{2.63}$$

The latter can be rearranged to make the acceleration appear in the equations of motion, hence getting

$$M_{\textcircled{\scriptsize i}} \star (\dot{\boldsymbol{\omega}}^{\textcircled{\scriptsize i}}_{\textcircled{\scriptsize i}/I})^S + \boldsymbol{\omega}^{\textcircled{\scriptsize i}}_{\textcircled{\scriptsize i}/I} \times \left(M_{\textcircled{\scriptsize i}} \star (\boldsymbol{\omega}^{\textcircled{\scriptsize i}}_{\textcircled{\scriptsize i}/I})^S\right) = \boldsymbol{W}^{\textcircled{\scriptsize i}}_i(O_{\textcircled{\scriptsize i}}). \tag{2.64}$$

In order to avoid using the swap, we can define an operator $H[\cdot] : \mathbb{R}^{8\times8} \mapsto \mathbb{R}^{8\times8}$ such that

$$H(M) \star \mathbf{a} \triangleq M \star \mathbf{a}^S. \tag{2.65}$$

If for example $H[\cdot]$ operator is applied to a block matrix $M = [M_1, M_2]$, where $M \in \mathbb{R}^{8\times8}$ and $M_1, M_2 \in \mathbb{R}^{8\times4}$, then

$$H(M) = H\left([M_1, M_2]\right) = [M_2, M_1]. \tag{2.66}$$

This applies to $M_{\textcircled{\scriptsize i}}$ leading to

$$H(M_{\textcircled{\scriptsize i}}) = \begin{bmatrix} 0 & 0_{1\times3} & 1 & 0_{1\times3} \\ 0_{3\times1} & 0_{3\times3} & 0_{3\times1} & m_{\textcircled{\scriptsize i}} I_3 \\ 1 & 0_{1\times3} & 0 & 0_{1\times3} \\ 0_{3\times1} & \bar{I}_{\textcircled{\scriptsize i}} & 0_{3\times1} & 0_{3\times3} \end{bmatrix}, \tag{2.67}$$

which can be used to rewrite Eq. (2.61) in a swap-free form:

$$\mathbf{H}^{\bullet_i}_{\bullet_i/I} = \mathrm{H}(\mathrm{M}_{\bullet_i}) \star \boldsymbol{\omega}^{\bullet_i}_{\bullet_i/I}. \tag{2.68}$$

In order to integrate the dynamics we will rely on the inverse of $\mathrm{H}(\mathrm{M}_{\bullet_i})$, which is defined as

$$\mathrm{H}(\mathrm{M}_{\bullet_i})^{-1} = \begin{bmatrix} 0 & 0_{1\times3} & 1 & 0_{1\times3} \\ 0_{3\times1} & 0_{3\times3} & 0_{3\times1} & \bar{\mathrm{I}}^{-1}_{\bullet_i} \\ 1 & 0_{1\times3} & 0 & 0_{1\times3} \\ 0_{3\times1} & \frac{1}{\mathrm{m}_{\bullet_i}}\mathrm{I}_3 & 0_{3\times1} & 0_{3\times3} \end{bmatrix}; \tag{2.69}$$

this can be proved verifying that $\mathrm{H}(\mathrm{M}_{\bullet_i})^{-1}\mathrm{H}(\mathrm{M}_{\bullet_i}) = \mathrm{H}(\mathrm{M}_{\bullet_i})\mathrm{H}(\mathrm{M}_{\bullet_i})^{-1} = \mathrm{I}_8$.

The i^{th} body's kinetic energy can be computed as

$$\mathrm{E}_{\mathrm{k}_i} = \frac{1}{2}(\boldsymbol{\omega}^{\bullet_i}_{\bullet_i/I})^{\mathrm{S}} \circ \left(\mathrm{M}_{\bullet_i} \star (\boldsymbol{\omega}^{\bullet_i}_{\bullet_i/I})^{\mathrm{S}}\right). \tag{2.70}$$

Considering a multibody system made of N rigid bodies whose centers of mass are at $\bullet_i$, Eq. (2.61) can be specialized for such a system yielding to

$$\mathbf{H}^{\mathrm{I}}_{\mathrm{S}}(\mathrm{O}_{\mathrm{I}}) = \sum_{i=1}^{N} \mathbf{q}_{\bullet_i/I}\mathbf{H}^{\bullet_i}_{\bullet_i}(\mathrm{O}_{\bullet_i})\mathbf{q}^{*}_{\bullet_i/I} = \sum_{i=1}^{N} \mathbf{q}_{\bullet_i/I}\left(\mathrm{M}_{\bullet_i} \star (\boldsymbol{\omega}^{\bullet_i}_{\bullet_i/I})^{\mathrm{S}}\right)\mathbf{q}^{*}_{\bullet_i/I}, \tag{2.71}$$

which represents the overall dual momentum for the system, computed about the origin of inertial frame I and expressed in the same frame. We can proceed in a similar fashion to generalize Eq. (2.70) for a multibody system, hence obtaining

$$\mathrm{E}_{\mathrm{k}} = \frac{1}{2}\sum_{i=1}^{N}(\boldsymbol{\omega}^{\bullet_i}_{\bullet_i/I})^{\mathrm{S}} \circ \left(\mathrm{M}_{\bullet_i} \star (\boldsymbol{\omega}^{\bullet_i}_{\bullet_i/I})^{\mathrm{S}}\right); \tag{2.72}$$

note that both Eqs. (2.71) and (2.72) provide constant quantities for

the case under analysis.

2.4.2 Dynamics

The previous sections laid out the concepts and relationships which characterize the dual quaternion description of a generic spacecraft mounted manipulator; the next step of our dissertation is to develop the Newton-Euler equations for the system, in a form which will be suitable for numerical simulation. After developing all the necessary equations, we also suggest a general solution routine which can be easily implemented in any numerical computing environment.

Eq. (2.64) provides the general Newton-Euler equation describing the combined translational-rotational motion of a 6-DOF rigid body; to the aim of our discussion these equations must be specialized to take into account the different nature of the forces acting on each body. We can rearrange Eq. (2.64) and move the nonlinear velocities term to the right-hand side, hence

$$\mathrm{H}(\mathrm{M}_{\mathfrak{B}_i})\dot{\boldsymbol{\omega}}^{\mathfrak{B}_i}_{\mathfrak{B}_i/\mathrm{I}} = -\boldsymbol{\omega}^{\mathfrak{B}_i}_{\mathfrak{B}_i/\mathrm{I}} \times \left(\mathrm{M}_{\mathfrak{B}_i} \star (\boldsymbol{\omega}^{\mathfrak{B}_i}_{\mathfrak{B}_i/\mathrm{I}})^{\mathrm{S}}\right) + \boldsymbol{W}^{\mathfrak{B}_i}_{i}(\mathrm{O}_{\mathfrak{B}_i}), \tag{2.73}$$

where in their turn the wrenches acting on body i are the sum of different contributions,

$$\begin{aligned}\boldsymbol{W}^{\mathfrak{B}_i}_{i}(\mathrm{O}_{\mathfrak{B}_i}) = \boldsymbol{W}^{\mathfrak{B}_i}_{\mathfrak{B}_i}(\mathrm{O}_{\mathfrak{B}_i}) - \sum_{j\in \mathrm{N}[C(:,i)]} \boldsymbol{W}^{\mathfrak{B}_i}_{\mathrm{act},j} + \sum_{j\in \mathrm{P}[C(:,i)]} \boldsymbol{W}^{\mathfrak{B}_i}_{\mathrm{act},j} \\ - \sum_{j\in \mathrm{N}[C(:,i)]} \boldsymbol{W}^{j}_{\mathfrak{B}_{i+1}/\mathfrak{B}_i} + \sum_{j\in \mathrm{P}[C(:,i)]} \boldsymbol{W}^{j}_{\mathfrak{B}_i/\mathfrak{B}_{i-1}}.\end{aligned} \tag{2.74}$$

Wrenches $\boldsymbol{W}^{\mathfrak{B}_i}_{\mathfrak{B}_i}(\mathrm{O}_{\mathfrak{B}_i})$ represent body forces, and may either be caused by a control action ($\boldsymbol{W}^{\mathfrak{B}_i}_{\mathfrak{B}_i,\mathrm{act}}$) or by exogenous phenomena, such as disturbances ($\boldsymbol{W}^{\mathfrak{B}_i}_{\mathfrak{B}_i,\text{non-act}}$); $\boldsymbol{W}^{\mathfrak{B}_i}_{\mathrm{act},j}$ arise from the actuation of the adjacent joints while the last two terms express the effect of reaction wrenches on the dynamics of the body. Note that while the first three terms are known, reaction forces must be computed at each step of the solution process; they are therefore treated as unknowns and

moved to the left-hand side of the Newton-Euler equation, which becomes

$$\begin{aligned} H(M_{\mathfrak{B}_i})\dot{\omega}^{\mathfrak{B}_i}_{\mathfrak{B}_i/I} + \sum_{j\in N[C(:,i)]} W^j_{\mathfrak{B}_{i+1}/\mathfrak{B}_i} - \sum_{j\in P[C(:,i)]} W^j_{\mathfrak{B}_i/\mathfrak{B}_{i-1}} = \\ - \omega^{\mathfrak{B}_i}_{\mathfrak{B}_i/I} \times \left(M_{\mathfrak{B}_i} \star (\omega^{\mathfrak{B}_i}_{\mathfrak{B}_i/I})^S \right) + W^{\mathfrak{B}_i}_{\mathfrak{B}_i}(O_{\mathfrak{B}_i}) + \\ - \sum_{j\in N[C(:,i)]} W^{\mathfrak{B}_i}_{act,j} + \sum_{j\in P[C(:,i)]} W^{\mathfrak{B}_i}_{act,j}. \end{aligned} \tag{2.75}$$

In order to solve for both the velocities and reaction forces we need to deploy another set of equations which relates dual accelerations and the constraints acting at each joint; knowing that every joint dual velocity can be expressed in joint coordinates as the difference between the velocities of its adjoining bodies, we obtain

$$\begin{aligned} \omega^i_{i/\mathfrak{B}_k} = q_{\mathfrak{B}_{i+1}/i}\, \omega^{\mathfrak{B}_{i+1}}_{\mathfrak{B}_{i+1}/I}\, q^*_{\mathfrak{B}_{i+1}/i} - q^*_{i/\mathfrak{B}_k}\, \omega^{\mathfrak{B}_k}_{\mathfrak{B}_k/I}\, q_{i/\mathfrak{B}_k}, \quad k = N[C(i,:)], \\ i = \{1,\dots,J\}. \end{aligned} \tag{2.76}$$

Taking the derivative of Eq. (2.76) yields

$$\begin{aligned} \dot{\omega}^i_{i/\mathfrak{B}_k} = q_{\mathfrak{B}_{i+1}/i}\, \dot{\omega}^{\mathfrak{B}_{i+1}}_{\mathfrak{B}_{i+1}/I}\, q^*_{\mathfrak{B}_{i+1}/i} - q^*_{i/\mathfrak{B}_k}\, \dot{\omega}^{\mathfrak{B}_k}_{\mathfrak{B}_k/I}\, q_{i/\mathfrak{B}_k} + \\ - q^*_{i/\mathfrak{B}_k}(\omega^{\mathfrak{B}_k}_{\mathfrak{B}_k/I} \times \omega^{\mathfrak{B}_k}_{i/\mathfrak{B}_k}) q_{i/\mathfrak{B}_k}. \end{aligned} \tag{2.77}$$

Applying Λ_i (see Table 2.9) to both sides, and recalling that $\Lambda_i \dot{\omega}^i_{i/\mathfrak{B}_k} = \mathbf{0}$ by construction, the set of equations to be added to Eq. (2.75) is

$$\Lambda_i \sum_{j\in P[C(i,:)]} \dot{\omega}^i_{\mathfrak{B}_j/I} - \Lambda_i \sum_{j\in N[C(i,:)]} \dot{\omega}^i_{\mathfrak{B}_j/I} = \Lambda_i(\omega^i_{\mathfrak{B}_k/I} \times \omega^i_{i/\mathfrak{B}_k}). \tag{2.78}$$

This set of equations can be cast in the form

$$\begin{bmatrix} \mathcal{S}_{11} & \mathcal{S}_{12} \\ \mathcal{S}_{21} & \mathcal{S}_{22} \end{bmatrix} \begin{bmatrix} \dot{\mathcal{Y}} \\ \mathcal{T} \end{bmatrix} = \begin{bmatrix} \mathcal{B}_1 \\ \mathcal{B}_2 \end{bmatrix}, \tag{2.79}$$

where $\mathcal{Y}$ and $\mathcal{T}$ were introduced in Eqs. (2.35) and (2.57).

The different blocks in Eq. (2.79) gather the terms of Eqs. (2.75) and (2.78), and are hereby characterized; $\mathcal{S}_{11} \in \mathbb{R}^{8N\times 8N}$ is a block diagonal matrix collecting the dual inertia matrices in the form

$$\mathcal{S}_{11} = \begin{bmatrix} H(M_{\mathfrak{s}_1}) & & & \cdots & 0_{8\times 8} \\ & \ddots & & & \vdots \\ & & H(M_{\mathfrak{s}_i}) & & \\ \vdots & & & \ddots & \\ 0_{8\times 8} & \cdots & & & H(M_{\mathfrak{s}_N}) \end{bmatrix}, \tag{2.80}$$

and its inverse $\mathcal{S}_{11}^{-1}$ can be easily recovered assembling the inverse of each sub-block (see Eq. (2.69)). $\mathcal{S}_{12} \in \mathbb{R}^{8N\times R}$ collects the frame transformations and mapping matrices to couple the reduced reaction wrenches in $\mathcal{T}$ with the rigid body dynamics; it can be built putting together block matrices $(\mathcal{S}_{12})_{ij} \in \mathbb{R}^{8\times r_j}$ as in

$$\mathcal{S}_{12} = \begin{bmatrix} (\mathcal{S}_{12})_{11} & & & \cdots & (\mathcal{S}_{12})_{1J} \\ & \ddots & & & \vdots \\ & & (\mathcal{S}_{12})_{ij} & & \\ \vdots & & & \ddots & \\ (\mathcal{S}_{12})_{N1} & \cdots & & & (\mathcal{S}_{12})_{NJ} \end{bmatrix}, \tag{2.81}$$

where

$$(S_{12})_{ij} = \begin{cases} -[\![\mathbf{q}^*_{\mathfrak{s}_i/j}]\!]_{\mathbf{L}}[\![\mathbf{q}_{\mathfrak{s}_i/j}]\!]_{\mathbf{R}}V_j, & \text{if } c_{ji} = 1, \\ 0_{8\times r_j}, & \text{if } c_{ji} = 0, \\ [\![\mathbf{q}_{j/\mathfrak{s}_i}]\!]_{\mathbf{L}}[\![\mathbf{q}^*_{j/\mathfrak{s}_i}]\!]_{\mathbf{R}}V_j, & \text{if } c_{ji} = -1. \end{cases} \tag{2.82}$$

Sub-block $\mathcal{S}_{21} \in \mathbb{R}^{R\times 8N}$ gathers the terms of Eq. (2.78), hence expressing the null accelerations of the constrained degrees of freedom of

the joints. Block matrices $(\mathcal{S}_{21})_{ij} \in \mathbb{R}^{r_i \times 8}$ are given by

$$(S_{21})_{ij} = \begin{cases} \Lambda_i [\![\mathbf{q}_{\mathfrak{o}_j/i}]\!]_L [\![\mathbf{q}^*_{\mathfrak{o}_j/i}]\!]_R, & \text{if } c_{ij} = 1, \\ 0_{r_i \times 8}, & \text{if } c_{ij} = 0, \\ -\Lambda_i [\![\mathbf{q}^*_{i/\mathfrak{o}_j}]\!]_L [\![\mathbf{q}_{i/\mathfrak{o}_j}]\!]_R, & \text{if } c_{ij} = -1, \end{cases} \tag{2.83}$$

and are located in $\mathcal{S}_{21}$,

$$\mathcal{S}_{21} = \begin{bmatrix} (\mathcal{S}_{21})_{11} & & & \cdots & (\mathcal{S}_{21})_{1N} \\ & \ddots & & & \vdots \\ & & (\mathcal{S}_{21})_{ij} & & \\ \vdots & & & \ddots & \\ (\mathcal{S}_{21})_{J1} & \cdots & & & (\mathcal{S}_{21})_{JN} \end{bmatrix}. \tag{2.84}$$

Sub-matrix $\mathcal{S}_{22} \in \mathbb{R}^{R \times R}$ bonds reaction wrenches and constraint equations, but since no such forces appear in these equations (they express a kinematic relationship, not a dynamic one), $\mathcal{S}_{22}$ is filled with zeros, $\mathcal{S}_{22} = 0_{R \times R}$.

The vectors $\mathcal{B}_1$ and $\mathcal{B}_2$ are the recollection of the right-hand side terms of Eqs. (2.75) and (2.78); these quantities are already known but often need to undergo a pose transformation into the suitable reference system. $\mathcal{B}_1 \in \mathbb{R}^{8N}$ gathers the right-hand side terms of the Newton-Euler equations, i.e. the nonlinear term $\boldsymbol{\omega} \times (M \star (\boldsymbol{\omega})^S)$ and the different loads applied to each body i; it is found stacking sub-vectors $(\mathcal{B}_1)_i \in \mathbb{R}^8$,

$$\mathcal{B}_1 = \left[(\mathcal{B}_1)_1, \cdots, (\mathcal{B}_1)_i, \cdots, (\mathcal{B}_1)_N \right]^T, \tag{2.85}$$

where

$$(\mathcal{B}_1)_i = -\boldsymbol{\omega}^{\mathfrak{o}_i}_{\mathfrak{o}_i/I} \times \left(M_{\mathfrak{o}_i} \star (\boldsymbol{\omega}^{\mathfrak{o}_i}_{\mathfrak{o}_i/I})^S \right) + \boldsymbol{W}^{\mathfrak{o}_i}_{\mathfrak{o}_i}(O_{\mathfrak{o}_i}) +$$

Recall that $\mathbf{W}^{\mathfrak{B}_i}_{\mathfrak{B}_i}$ includes contributions both due to the control input and to exogenous phenomena, so $\mathbf{W}^{\mathfrak{B}_i}_{\mathfrak{B}_i} = \mathbf{W}^{\mathfrak{B}_i}_{\mathfrak{B}_i,act} + \mathbf{W}^{\mathfrak{B}_i}_{\mathfrak{B}_i,non\text{-}act}$

$$- \sum_{j \in N[C(:,i)]} \mathbf{q}_{j/\mathfrak{B}_i} \mathbf{W}^j_{act,j}(O_j) \mathbf{q}^*_{j/\mathfrak{B}_i} + \sum_{j \in P[C(:,i)]} \mathbf{q}^*_{\mathfrak{B}_i/j} \mathbf{W}^j_{act,j}(O_j) \mathbf{q}_{\mathfrak{B}_i/j}. \tag{2.86}$$

Likewise, $\mathcal{B}_2 \in \mathbb{R}^R$ stacks the right-hand side terms of Eq. (2.78); its sub-vectors $(\mathcal{B}_2)_i \in \mathbb{R}^{r_i}$ are given by

$$\begin{aligned}(\mathcal{B}_2)_i &= \Lambda_i \mathbf{q}^*_{i/\mathfrak{B}_k} (\boldsymbol{\omega}^{\mathfrak{B}_k}_{\mathfrak{B}_k/I} \times \boldsymbol{\omega}^{\mathfrak{B}_k}_{i/\mathfrak{B}_k}) \mathbf{q}_{i/\mathfrak{B}_k} \\ &= \Lambda_i \mathbf{q}^*_{i/\mathfrak{B}_k} \boldsymbol{\omega}^{\mathfrak{B}_k}_{\mathfrak{B}_k/I} \mathbf{q}_{i/\mathfrak{B}_k} \times \boldsymbol{\omega}^i_{i/\mathfrak{B}_k}, \quad k = N[C(i,:)],\end{aligned} \tag{2.87}$$

and then collected in

$$\mathcal{B}_2 = \left[(\mathcal{B}_2)_1, \cdots, (\mathcal{B}_2)_i, \cdots, (\mathcal{B}_2)_J \right]^T. \tag{2.88}$$

Note that the terms featured in $(\mathcal{B}_1)_i$ are all expressed in body coordinates $\mathfrak{B}_i$ as they describe the rigid body dynamics, while $(\mathcal{B}_2)_i$ must be expressed in joint frames.

If for example we consider the first body, expanding Eq. (2.79) and exploiting the aforementioned definitions we get the dynamics equations of the satellite base in the form

$$\begin{aligned}\mathrm{H}(\mathrm{M}_{\mathfrak{B}_1}) \star \dot{\boldsymbol{\omega}}^{\mathfrak{B}_1}_{\mathfrak{B}_1/I} + [\![\mathbf{q}_{1/\mathfrak{B}_1}]\!]_L [\![\mathbf{q}^*_{1/\mathfrak{B}_1}]\!]_R V_1 \tilde{\mathbf{W}}^1_{\mathfrak{B}_1/\mathfrak{B}_2} = \\ - \boldsymbol{\omega}^{\mathfrak{B}_1}_{\mathfrak{B}_1/I} \times \left(\mathrm{M}_{\mathfrak{B}_1} \star (\boldsymbol{\omega}^{\mathfrak{B}_1}_{\mathfrak{B}_1/I})^S \right) + \mathbf{W}^{\mathfrak{B}_1}_{\mathfrak{B}_1}(O_{\mathfrak{B}_1}) + \\ - \mathbf{q}_{1/\mathfrak{B}_1} \mathbf{W}^1_{act,1} \mathbf{q}^*_{1/\mathfrak{B}_1}.\end{aligned} \tag{2.89}$$

The same can be done for the set of constraint equations, and considering $i = 1$ (i.e. the joint connecting the manipulator to the base) we get

$$\begin{aligned}\Lambda_1 [\![\mathbf{q}_{\mathfrak{B}_2/1}]\!]_L [\![\mathbf{q}^*_{\mathfrak{B}_2/1}]\!]_R \dot{\boldsymbol{\omega}}^{\mathfrak{B}_2}_{\mathfrak{B}_2/I} - \Lambda_1 [\![\mathbf{q}^*_{1/\mathfrak{B}_1}]\!]_L [\![\mathbf{q}_{1/\mathfrak{B}_1}]\!]_R \dot{\boldsymbol{\omega}}^{\mathfrak{B}_1}_{\mathfrak{B}_1/I} = \\ \Lambda_1 \mathbf{q}^*_{1/\mathfrak{B}_1} \boldsymbol{\omega}^{\mathfrak{B}_1}_{\mathfrak{B}_1/I} \mathbf{q}_{1/\mathfrak{B}_1} \times \boldsymbol{\omega}^1_{1/\mathfrak{B}_1}.\end{aligned} \tag{2.90}$$

The solution of Eq. (2.79) allows to recover both the dual velocity of every rigid body in the system and the reaction wrenches arising

from the joint action between adjoining bodies, evolving as

$$\begin{bmatrix} \dot{\mathcal{Y}} \\ \mathcal{T} \end{bmatrix} = \mathcal{S}^{-1} \begin{bmatrix} \mathcal{B}_1 \\ \mathcal{B}_2 \end{bmatrix}, \tag{2.91}$$

where

$$\mathcal{S} \triangleq \begin{bmatrix} \mathcal{S}_{11} & \mathcal{S}_{12} \\ \mathcal{S}_{21} & \mathcal{S}_{22} \end{bmatrix}. \tag{2.92}$$

Exploiting the easily invertible block-diagonal structure of $\mathcal{S}_{11}$ and the fact that $\mathcal{S}_{22} = 0_{R\times R}$, direct computation of the large matrix $\mathcal{S}^{-1}$ can be recast into a more computationally-friendly procedure. Once defined the Schur complement of $\mathcal{S}_{11}$ as

$$\mathcal{S}/\mathcal{S}_{11} \triangleq -\mathcal{S}_{21}\mathcal{S}_{11}^{-1}\mathcal{S}_{12} \tag{2.93}$$

the inverse of $\mathcal{S}$ becomes

$$\mathcal{S}^{-1} = \begin{bmatrix} \mathcal{S}_{11}^{-1} + \mathcal{S}_{11}^{-1}\mathcal{S}_{12}(\mathcal{S}/\mathcal{S}_{11})^{-1}\mathcal{S}_{21}\mathcal{S}_{11}^{-1} & -\mathcal{S}_{11}^{-1}\mathcal{S}_{12}(\mathcal{S}/\mathcal{S}_{11})^{-1} \\ -(\mathcal{S}/\mathcal{S}_{11})^{-1}\mathcal{S}_{21}\mathcal{S}_{11}^{-1} & (\mathcal{S}/\mathcal{S}_{11})^{-1} \end{bmatrix}; \tag{2.94}$$

note that if the masses and inertias are constant - as it is in our case - $\mathcal{S}_{11}^{-1}$ can be computed offline once and for all at the beginning of the numerical routine. By expansion of Eq. (2.91), the system's solution has the form

$$\begin{aligned} \mathcal{T} &= \left(\mathcal{S}_{21}\mathcal{S}_{11}^{-1}\mathcal{S}_{12}\right)^{-1}\left(\mathcal{S}_{21}\mathcal{S}_{11}^{-1}\mathcal{B}_1 - \mathcal{B}_2\right), \\ \dot{\mathcal{Y}} &= -\mathcal{S}_{11}^{-1}\mathcal{S}_{12}\mathcal{T} + \mathcal{S}_{11}^{-1}\mathcal{B}_1 \\ &= -\mathcal{S}_{11}^{-1}\mathcal{S}_{12}\left(\mathcal{S}_{21}\mathcal{S}_{11}^{-1}\mathcal{S}_{12}\right)^{-1}\left(\mathcal{S}_{21}\mathcal{S}_{11}^{-1}\mathcal{B}_1 - \mathcal{B}_2\right) + \mathcal{S}_{11}^{-1}\mathcal{B}_1. \end{aligned} \tag{2.95}$$

The complete characterization of the system's coupled kinematics and dynamics is therefore allowed by the solution of the system of ODEs described by Eqs. (2.43), (2.58) and (2.95). The system's

evolution can then be rearranged in the form

$$\dot{x} = f(x, u, w), \tag{2.96}$$

where

$$x \triangleq \left[q_{\mathcal{B}_1/I}, \Gamma, \mathcal{Y} \right]^T \in \mathbb{R}^{79} \tag{2.97}$$

is the state vector,

$$u \triangleq \left[\mathcal{W}^{\mathcal{B}_1}_{\mathcal{B}_1,\text{act}}, \mathcal{W}^{1}_{\text{act},1}, \cdots, \mathcal{W}^{J}_{\text{act},J} \right]^T \in \mathbb{R}^{64} \tag{2.98}$$

is the control input and

$$w \triangleq \left[\mathcal{W}^{\mathcal{B}_1}_{\mathcal{B}_1,\text{non-act}}, \cdots, \mathcal{W}^{\mathcal{B}_N}_{\mathcal{B}_N,\text{non-act}} \right]^T \in \mathbb{R}^{64} \tag{2.99}$$

is the vector collecting exogenous inputs.

2.4.3 Computer procedure

The relationships shown in the previous sections can be rearranged in an algorithm-like fashion to build a computer subroutine able to simulate the evolution of the state x, starting from an initial condition x_0; the procedure displayed in Algorithm 1 can be used to solve the coupled kinematics and dynamics for any configuration of a spacecraft mounted manipulator, as long as its physical description is compliant with what already discussed.

Moreover, Algorithm 1 will provide a valuable tool to prove the correctness of our approach; starting from non-null initial conditions we can simulate the system in absence of external forces and disturbances to verify that the overall dual momentum $\mathbf{H}^I_S(O_I)$ is null, while the kinetic energy E_k must remain constant due to the absence of dissipative forces.

Algorithm 1 Kinematics and dynamics of a spacecraft-mounted manipulator (SMM)

Input: $x_0, q_{i/\mathfrak{o}_k}, q_{\mathfrak{o}_{i+1}/i}, r^{\mathfrak{o}_k}_{i/\mathfrak{o}_k}, \boldsymbol{W}^{i}_{\text{act},i}, \boldsymbol{W}^{\mathfrak{o}_i}_{\mathfrak{o}_i}, M_{\mathfrak{o}_i}, \mathcal{S}^{-1}_{11}, C, V_i, \Lambda_i, L_{J_i}, t_f$
Output: $\dot{x}$

function SMMDYNAMICS
  while $t < t_f$ **do**
    Extract $\mathbf{q}_{\mathfrak{o}_1/I}, \Gamma, \mathcal{Y}$ from $\mathbf{x}$
    Compute $\dot{\mathbf{q}}_{\mathfrak{o}_1/I}$ from Eq. (2.43)
    for $i = 1 : J$ **do**
      if $i \in \{R, S\}$ **then** ▷ Select joint type
        Update $q_{i/\mathfrak{o}_k}$ using Γ_{J_i}
      else if $i \in \{P, U\}$ **then**
        Update $r^{\mathfrak{o}_k}_{i/\mathfrak{o}_k}$ using Γ_{J_i}
      else
        Update $q_{i/\mathfrak{o}_k}, r^{\mathfrak{o}_k}_{i/\mathfrak{o}_k}$ using Γ_{J_i}
      Compute $\mathbf{q}_{i/\mathfrak{o}_k}$ using Eq. (2.40)
      Compute $\dot{\Gamma}_{J_i}$ using Eq. (2.58)
    for $i = 1 : N$ **do** ▷ Assemble $\mathcal{S}_{12}$
      for $j = 1 : J$ **do**
        $c_{ji} = C(j, i)$
        Compute $(\mathcal{S}_{12})_{ij}$ using Eq. (2.82)
    for $i = 1 : J$ **do** ▷ Assemble $\mathcal{S}_{21}$
      for $j = 1 : N$ **do**
        $c_{ij} = C(i, j)$
        Compute $(\mathcal{S}_{21})_{ij}$ using Eq. (2.83)
    Compute $\mathcal{S}/\mathcal{S}_{11}$ using Eq. (2.93)
    Compute $(\mathcal{S}/\mathcal{S}_{11})^{-1}$
    for $i = 1 : N$ **do** ▷ Assemble $\mathcal{B}_1$
      Compute $(\mathcal{B}_1)_i$ using Eq. (2.86)
    for $i = 1 : J$ **do** ▷ Assemble $\mathcal{B}_1$
      Compute $(\mathcal{B}_2)_i$ using Eq. (2.87)
    Compute $\mathcal{T}, \dot{\mathcal{Y}}$ using Eq. (2.95)
    Assemble $\dot{x}$ from $\dot{\mathbf{q}}_{\mathfrak{o}_1/I}, \dot{\Gamma}, \dot{\mathcal{Y}}$
    return $\dot{x}$

Chapter 3

Spacecraft-manipulator control

3.1 Introduction

After deriving in a general way the kinematics and dynamics of a spacecraft mounted manipulator, we want to exploit the framework described in Chapter 2 to better understand its potential and deepen our understanding of the system itself. Although the model in Eq. (2.96) is already capable of simulating the system's behaviour when excited by any force/torque described by one of the types listed in the model, we still have to design and/or characterize the system's inputs. A first remark concerning the exogenous inputs presented in Eq. (2.99) has to be made; vector w collects all the forces acting on the system which have an external origin, i.e. are caused by phenomena not accounted by the model itself. Note that any type of environmental force (gravity gradient, atmospheric drag, solar radiation pressure, . . .) will act as an exogenous input to the system and therefore fall within the w vector. Many of these phenomena have been modeled in the past and their effects on space systems are well known; however, none of them has been considered to the purpose of our study, and this choice has a twofold justification. On the one hand, the main orbital perturbations are accurately studied and described by a good deal of the space-related scientific literature, so we can reasonably assume that their action will be successfully

counteracted with ad-hoc choices during the mission design. If we take these for granted when dealing with our study, there is no reason in taking perturbations into account a second time. On the other hand, the space environment has most of the time a non-negligible effect when a long time window is considered; in this case we can witness orbit degradation, changes in the satellite attitude, and a number of other undesired effects. To the aim of our work no such time interval is considered, as we are mostly interested in maneuvers that are likely to be considered short, if compared with a characteristic orbital time.

Besides orbital perturbations, all the other disturbances taking place during a space mission can be considered as exogenous inputs; these can be caused by inaccuracy in the model, noisy measurements and every other phenomenon whose effect cannot be foreseen due to poor knowledge and/or random nature of the phenomenon itself. The best way to counteract this is to exploit modern filtering techniques to blend the available knowledge of the model with the information coming from sensors; the estimation problem, although interesting and essential for the successful outcome of the whole design process, is however out of the scope of this work. In light of these considerations, we choose to neglect exogenous inputs, so $w = 0$; the system will only be excited by the control action, hence $\dot{x} = f(x, u)$.

The design of the control input $\mathbf{u}$ will play a major part in the following of our discussion; our purpose is to lay out some general ideas which will be applicable to any type of SMM model coherent with the one in Chapter 2. This framework can be exploited to perform a number of different tasks involving coordinated control of the base and of its manipulator, but it can also be specialized at the occurrence to focus on a particular aspect of the problem, e.g. to only study the end-effector trajectory tracking or the attitude stabilization of the base. The dual quaternion algebra will prove its value in formulating control laws descending from the well known attitude-only quaternion-based controllers, whose ef-

fect is now broadened to the control of position and attitude of the whole spacecraft-manipulator system; the end-effector control will be performed in the task space, hence resulting in a more intuitive formulation of both the control target and policies.

In order to achieve these results, we will develop control policies with the goal of performing *pose tracking* maneuvers involving both the satellite base and the manipulator; these can be thought of as representative of a large class of possible OOS tasks, such as docking, refueling, inspection, berthing ...

3.1.1 Case study

To the aim of developing the different control strategies, we need to consider a model with a known topology; we will deal with the analysis of a 6R arm attached to a satellite base through a cart which will be modeled as a prismatic (P) joint; our robot is therefore a redundant one, identified by the P6R acronym (Prismatic + 6 Revolute). Recalling the definitions introduced in Sec. 2.3.2, our case study configuration is characterized as in Table 3.1 and Eqs. (3.1) and (3.2).

Parameter	Description	Quantity
B	Branches	1
N	Bodies	8
J	Joints	7
D	DOFs allowed by the joints	7
R	DOFs constrained by the joints	35

Table 3.1: Topology of a P6R spacecraft-mounted manipulator.

The branch termination vector Eq. (2.34) is

$$\mathsf{T} = \begin{bmatrix} 0 & 0 & 0 & 0 & 0 & 0 & 0 & 1 \end{bmatrix}^{\mathsf{T}}, \tag{3.1}$$

while the incidence matrix Eq. (2.33) will be

$$C = \begin{array}{c} \\ \text{Joint } J_1 \\ \text{Joint } J_2 \\ \text{Joint } J_3 \\ \text{Joint } J_4 \\ \text{Joint } J_5 \\ \text{Joint } J_6 \\ \text{Joint } J_7 \end{array} \begin{array}{c} \begin{array}{cccccccc} \textcircled{1} & \textcircled{2} & \textcircled{3} & \textcircled{4} & \textcircled{5} & \textcircled{6} & \textcircled{7} & \textcircled{8} \end{array} \\ \begin{bmatrix} -1 & 1 & 0 & 0 & 0 & 0 & 0 & 0 \\ 0 & -1 & 1 & 0 & 0 & 0 & 0 & 0 \\ 0 & 0 & -1 & 1 & 0 & 0 & 0 & 0 \\ 0 & 0 & 0 & -1 & 1 & 0 & 0 & 0 \\ 0 & 0 & 0 & 0 & -1 & 1 & 0 & 0 \\ 0 & 0 & 0 & 0 & 0 & -1 & 1 & 0 \\ 0 & 0 & 0 & 0 & 0 & 0 & -1 & 1 \end{bmatrix} \end{array}. \tag{3.2}$$

3.2 Overview on feedback linearization

The problem of designing a coordinated controller for a spacecraft-mounted manipulator is a complex one, since there is the necessity to deal with a large set of nonlinear-coupled differential equations which are the mathematical counterpart of a complex physical system. In order to address such complexities the proposed approach relies on the *feedback linearization* theory [52], which features a set of useful tools to reduce a nonlinear system to a fully or partially linearized one. This kind of procedure is not to be confused with the conventional (or Jacobian) linearization, which involves linear approximations of the state dynamics; feedback linearization is instead achieved by exact full or partial state feedback. This means that, when considering a class of nonlinear systems of the form

$$\begin{aligned} \dot{x} &= f(x) + g(x)u \\ y &= h(x), \end{aligned} \tag{3.3}$$

we want to design a state feedback controller evolving as

$$u = \alpha(x) + \beta(x)\mu \tag{3.4}$$

and a change of variables

$$z = T(x) \tag{3.5}$$

which transform Eq. (3.3) in an equivalent linear - or partially linear - system. Note that the map T must be invertible, i.e. the inverse map $T^{-1}(\cdot)$ must exist and be defined such that $x = T^{-1}(z), \forall z \in T(D)$, where D is the domain of T. Moreover, both the map $T(\cdot)$ and its inverse $T^{-1}(\cdot)$ are required to be continuously differentiable in D, thus T is a *diffeomorphism* in D.

The following ideas stem from the *Input/Output* linearization technique, a specific approach to the feedback linearization framework, which encompasses linearization of the input/output map, while the state is only partially linearized. To achieve this, we consider a multi-input multi-output nonlinear system represented by

$$\begin{aligned} \dot{x} &= f(x) + \sum_{i=1}^{m} g_i(x)u_i \\ y_1 &= h_1(x), \ldots, y_m = h_m(x), \end{aligned} \tag{3.6}$$

where $x \in D \subseteq \mathbb{R}^n$ is the state vector, $u = [u_1, \cdots, u_m]^T \in \mathbb{R}^m$ is the input vector and $y = [y_1, \cdots, y_m]^T \in \mathbb{R}^m$ is the output vector. The output can be recursively differentiated with respect to time to make the control input appear in its expression; using Eq. (3.3), this leads to

$$\dot{y} = \frac{\partial h}{\partial x}[f(x) + g(x)u] \triangleq \mathcal{L}_f h(x) + \mathcal{L}_g h(x)u, \tag{3.7}$$

where by definition

$$\mathcal{L}_f h(x) \triangleq \frac{\partial h}{\partial x} f(x) \tag{3.8}$$

is the Lie derivative of h along vector field f. Note that, according to this notation,

$$\mathcal{L}_g \mathcal{L}_f^k h(x) = \frac{\partial (\mathcal{L}_f^k h)}{\partial x} g(x). \tag{3.9}$$

Carrying out the recursive differentiation of $y_i, i = 1, \ldots, m$ in

Eq. (3.6), having defined $y_i^{(k)}$ as the k^{th}-order time derivative of y_i, if $h_i(x)$ satisfies

$$\begin{aligned} &\mathcal{L}_{g_j}\mathcal{L}_f^{k-1}h_i(x) = 0,\ k = 1,\dots,\rho_i - 1,\ j = 1,\dots,m \quad \text{and} \\ &\mathcal{L}_{g_j}\mathcal{L}_f^{\rho_i-1}h_i(x) \neq 0, \end{aligned} \tag{3.10}$$

then u_j does not appear in the expressions of $y_i, \dot{y}_i, \dots, y^{(\rho_i-1)}$ and appears in $y^{(\rho_i)}$ obtained as

$$y^{(\rho_i)} = \mathcal{L}_f^{\rho_i}h_i(x) + \sum_{j=1}^{m} \mathcal{L}_{g_j}\mathcal{L}_f^{\rho_i-1}h_i(x)u_j. \tag{3.11}$$

Using a compact notation for the sake of brevity,

$$y^{(\rho)} = D(x) + E(x)u, \tag{3.12}$$

where

$$y^{(\rho)} = \left[y_1^{(\rho_1)}, \cdots, y_m^{(\rho_m)}\right]^T \in \mathbb{R}^m, \tag{3.13}$$

$$D(x) = \begin{bmatrix} \mathcal{L}_f^{\rho_1}h_1(x) \\ \vdots \\ \mathcal{L}_f^{\rho_m}h_m(x) \end{bmatrix} \in \mathbb{R}^m, \tag{3.14}$$

$$E(x) = \begin{bmatrix} \mathcal{L}_{g_1}\mathcal{L}_f^{\rho_1-1}h_1(x) & \cdots & \mathcal{L}_{g_m}\mathcal{L}_f^{\rho_1-1}h_1(x) \\ \vdots & \ddots & \vdots \\ \mathcal{L}_{g_1}\mathcal{L}_f^{\rho_m-1}h_m(x) & \cdots & \mathcal{L}_{g_m}\mathcal{L}_f^{\rho_m-1}h_m(x) \end{bmatrix} \in \mathbb{R}^{m\times m}. \tag{3.15}$$

If $E(x)$ is non-singular, the feedback control law consists in

$$u = E(x)^{-1}\left(\mu - D(x)\right) = R(x) + Q(x)\mu, \tag{3.16}$$

which substituted in Eq. (3.12) yields the linearized differential input/output map

$$y^{(\rho)} = \mu. \tag{3.17}$$

Eq. (3.17) is equivalent to a chain of ρ integrators, and the integer $\rho = \sum_{i=1}^{m} \rho_i$ is called the *relative degree* of the system.

Theorem 3.1. *We can suppose the system in Eq. (3.6) to have relative degree $\rho \leqslant n$ in D. If $\rho = n$, then for every $x_0 \in D$, a neighborhood N of x_0 exists such that the map*

$$T(x) = \begin{bmatrix} h(x) \\ \mathcal{L}_f h(x) \\ \vdots \\ \mathcal{L}_f^{n-1} h(x) \end{bmatrix} \tag{3.18}$$

restricted to N, is a diffeomorphism on N. If $\rho < n$, a neighborhood N of x_0, $\forall x_0 \in D$, and smooth functions $\eta_1(x), \ldots, \eta_{n-\rho}(x)$ exist such that

$$\frac{\partial \eta_i}{\partial x} g(x) = 0, \quad \forall i \; 1 \leqslant i \leqslant n - \rho, \forall x \in N, \tag{3.19}$$

and the map

$$z = T(x) = \begin{bmatrix} \eta_1(x) \\ \vdots \\ \eta_{n-\rho}(x) \\ \hline h(x) \\ \vdots \\ \mathcal{L}_f^{\rho-1} h(x) \end{bmatrix} = \begin{bmatrix} \eta(x) \\ \hline \xi(x) \end{bmatrix}, \tag{3.20}$$

restricted to N, is a diffeomorphism on N.

Proof. See [52]. □

Note that Eq. (3.19) ensures that the control input u cancels out when we compute

$$\dot{\eta}_i = \frac{\partial \eta_i}{\partial x} \left(f(x) + g(x)u \right). \tag{3.21}$$

The change of variables in Eq. (3.20) and the control input in Eq. (3.16) transform the system of Eq. (3.6) into

$$\begin{aligned} \dot{\eta} &= \vartheta(\eta, \xi) \\ \dot{\xi} &= A\xi + B\mu \\ &\quad A\xi + BQ(x)^{-1}\left(u - R(x)\right) \\ y &= C\xi, \end{aligned} \tag{3.22}$$

where $\eta \in \mathbb{R}^{n-\rho}$ is known as the internal part, $\xi \in \mathbb{R}^{\rho}$ as the external part. Recalling the definition of $y^{(\rho)}$ in Eq. (3.11) and of ξ in Eq. (3.20), it is straightforward to verify that $\xi = [y, \dot{y}, \cdots, y^{(\rho)}]^T$; hence A, B, C represent a chain of integrators in canonical form, as in

$$\begin{aligned} \dot{\xi} &= \underbrace{\begin{bmatrix} 0_{m\times m} & I_{m\times m} & 0_{m\times m} & \cdots & \cdots & 0_{m\times m} \\ 0_{m\times m} & 0_{m\times m} & I_{m\times m} & & & 0_{m\times m} \\ \vdots & & & \ddots & & \vdots \\ 0_{m\times m} & & & & 0_{m\times m} & I_{m\times m} \\ 0_{m\times m} & 0_{m\times m} & 0_{m\times m} & \cdots & 0_{m\times m} & 0_{m\times m} \end{bmatrix}}_{A\in\mathbb{R}^{m\rho\times m\rho}} \xi + \underbrace{\begin{bmatrix} 0_{m\times m} \\ 0_{m\times m} \\ \vdots \\ 0_{m\times m} \\ I_{m\times m} \end{bmatrix}}_{B\in\mathbb{R}^{m\rho\times m}} \mu, \\ y &= \underbrace{\begin{bmatrix} I_{m\times m} & 0_{m\times m} & \cdots & 0_{m\times m} \end{bmatrix}}_{C\in\mathbb{R}^{m\times m\rho}} \xi. \end{aligned} \tag{3.23}$$

Note that the linearizing feedback control makes the internal dynamics $\vartheta(\eta, \xi)$ unobservable from the output; in order to ensure stability of the whole system, it is therefore required that the zero dynamics are stable, so the choice of η must respect the condition $\vartheta(\eta_0, 0) = 0$ [52].

We will now briefly show how the previously outlined theory leads to some meaningful results in terms of both system stabilization and reference tracking; we start by considering a partially feedback linearizable system of the form described in Eq. (3.22),

where

$$z = T(x) = \begin{bmatrix} \eta \\ \xi \end{bmatrix} \tag{3.24}$$

is a diffeomorphism on a domain $D \subset \mathbb{R}^n$, $D_z = T(D)$ contains the origin, A, B is controllable, $\vartheta(0,0) = 0$ and $\vartheta(\eta, \xi)$, $Q(x)^{-1}$, $R(x)$ are continuously differentiable. The state feedback control

$$u = R(x) + Q(x)\mu \tag{3.25}$$

reduces Eq. (3.22) to the form

$$\begin{aligned} \dot{\eta} &= \vartheta(\eta, \xi) \\ \dot{\xi} &= A\xi + B\mu, \end{aligned} \tag{3.26}$$

where the output y has been dropped as it has no role in the system's stabilization. By choosing $\mu = -K\xi$, the system becomes

$$\begin{aligned} \dot{\eta} &= \vartheta(\eta, \xi) \\ \dot{\xi} &= (A - BK)\xi, \end{aligned} \tag{3.27}$$

which reaches asymptotic stability in the origin if $(A-BK)$ is Hurwitz and if the origin of $\dot{\eta} = \vartheta(\eta, 0)$ is asymptotically stable.

Similar ideas [52] can be exploited if we want to track a reference $r(t)$. We define a reference signal vector $\mathcal{R}$ collecting the reference signal $r(t)$ and its derivatives up to the $(\rho - 1)^{\text{th}}$-order,

$$\mathcal{R} = \begin{bmatrix} r \\ \vdots \\ r^{(\rho-1)} \end{bmatrix}. \tag{3.28}$$

Exploiting knowledge of $\mathcal{R}$, we define a change of variables $e = \xi - \mathcal{R}$, which transforms Eq. (3.22) into

$$\begin{aligned} \dot{\eta} &= \vartheta(\eta, e + \mathcal{R}) \\ \dot{e} &= Ae + B\left(Q(x)^{-1}\left(u - R(x)\right) - r^{(\rho)}\right). \end{aligned} \tag{3.29}$$

If a state feedback control in the form

$$u = R(x) + Q(x)\left(\mu + r^{(\rho)}\right) \tag{3.30}$$

is applied to Eq. (3.29), then the system is reduced to

$$\begin{aligned} \dot{\eta} &= \vartheta(\eta, e + \mathcal{R}) \\ \dot{e} &= Ae + B\mu, \end{aligned} \tag{3.31}$$

and therefore tracking capability is ensured under the same conditions expressed for the system in Eq. (3.27).

3.3 Dual quaternion based feedback linearization

Having sorted out some main ideas regarding feedback linearization techniques, we can move to the description of how these concepts can be applied to the problem of controlling the spacecraft-manipulator; we will show how this framework allow us to both stabilize the system and track a reference signal.

3.3.1 Stabilization

First of all, the system model presented in Eq. (2.96) must be rearranged in the form proposed by Eq. (3.3); in order to do that we note that the state evolution can be expressed as

$$\begin{bmatrix} \dot{q}_{\mathfrak{o}_1/I} \\ \dot{\Gamma}_{J_1} \\ \vdots \\ \dot{\Gamma}_{J_J} \\ \dot{y} \end{bmatrix} = \begin{bmatrix} \frac{1}{2} q_{\mathfrak{o}_1/I} \omega^{\mathfrak{o}_1}_{\mathfrak{o}_1/I} \\ L_{J_1} \omega^{1}_{1/\mathfrak{o}_1} \\ \vdots \\ L_{J_J} \omega^{J}_{J/\mathfrak{o}_J} \\ \mathcal{S}_{11}^{-1}(\mathcal{B}_1 - \mathcal{S}_{12}\mathcal{T}) \end{bmatrix}, \tag{3.32}$$

where the control input only appears in the equation of $\dot{y}$, which can be expanded in the form

$$\dot{y} = \mathcal{S}_{11}^{-1}\left(I_{8\times 8} - \mathcal{S}_{12}\left(\mathcal{S}_{21}\mathcal{S}_{11}^{-1}\mathcal{S}_{12}\right)^{-1}\mathcal{S}_{21}\mathcal{S}_{11}^{-1}\right)\mathcal{B}_1 + \mathcal{S}_{11}^{-1}\mathcal{S}_{12}\left(\mathcal{S}_{21}\mathcal{S}_{11}^{-1}\mathcal{S}_{12}\right)^{-1}\mathcal{B}_2. \tag{3.33}$$

We can write $\mathcal{B}_1 = \mathcal{B}_{1,act} + \mathcal{B}_{1,non\text{-}act}$, where $\mathcal{B}_{1,act}$ gathers the actuation terms present in $\mathcal{B}_1$, while $\mathcal{B}_{1,non\text{-}act}$ collects the nonlinear terms. Specifically,

Note that we are assuming $\mathbf{W}^{\mathfrak{B}_i}_{\mathfrak{B}_i,non\text{-}act} = 0$

$$\left(\mathcal{B}_{1,non\text{-}act}\right)_i = -\boldsymbol{\omega}^{\mathfrak{B}_i}_{\mathfrak{B}_i/I} \times \left(M_{\mathfrak{B}_i} \star (\boldsymbol{\omega}^{\mathfrak{B}_i}_{\mathfrak{B}_i/I})^S\right), \quad i = 1, \ldots, N. \tag{3.34}$$

and

$$\begin{aligned}
\left(\mathcal{B}_{1,act}\right)_1 &= \mathbf{W}^{\mathfrak{B}_1}_{\mathfrak{B}_1,act} - \mathbf{q}_{1/\mathfrak{B}_1}\mathbf{W}^1_{act,1}(O_1)\mathbf{q}^*_{1/\mathfrak{B}_1}, \\
\left(\mathcal{B}_{i,act}\right)_i &= \sum_{j\in P[C(:,i)]} \mathbf{q}^*_{\mathfrak{B}_i/j}\mathbf{W}^j_{act,j}(O_j)\mathbf{q}_{\mathfrak{B}_i/j} - \sum_{j\in N[C(:,i)]} \mathbf{q}_{j/\mathfrak{B}_i}\mathbf{W}^j_{act,j}(O_j)\mathbf{q}^*_{j/\mathfrak{B}_i}, \\
& \qquad\qquad i = 2, \ldots, N.
\end{aligned} \tag{3.35}$$

The control input u can be put into evidence by writing $\mathcal{B}_{1,act} = \mathcal{B}_u u$, having defined $\mathcal{B}_u \in \mathbb{R}^{64\times 64}$ as

$$\mathcal{B}_u = \begin{bmatrix}
I_{8\times 8} & -Q(\mathbf{q}^*_{1/\mathfrak{B}_1})_R & 0_{8\times 8} & \cdots & \cdots & 0_{8\times 8} \\
0_{8\times 8} & Q(\mathbf{q}^*_{\mathfrak{B}_2/1})_L & -Q(\mathbf{q}^*_{2/\mathfrak{B}_2})_R & \cdots & \cdots & 0_{8\times 8} \\
\vdots & & & \ddots & & \vdots \\
\vdots & & & & Q(\mathbf{q}^*_{\mathfrak{B}_7/6})_L & -Q(\mathbf{q}^*_{7/\mathfrak{B}_7})_R \\
0_{8\times 8} & \cdots & \cdots & \cdots & 0_{8\times 8} & Q(\mathbf{q}^*_{\mathfrak{B}_8/7})_L
\end{bmatrix}, \tag{3.36}$$

given

$$\begin{aligned}
Q(\mathbf{q}^*_{X/Y})_L &= [\![\mathbf{q}^*_{X/Y}]\!]_L [\![\mathbf{q}_{X/Y}]\!]_R, \\
Q(\mathbf{q}^*_{X/Y})_R &= [\![\mathbf{q}_{X/Y}]\!]_L [\![\mathbf{q}^*_{X/Y}]\!]_R.
\end{aligned} \tag{3.37}$$

Rearranging Eq. (3.33) with this decomposition of $\mathcal{B}_1$ allows to express $\dot{y}$ as

$$\dot{y} = \Phi(x) + \Psi(x)u, \tag{3.38}$$

where $\Phi(x) \in \mathbb{R}^{64}$ is

$$\Phi(x) = \mathcal{S}_{11}^{-1}\left(I_{8\times 8} - \mathcal{S}_{12}\left(\mathcal{S}_{21}\mathcal{S}_{11}^{-1}\mathcal{S}_{12}\right)^{-1}\mathcal{S}_{21}\mathcal{S}_{11}^{-1}\right)\mathcal{B}_{1,\text{non-act}} + \\ + \mathcal{S}_{11}^{-1}\mathcal{S}_{12}\left(\mathcal{S}_{21}\mathcal{S}_{11}^{-1}\mathcal{S}_{12}\right)^{-1}\mathcal{B}_2 \tag{3.39}$$

and $\Psi(x) \in \mathbb{R}^{64\times 64}$ is

$$\Psi(x) = \mathcal{S}_{11}^{-1}\left(I_{8\times 8} - \mathcal{S}_{12}\left(\mathcal{S}_{21}\mathcal{S}_{11}^{-1}\mathcal{S}_{12}\right)^{-1}\mathcal{S}_{21}\mathcal{S}_{11}^{-1}\right)\mathcal{B}_u. \tag{3.40}$$

We can now express the state evolution in a form suitable for feedback linearization, i.e.

$$\underbrace{\begin{bmatrix} \dot{q}_{\mathfrak{o}_1/I} \\ \dot{\Gamma}_{J_1} \\ \vdots \\ \dot{\Gamma}_{J_J} \\ \dot{y} \end{bmatrix}}_{\dot{x}\in\mathbb{R}^{79}} = \underbrace{\begin{bmatrix} \frac{1}{2}q_{\mathfrak{o}_1/I}\omega^{\mathfrak{o}_1}_{\mathfrak{o}_1/I} \\ L_{J_1}\omega^{1}_{1/\mathfrak{o}_1} \\ \vdots \\ L_{J_J}\omega^{J}_{J/\mathfrak{o}_J} \\ \Phi(x) \end{bmatrix}}_{f(x)\in\mathbb{R}^{79}} + \underbrace{\begin{bmatrix} 0_{8\times 64} \\ 0_{1\times 64} \\ \vdots \\ 0_{1\times 64} \\ \Psi(x) \end{bmatrix}}_{g(x)\in\mathbb{R}^{79\times 64}} u. \tag{3.41}$$

The proposed output is now

$$y = \begin{bmatrix} \tilde{\omega}^{\mathfrak{o}_1}_{\mathfrak{o}_1/I} \\ \dot{\Gamma} \end{bmatrix} \in \mathbb{R}^{13}. \tag{3.42}$$

Note that when a vector dual quaternion $q \in \mathbb{H}_d^v$ has a tilde accent as in $\tilde{q}$, this means that the first and fifth row associated with its null components have been removed; recalling the mapping matrices of

Sec. 2.3.4, $\tilde{\mathbf{q}} = E_{15}\mathbf{q}$, so

$$\dot{\tilde{\omega}}^{\mathcal{B}_1}_{\mathcal{B}_1/I} = E_{15}\dot{\omega}^{\mathcal{B}_1}_{\mathcal{B}_1/I}. \tag{3.43}$$

A similar operation can be carried out on the input vector u; we know from Eq. (2.98) that $u \in \mathbb{R}^{64}$, corresponding to an 8x1 dual actuation wrench on the base and on each of the joints. However, all the joint actuation wrenches $\boldsymbol{W}^i_{act,i}$, $i = 1, \ldots, J$ have null entries in correspondence of the locked degrees of freedom (e.g., there is no actuation along a translation-related degree of freedom for a revolute joint). To take this into account, we squeeze u into a reduced form $\tilde{u} \in \mathbb{R}^{13}$ which only collects the nonzero components of u. In detail,

$$u = V_{map,all}\tilde{u}, \tag{3.44}$$

having defined the block-diagonal matrix $V_{map,all} \in \mathbb{R}^{64\times 13}$ as

$$V_{map,all} = \begin{bmatrix} V_{act,base} & 0_{8\times1} & 0_{8\times1} & \cdots & \cdots & 0_{8\times1} \\ 0_{8\times6} & V_{act,prism} & 0_{8\times1} & & & 0_{8\times1} \\ 0_{8\times6} & 0_{8\times1} & V_{act,rev} & & & 0_{8\times1} \\ \vdots & & & \ddots & & \vdots \\ \vdots & & & & V_{act,rev} & 0_{8\times1} \\ 0_{8\times6} & \cdots & \cdots & \cdots & 0_{8\times1} & V_{act,rev} \end{bmatrix}, \tag{3.45}$$

and

$$\begin{aligned} V_{act,base} &= E_{15}^T \in \mathbb{R}^{8\times6}, \\ V_{act,prism} &= E_{1235678}^T \in \mathbb{R}^{8\times1}, \\ V_{act,rev} &= E_{1234567}^T \in \mathbb{R}^{8\times1}. \end{aligned} \tag{3.46}$$

Once the output is defined (Eq. (3.42)) we want to obtain an input/output differential relationship in the form described by Eq. (3.11); in this case this is achieved in a straightforward manner computing the first-order time derivative of y, which already leads to an input-

dependent expression in the form

$$\underbrace{\begin{bmatrix}\dot{\tilde{\omega}}^{\mathfrak{G}_1}_{\mathfrak{G}_1/I}\\ \ddot{\Gamma}\end{bmatrix}}_{\dot{y}} = \underbrace{\begin{bmatrix}\left(\tilde{\Phi}(x)\right)_1\\ \Delta(x)\end{bmatrix}}_{D(x)\in\mathbb{R}^{13}} + \underbrace{\begin{bmatrix}\left(\tilde{\Psi}(x)\right)_1\\ H(x)\end{bmatrix} V_{map,all}}_{E(x)\in\mathbb{R}^{13\times 13}} \tilde{u} \\ = D(x) + E(x)\tilde{u}. \tag{3.47}$$

Note that $(\Phi(x))_i$ and $(\Psi(x))_i$ are the rows of $\Phi(x), \Psi(x)$ associated with the dual acceleration of the i^{th} body, while the following steps have to be made in order to define $D(x), E(x)$. First, we have to put in evidence the dependence of $\ddot{\Gamma}$ on the control input, rearranging Eq. (2.77); using that $\dot{\omega}^{\mathfrak{G}_{i+1}}_{\mathfrak{G}_{i+1}/I} = (\Phi(x))_{i+1} + (\Psi(x))_{i+1}\, u$,

$$\begin{aligned}\dot{\omega}^{i}_{i/\mathfrak{G}_k} &= q_{\mathfrak{G}_{i+1}/i}\left[(\Phi(x))_{i+1} + (\Psi(x))_{i+1}\, u\right] q^*_{\mathfrak{G}_{i+1}/i} - q^*_{i/\mathfrak{G}_k}\Big[(\Phi(x))_k + \\ &\quad + (\Psi(x))_k\, u\Big] q_{i/\mathfrak{G}_k} - q^*_{i/\mathfrak{G}_k}(\omega^{\mathfrak{G}_k}_{\mathfrak{G}_k/I} \times \omega^{\mathfrak{G}_k}_{i/\mathfrak{G}_k}) q_{i/\mathfrak{G}_k} \\ &= Q(q^*_{\mathfrak{G}_{i+1}/i})_R\, (\Phi(x))_{i+1} - Q(q^*_{i/\mathfrak{G}_k})_L \left[(\Phi(x))_k + \omega^{\mathfrak{G}_k}_{\mathfrak{G}_k/I} \times \omega^{\mathfrak{G}_k}_{i/\mathfrak{G}_k}\right] + \\ &\quad + \left[Q(q^*_{\mathfrak{G}_{i+1}/i})_R\, (\Psi(x))_{i+1} - Q(q^*_{i/\mathfrak{G}_k})_L\, (\Psi(x))_k\right] u, \quad k = N[C(i,:)].\end{aligned} \tag{3.48}$$

Hence,

$$\ddot{\Gamma}_{J_i} = \underbrace{L_{J_i}\left\{Q(q^*_{\mathfrak{G}_{i+1}/i})_R\, (\Phi(x))_{i+1} - Q(q^*_{i/\mathfrak{G}_k})_L \left[(\Phi(x))_k + \omega^{\mathfrak{G}_k}_{\mathfrak{G}_k/I} \times \omega^{\mathfrak{G}_k}_{i/\mathfrak{G}_k}\right]\right\}}_{(\Delta(x))_i} + \\ + \underbrace{L_{J_i}\left\{\left[Q(q^*_{\mathfrak{G}_{i+1}/i})_R\, (\Psi(x))_{i+1} - Q(q^*_{i/\mathfrak{G}_k})_L\, (\Psi(x))_k\right]\right\}}_{(H(x))_i\in\mathbb{R}^{1\times 64}} u. \tag{3.49}$$

We can now proceed with the change of variables highlighted in Eq. (3.20); note that the output was differentiated only one time to make the input appear, so $\rho = \sum_{i=1}^{m} \rho^{(i)} = 13$. The unobservable dynamics η are given by $q_{1/\mathfrak{G}_i}$ and Γ, so $n - \rho = 15$. This leads to the

definition of

$$\eta = \begin{bmatrix} q_{1/\mathcal{B}_i} \\ \Gamma \end{bmatrix} \in \mathbb{R}^{15}, \qquad \xi = \begin{bmatrix} \tilde{\omega}^{\mathcal{B}_1}_{\mathcal{B}_1/I} \\ \dot{\Gamma} \end{bmatrix} \in \mathbb{R}^{13}, \tag{3.50}$$

which are stacked in

$$z = \left[\begin{array}{c} \eta \\ \hline \xi \end{array}\right] \in \mathbb{R}^{28}. \tag{3.51}$$

The change of variables is enabled by the diffeomorphism $T(x)$,

$$\underbrace{\left[\begin{array}{c} q_{\mathcal{B}_1/I} \\ \Gamma \\ \hline \tilde{\omega}^{\mathcal{B}_1}_{\mathcal{B}_1/I} \\ \dot{\Gamma} \end{array}\right]}_{z} = \underbrace{\left[\begin{array}{c|ccc} I_{15\times 15} & \multicolumn{3}{c}{0_{15\times 64}} \\ \hline & A_{\mathcal{B}_1} & \cdots & 0 & 0 \\ & \vdots & \ddots & \vdots & \vdots \\ 0_{13\times 15} & 0 & \cdots & A_{62} & 0 \\ & 0 & \cdots & A_{71} & A_{72} \end{array}\right]}_{T(x)} \left[\begin{array}{c} q_{\mathcal{B}_1/I} \\ \Gamma \\ \hline y \end{array}\right], \tag{3.52}$$

where

$$\begin{aligned} A_{\mathcal{B}_1} &= E_{15} \in \mathbb{R}^{6\times 8}, \\ A_{i1} &= -L_{J_i} Q(q^*_{i/\mathcal{B}_k})_L \in \mathbb{R}^{1\times 8}, \qquad i = 1, \dots, J \\ A_{i2} &= L_{J_i} Q(q^*_{\mathcal{B}_{i+1}/i})_R \in \mathbb{R}^{1\times 8}. \end{aligned} \tag{3.53}$$

The evolution of the transformed system recalls Eq. (3.22), where in this case the internal dynamics $\dot{\eta} = \vartheta(\eta, \xi)$ are specified by

$$\begin{bmatrix} \dot{q}_{\mathcal{B}_1/I} \\ \dot{\Gamma}_{J_1} \\ \vdots \\ \dot{\Gamma}_{J_J} \end{bmatrix} = \begin{bmatrix} \frac{1}{2} q_{\mathcal{B}_1/I} \omega^{\mathcal{B}_1}_{\mathcal{B}_1/I} \\ L_{J_1} \omega^1_{1/\mathcal{B}_1} \\ \vdots \\ L_{J_J} \omega^J_{J/\mathcal{B}_J} \end{bmatrix}, \tag{3.54}$$

which fulfill the stability condition $\vartheta(\eta_0, 0) = 0$, hence allowing stabilization of the entire system. The dynamics of the external part ξ

evolve as

$$\dot{\xi} = D(x) + E(x)\tilde{u}. \tag{3.55}$$

If we choose the control $\tilde{u}$ as

$$\tilde{u} = E(x)^{-1}\left(\mu - D(x)\right), \tag{3.56}$$

Eq. (3.55), which describes the linearizable part of the system, becomes

$$\dot{\xi} = \mu, \tag{3.57}$$

which is feedback stabilized by an appropriate choice of μ, e.g., $\mu = -K\xi$, with K positive definite.

3.3.2 Reference tracking

Exploiting the relationships in Sec. 3.3.1, it is also possible to rearrange the equations such that a different task is achieved by the control, namely the tracking of a reference signal $r(t)$ whose derivatives up to the ρ order are available on-line. Once more, the key idea is the one of exploiting a change of variables $\xi \mapsto e$, where $e = \xi - \mathcal{R}$.

Assume we want to perform simultaneous velocity control of both the base and end-effector of the manipulator; we may want to choose an output as

$$y = \begin{bmatrix} \tilde{\omega}^{\mathcal{F}_1}_{\mathcal{F}_1/I} \\ \tilde{\omega}^{\mathcal{F}_8}_{\mathcal{F}_8/I} \end{bmatrix} \in \mathbb{R}^{12}, \tag{3.58}$$

while the known reference signal would be

$$\mathcal{R} = \begin{bmatrix} \tilde{\omega}^{\mathcal{F}_1}_{S/I} \\ \tilde{\omega}^{\mathcal{F}_8}_{E/I} \end{bmatrix} \in \mathbb{R}^{12}. \tag{3.59}$$

In order to make the control input u appear, y only needs to be

differentiated once, hence getting

$$\underbrace{\begin{bmatrix}\dot{\tilde{\omega}}^{\mathcal{B}_1}_{\mathcal{B}_1/I}\\ \dot{\tilde{\omega}}^{\mathcal{B}_8}_{\mathcal{B}_8/I}\end{bmatrix}}_{\dot{y}} = \underbrace{\begin{bmatrix}\left(\tilde{\Phi}(x)\right)_1\\ \left(\tilde{\Phi}(x)\right)_8\end{bmatrix}}_{D(x)\in\mathbb{R}^{12}} + \underbrace{\begin{bmatrix}\left(\tilde{\Psi}(x)\right)_1\\ \left(\tilde{\Psi}(x)\right)_8\end{bmatrix} V_{map,all}}_{E(x)\in\mathbb{R}^{12\times 13}} \tilde{u}. \tag{3.60}$$

In this case matrix $E(x)$ is rectangular because of the redundant nature of the problem - note that we are trying to control the 12 independent nonzero entries of $\tilde{\omega}^{\mathcal{B}_1}_{\mathcal{B}_1/I}, \tilde{\omega}^{\mathcal{B}_8}_{\mathcal{B}_8/I}$ having 13 control inputs. The problem can however be successfully addressed if $E(x)$ has full column rank, and therefore a pseudoinverse $E(x)^+ \in \mathbb{R}^{13\times 12}$ exists such that $E^+E = I_{13\times 13}$.

By definition of ξ, once more it is straightforward to verify that $\xi = y$, and the diffeomorphism $T(x) : x \mapsto z$ is described by

$$\underbrace{\left[\begin{array}{c} q_{\mathcal{B}_1/I}\\ \Gamma\\ \hline \tilde{\omega}^{\mathcal{B}_1}_{\mathcal{B}_1/I}\\ \tilde{\omega}^{\mathcal{B}_8}_{\mathcal{B}_8/I}\end{array}\right]}_{z\in\mathbb{R}^{27}} = \underbrace{\left[\begin{array}{c|cc} I_{15\times 15} & 0_{15\times 64} & \\ \hline 0_{12\times 15} & A_{11} & 0_{6\times 56}\\ & 0_{6\times 56} & A_{81}\end{array}\right]\left[\begin{array}{c} q_{\mathcal{B}_1/I}\\ \Gamma\\ \hline y\end{array}\right]}_{T(x)}, \tag{3.61}$$

where

$$A_{11} = A_{81} = E_{15} \in \mathbb{R}^{6\times 8}. \tag{3.62}$$

Note that the velocities $\omega^{\mathcal{B}_i}_{\mathcal{B}_i/I}, i = 2,\dots,N-1$ are considered observable due to Eq. (2.53); if the Jacobian $\boldsymbol{J}(\mathbf{q},\zeta)$ is invertible, then a relationship in the form $\omega^{\mathcal{B}_i}_{\mathcal{B}_i/I} = \mathcal{F}\left(\omega^{\mathcal{B}_1}_{\mathcal{B}_1/I}, \omega^{\mathcal{B}_8}_{\mathcal{B}_8/I}\right)$ exists and is unique.

In order to obtain the error dynamics $\dot{e} = \dot{\xi} - \dot{\mathcal{R}}$, we first differentiate ξ, and from Eq. (3.60)

$$\dot{\xi} = D(x) + E(x)\tilde{u}. \tag{3.63}$$

By assumption $\dot{\mathcal{R}}$ is known, hence

$$\begin{aligned}\dot{e} &= D(x) + E(x)\tilde{u} - \dot{\mathcal{R}} \\ &= \underbrace{D(x) - \dot{\mathcal{R}}}_{\Xi \in \mathbb{R}^{12}} + E(x)\tilde{u}.\end{aligned} \tag{3.64}$$

If

$$\tilde{u} = E(x)^{+} \left(\mu - \Xi(x)\right), \tag{3.65}$$

then again

$$\dot{e} = \mu, \tag{3.66}$$

and upon fulfillment of the previous considerations on the design of μ, the error is driven towards zero, i.e. the transformed state is able to track the reference $\mathcal{R}$.

3.4 Derivation of nominal control laws

The ideas developed up to now prove that, by exploitation of a general kinematic/dynamic framework based on the dual quaternion formalism, whose equations have been rearranged in a form suitable for feedback linearization, it is possible to design a control strategy in which the control input u is obtained upon definition of a much simpler linearized control input μ, which in its turn is in charge of leading the linearized dynamics to zero.

We now want to narrow our analysis to the design of some specific control laws for the spacecraft-manipulator system characterized by the topology in Sec. 3.1; as anticipated in Chapter 1, this choice is motivated by the configuration of the UR10e manipulator of the *Dynamics and Control System Laboratory* (DCSL), a testbed whose purpose is to help the researchers understand and design the interactions between a manipulator and a spaceborne platform, be it a service satellite, a bigger structure like the ISS, etc. The presence of another experimental facility (see [53]) aimed at reproducing a 5DOFs free floating base and its maneuvers (mainly autonomous

rendez-vous and docking operations), further motivates the modeling and design choices carried out in the following.

In order to faithfully describe the facility we need to point out some aspects of the modeling phase which will impact the control design strategy; first of all, as the UR10e is clearly not floating but is constrained to the wall through a prismatic joint, we modeled the wall as a free-floating base whose mass is much larger than the one of the manipulator itself. In this way we both conserve the structure of the equations in Chapter 2, which describe the base as free-floating, and successfully describe the physics of the experimental platform of interest. Moreover, in order to retain the general analysis carried out in the previous sections, we draw a parallel between the problem of controlling the position of the prismatic joint and the case in which all the 6DOFs of the base have to be controlled; even if we are interested in dealing only with the translational movement of the P joint, the equations could be effortlessly expanded to cover the multi-dimensional case in which the spatial movement of a rigid body has to be controlled.

We want in this way to both build an accurate simulation environment coherent with the experimental platform of the DCSL, and to provide some useful insights for anyone interested in using the proposed approach in the study of a real space system.

3.4.1 Arm stabilization

In a number of different cases during the operational life of a spacecraft-mounted manipulator, the robot arm may need to maintain a certain configuration described by Γ_d, even if subjected to forces/torques which act as disturbances; this problem can be referred to as a stabilization one, and can be tackled using the ideas explained in Sec. 3.3.1. Using the model in Sec. 3.1.1 we will consider the stabilization of the 6 revolute joints of an UR10e manipulator.

If we choose the output of the system to describe the angular

rates of the joints, we obtain

$$y = \dot{\Gamma} \in \mathbb{R}^6. \tag{3.67}$$

By taking the derivative of y, we make the control input appear exploiting the relation in Eq. (3.49), where in this case we drop the prismatic joint, hence

$$\ddot{\Gamma}_{J_i} = (\Delta(x))_i + (H(x))_i u, \ i = 2, \dots, J. \tag{3.68}$$

Performing the change of variables introduced in Eq. (3.20), the new system becomes

$$\underbrace{\left[\begin{array}{c} q_{\mathfrak{o}_1/I} \\ \hline \Gamma \\ \hline \dot{\Gamma} \end{array}\right]}_{z} = \underbrace{\left[\begin{array}{c|cccc} I_{15\times 15} & 0_{15\times 64} & & & \\ \hline & 0 & A_{21} & A_{22} & \cdots & 0 \\ & 0 & 0 & A_{31} & \cdots & 0 \\ 0_{6\times 15} & \vdots & \vdots & \vdots & \ddots & \vdots \\ & 0 & 0 & 0 & \cdots & A_{72} \end{array}\right]}_{T(x)} \left[\begin{array}{c} q_{\mathfrak{o}_1/I} \\ \hline \Gamma \\ \hline y \end{array}\right], \tag{3.69}$$

where again

$$\begin{aligned} A_{i1} &= -L_{J_i} Q(q^*_{i/\mathfrak{o}_k})_L \in \mathbb{R}^{1\times 8}, \\ A_{i2} &= L_{J_i} Q(q^*_{\mathfrak{o}_{i+1}/i})_R \in \mathbb{R}^{1\times 8}, \qquad i = 2, \dots, J. \end{aligned} \tag{3.70}$$

According to the feedback linearization procedure, for this specific case $\xi = y$, hence the dynamics of the transformed state will be described by

$$\dot{\xi} = \underbrace{\Delta(x)}_{D(x)} + \underbrace{H(x)V_{map,arm}}_{E(x)} \tilde{u}, \tag{3.71}$$

$$V_{map,arm} = \begin{bmatrix} 0_{8\times1} & 0_{8\times1} & \cdots & \cdots & 0_{8\times1} \\ 0_{8\times1} & 0_{8\times1} & & & 0_{8\times1} \\ V_{act,rev} & 0_{8\times1} & & & 0_{8\times1} \\ \vdots & & \ddots & & \vdots \\ 0_{8\times1} & & & V_{act,rev} & 0_{8\times1} \\ 0_{8\times1} & 0_{8\times1} & \cdots & 0_{8\times1} & V_{act,rev} \end{bmatrix}, \tag{3.72}$$

where $V_{act,rev}$ is defined by Eq. (3.46). Eq. (3.71) is then feedback linearized by

$$\tilde{u} = E(x)^{-1}\left(\mu - D(x)\right) \tag{3.73}$$

which yields

$$\dot{\xi} = \mu. \tag{3.74}$$

In order to design μ we advocate the use of a candidate Lyapunov function defined as

$$V = \frac{1}{2}\left(\Gamma - \Gamma_d\right)^T K_p \left(\Gamma - \Gamma_d\right) + \frac{1}{2}\dot{\Gamma}^T K_v \dot{\Gamma}, \tag{3.75}$$

for the equilibrium points $\dot{\Gamma} = 0$, $\Gamma = \Gamma_d$. Note that the proposed function is a valid one as

$$V\left(\Gamma = \Gamma_d, \dot{\Gamma} = 0\right) = 0, \tag{3.76}$$

and

$$V\left(\Gamma, \dot{\Gamma}\right) > 0,\ \forall \left(\Gamma, \dot{\Gamma}\right) \in \mathbb{R}^6 \setminus \{\Gamma_d, 0\}. \tag{3.77}$$

In order to asymptotically stabilize the system of Eq. (3.74) at the desired equilibrium points, following the Lyapunov stability criterion in [54], we want to compute μ so that

$$\dot{V} = -\dot{\Gamma}^T K_s \dot{\Gamma}. \tag{3.78}$$

Differentiating Eq. (3.75) we obtain

$$\dot{V} = \dot{\Gamma}^T K_p \left(\Gamma - \Gamma_d\right) + \dot{\Gamma}^T K_v \ddot{\Gamma}; \tag{3.79}$$

recalling that $\ddot{\Gamma} = \mu$, equating Eq. (3.78) and Eq. (3.79),

$$K_\nu \mu + K_p \left(\Gamma - \Gamma_d\right) = -K_s \dot{\Gamma}, \tag{3.80}$$

from which

$$\mu = K_\nu^{-1} \left(-K_s \dot{\Gamma} - K_p \left(\Gamma - \Gamma_d\right)\right). \tag{3.81}$$

Substituting μ into Eq. (3.73) the actual control input vector $\tilde{u}$ can be recovered as

$$\tilde{u} = E(x)^{-1} \left(K_\nu^{-1} \left(-K_s \dot{\Gamma} - K_p \left(\Gamma - \Gamma_d\right)\right) - D(x)\right). \tag{3.82}$$

3.4.2 Simultaneous base/end-effector pose tracking

After dealing with the problem of driving the joint coordinates and rates to a desired stationary condition, we now suggest a possible strategy to simultaneously control the linear position and velocity of the base, along with the dual pose and velocity of the end-effector; our aim is to track a time-variant reference, with the purpose of simulating a coordinate maneuver accomplished by both the base and end-effector of the spacecraft-manipulator system.

With reference to the system described in Sec. 3.1, the notation will address the second body (the child body with respect to the prismatic joint) as equivalent to a new base, so $\mathcal{B}_B = \mathcal{B}_2$. The reference pose, velocity and acceleration of the base will be marked with a S subscript/superscript and will be expressed in the inertial I frame, hence

$$\begin{aligned}
q_{S/I} &= q_{S/I} + \epsilon \frac{1}{2} r^I_{S/I} q_{S/I}, \\
\omega^I_{S/I} &= \omega^I_{S/I} + \epsilon(v^I_{S/I} + r^I_{S/I} \times \omega^I_{S/I}), \\
\dot{\omega}^I_{S/I} &= \dot{\omega}^I_{S/I} + \epsilon(\dot{v}^I_{S/I} - \dot{\omega}^I_{S/I} \times r^I_{S/I} - \omega^I_{S/I} \times v^I_{S/I}).
\end{aligned} \tag{3.83}$$

In a similar fashion, the reference for the end effector will be denoted

by E,

$$\begin{aligned}
q_{E/I} &= q_{E/I} + \epsilon\frac{1}{2}r^I_{E/I}q_{E/I},\\
\omega^I_{E/I} &= \omega^I_{E/I} + \epsilon(v^I_{E/I} + r^I_{E/I} \times \omega^I_{E/I}),\\
\dot{\omega}^I_{E/I} &= \dot{\omega}^I_{E/I} + \epsilon(\dot{v}^I_{E/I} - \dot{\omega}^I_{E/I} \times r^I_{E/I} - \omega^I_{E/I} \times v^I_{E/I}).
\end{aligned} \tag{3.84}$$

Note that the trajectory generator is in charge of providing $q_{S/I}$, $r^I_{S/I}$, $\omega^I_{S/I}$, $v^I_{S/I}$, $q_{E/I}$, $r^I_{E/I}$, $\omega^I_{E/I}$, $v^I_{E/I}$ at every time step, and these quantities in their turn will be transformed into dual quaternions by the model. Once the reference condition is available, in order to compute the error we want to express all the quantities in the correspondent body axes, so the necessary pose transformations are carried out,

$$\begin{aligned}
\omega^{\mathfrak{o}_B}_{S/I} &= q^*_{\mathfrak{o}_B/I}\omega^I_{S/I}q_{\mathfrak{o}_B/I},\\
\dot{\omega}^{\mathfrak{o}_B}_{S/I} &= q^*_{\mathfrak{o}_B/I}\dot{\omega}^I_{S/I}q_{\mathfrak{o}_B/I},\\
\omega^{\mathfrak{o}_8}_{E/I} &= q^*_{\mathfrak{o}_8/I}\omega^I_{E/I}q_{\mathfrak{o}_8/I},\\
\dot{\omega}^{\mathfrak{o}_8}_{E/I} &= q^*_{\mathfrak{o}_8/I}\dot{\omega}^I_{E/I}q_{\mathfrak{o}_8/I}.
\end{aligned} \tag{3.85}$$

The relative pose errors are then retrieved, according to the relations

$$\begin{aligned}
q_{\mathfrak{o}_B/S} &= q^*_{S/I}q_{\mathfrak{o}_B/I},\\
q_{\mathfrak{o}_8/E} &= q^*_{E/I}q_{\mathfrak{o}_8/I};
\end{aligned} \tag{3.86}$$

note that a null error state is represented by unit dual quaternion errors, $q_{\mathfrak{o}_B/S} = \mathbf{1}$ and $q_{\mathfrak{o}_8/E} = \mathbf{1}$. The evolution of the relative error kinematics is obtained with

$$\begin{aligned}
\dot{q}_{\mathfrak{o}_B/S} &= \frac{1}{2}q_{\mathfrak{o}_B/S}\omega^{\mathfrak{o}_B}_{\mathfrak{o}_B/S},\\
\dot{q}_{\mathfrak{o}_8/E} &= \frac{1}{2}q_{\mathfrak{o}_8/E}\omega^{\mathfrak{o}_8}_{\mathfrak{o}_8/E},
\end{aligned} \tag{3.87}$$

where

$$\begin{aligned} \boldsymbol{\omega}^{\mathfrak{o}_B}_{\mathfrak{o}_B/S} &= \boldsymbol{\omega}^{\mathfrak{o}_B}_{\mathfrak{o}_B/I} - \boldsymbol{\omega}^{\mathfrak{o}_B}_{\mathfrak{o}_S/I}, \\ \boldsymbol{\omega}^{\mathfrak{o}_8}_{\mathfrak{o}_8/E} &= \boldsymbol{\omega}^{\mathfrak{o}_8}_{\mathfrak{o}_8/I} - \boldsymbol{\omega}^{\mathfrak{o}_8}_{\mathfrak{o}_E/I}, \end{aligned} \tag{3.88}$$

and, when the relative velocity error is null, $\boldsymbol{\omega}^{\mathfrak{o}_B}_{\mathfrak{o}_B/S} = \boldsymbol{\omega}^{\mathfrak{o}_8}_{\mathfrak{o}_8/E} = \boldsymbol{0}$. The relative dual accelerations between the bodies and their reference value can be accordingly stated as

$$\begin{aligned} \dot{\boldsymbol{\omega}}^{\mathfrak{o}_B}_{\mathfrak{o}_B/S} &= \dot{\boldsymbol{\omega}}^{\mathfrak{o}_B}_{\mathfrak{o}_B/I} - \dot{\boldsymbol{\omega}}^{\mathfrak{o}_B}_{\mathfrak{o}_S/I}, \\ \dot{\boldsymbol{\omega}}^{\mathfrak{o}_8}_{\mathfrak{o}_8/E} &= \dot{\boldsymbol{\omega}}^{\mathfrak{o}_8}_{\mathfrak{o}_8/I} - \dot{\boldsymbol{\omega}}^{\mathfrak{o}_8}_{\mathfrak{o}_E/I}. \end{aligned} \tag{3.89}$$

Once all these quantities are defined, as introduced in Eqs. (3.58) and (3.59), we build

$$y = \begin{bmatrix} \tilde{\boldsymbol{\omega}}^{\mathfrak{o}_B}_{\mathfrak{o}_B/I} \\ \tilde{\boldsymbol{\omega}}^{\mathfrak{o}_8}_{\mathfrak{o}_8/I} \end{bmatrix} \text{ and } \mathcal{R} = \begin{bmatrix} \tilde{\boldsymbol{\omega}}^{\mathfrak{o}_B}_{S/I} \\ \tilde{\boldsymbol{\omega}}^{\mathfrak{o}_8}_{E/I} \end{bmatrix}, \tag{3.90}$$

so the error becomes

$$e = \begin{bmatrix} \tilde{\boldsymbol{\omega}}^{\mathfrak{o}_B}_{\mathfrak{o}_B/S} \\ \tilde{\boldsymbol{\omega}}^{\mathfrak{o}_8}_{\mathfrak{o}_8/E} \end{bmatrix}. \tag{3.91}$$

The following steps closely mimic the procedure outlined from Eq. (3.60) to Eq. (3.65); once more, after feedback linearizing we get a linear differential relation between the evolution of the error and the linearized control input vector, $\dot{e} = \mu$. The problem lies now in the design of μ such that the state is driven towards the desired condition, not only in terms of dual velocities but also in terms of dual poses.

Since the desired condition corresponds to $\mathbf{q}_{\mathfrak{o}_B/S}, \mathbf{q}_{\mathfrak{o}_8/E} \to \boldsymbol{1}$, $\boldsymbol{\omega}^{\mathfrak{o}_B}_{\mathfrak{o}_B/S}, \boldsymbol{\omega}^{\mathfrak{o}_8}_{\mathfrak{o}_8/E} \to \boldsymbol{0}$, we consider a candidate control Lyapunov function (CLF) for equilibrium points $\mathbf{q}_{\mathfrak{o}_B/S} = \boldsymbol{1}$, $\mathbf{q}_{\mathfrak{o}_8/E} = \boldsymbol{1}$, $\boldsymbol{\omega}^{\mathfrak{o}_B}_{\mathfrak{o}_B/S} = \boldsymbol{0}$, $\boldsymbol{\omega}^{\mathfrak{o}_8}_{\mathfrak{o}_8/E} = \boldsymbol{0}$,

$$V\left(\mathbf{q}_{\mathbf{o}_B/S}, \boldsymbol{\omega}^{\mathbf{o}_B}_{\mathbf{o}_B/S}, \mathbf{q}_{\mathbf{o}_8/E}, \boldsymbol{\omega}^{\mathbf{o}_8}_{\mathbf{o}_8/E}\right) = \frac{1}{2}(\boldsymbol{\omega}^{\mathbf{o}_B}_{\mathbf{o}_B/S})^S \circ \left(K_{\mathbf{o}_B} \star (\boldsymbol{\omega}^{\mathbf{o}_B}_{\mathbf{o}_B/S})^S\right) + \\ + p_{\mathbf{o}_B}(\mathbf{q}_{\mathbf{o}_B/S} - \mathbf{1}) \circ (\mathbf{q}_{\mathbf{o}_B/S} - \mathbf{1}) + \frac{1}{2}(\boldsymbol{\omega}^{\mathbf{o}_8}_{\mathbf{o}_8/E})^S \circ \left(K_{\mathbf{o}_8} \star (\boldsymbol{\omega}^{\mathbf{o}_8}_{\mathbf{o}_8/E})^S\right) + \\ + p_{\mathbf{o}_8}(\mathbf{q}_{\mathbf{o}_8/E} - \mathbf{1}) \circ (\mathbf{q}_{\mathbf{o}_8/E} - \mathbf{1}), \quad (3.92)$$

where $p_{\mathbf{o}_B}, p_{\mathbf{o}_8} > 0$ are tunable scalar gains and $K_{\mathbf{o}_B}, K_{\mathbf{o}_8} \in \mathbb{R}^{8\times 8}$ are diagonal gain matrices. Note that V is a valid control Lyapunov function as

$$V\left(\mathbf{q}_{\mathbf{o}_B/S} = \mathbf{1}, \boldsymbol{\omega}^{\mathbf{o}_B}_{\mathbf{o}_B/S} = \mathbf{0}, \mathbf{q}_{\mathbf{o}_8/E} = \mathbf{1}, \boldsymbol{\omega}^{\mathbf{o}_8}_{\mathbf{o}_8/E}\mathbf{0}\right) = 0, \quad (3.93)$$

and

$$V\left(\mathbf{q}_{\mathbf{o}_B/S}, \boldsymbol{\omega}^{\mathbf{o}_B}_{\mathbf{o}_B/S}, \mathbf{q}_{\mathbf{o}_8/E}, \boldsymbol{\omega}^{\mathbf{o}_8}_{\mathbf{o}_8/E}\right) > 0, \\ \forall (\mathbf{q}_{\mathbf{o}_B/S}, \boldsymbol{\omega}^{\mathbf{o}_B}_{\mathbf{o}_B/S}, \mathbf{q}_{\mathbf{o}_8/E}, \boldsymbol{\omega}^{\mathbf{o}_8}_{\mathbf{o}_8/E}) \in \mathbb{H}^u_d \times \mathbb{H}^v_d \times \mathbb{H}^u_d \times \mathbb{H}^v_d \setminus \{\mathbf{1}, \mathbf{0}, \mathbf{1}, \mathbf{0}\}. \quad (3.94)$$

In order to stabilize the system at the desired equilibrium point, according to the Lyapunov stability criterion we want to impose a negative value of $\dot{V}$; taking the time derivative of V,

$$\dot{V} = (\boldsymbol{\omega}^{\mathbf{o}_B}_{\mathbf{o}_B/S})^S \circ \left(K_{\mathbf{o}_B} \star (\dot{\boldsymbol{\omega}}^{\mathbf{o}_B}_{\mathbf{o}_B/S})^S\right) + 2p_{\mathbf{o}_B}(\mathbf{q}_{\mathbf{o}_B/S} - \mathbf{1}) \circ \dot{\mathbf{q}}_{\mathbf{o}_B/S} + \\ + (\boldsymbol{\omega}^{\mathbf{o}_8}_{\mathbf{o}_8/E})^S \circ \left(K_{\mathbf{o}_8} \star (\dot{\boldsymbol{\omega}}^{\mathbf{o}_8}_{\mathbf{o}_8/E})^S\right) + 2p_{\mathbf{o}_8}(\mathbf{q}_{\mathbf{o}_8/E} - \mathbf{1}) \circ \dot{\mathbf{q}}_{\mathbf{o}_8/E}, \quad (3.95)$$

and recalling that if $\mathbf{a}, \mathbf{b}, \mathbf{c} \in \mathbb{H}_d$ [23]

$$\mathbf{a} \circ (\mathbf{b}\mathbf{c}) = (\mathbf{b})^S \circ ((\mathbf{a})^S \mathbf{c}^*) = (\mathbf{c})^S \circ (\mathbf{b}^*(\mathbf{a})^S), \quad (3.96)$$

Eq. (3.95) can be expressed as

$$\dot{V} = (\boldsymbol{\omega}^{\mathbf{o}_B}_{\mathbf{o}_B/S})^S \circ \left(K_{\mathbf{o}_B} \star (\dot{\boldsymbol{\omega}}^{\mathbf{o}_B}_{\mathbf{o}_B/I} - \dot{\boldsymbol{\omega}}^{\mathbf{o}_B}_{\mathbf{o}_S/I})^S + p_{\mathbf{o}_B} \mathbf{q}^*_{\mathbf{o}_B/S}(\mathbf{q}_{\mathbf{o}_B/S} - \mathbf{1})^S\right) + \\ + (\boldsymbol{\omega}^{\mathbf{o}_8}_{\mathbf{o}_8/E})^S \circ \left(K_{\mathbf{o}_8} \star (\dot{\boldsymbol{\omega}}^{\mathbf{o}_8}_{\mathbf{o}_8/I} - \dot{\boldsymbol{\omega}}^{\mathbf{o}_8}_{\mathbf{o}_E/I})^S + p_{\mathbf{o}_8} \mathbf{q}^*_{\mathbf{o}_8/E}(\mathbf{q}_{\mathbf{o}_8/E} - \mathbf{1})^S\right). \quad (3.97)$$

By imposing that

$$\dot{V} = -k_{\mathbb{B}}(\omega^{\mathbb{B}}_{\mathbb{B}/S})^S \circ (\omega^{\mathbb{B}}_{\mathbb{B}/S})^S - k_{\mathbb{S}}(\omega^{\mathbb{S}}_{\mathbb{S}/E})^S \circ (\omega^{\mathbb{S}}_{\mathbb{S}/E})^S, \tag{3.98}$$

if we equate the right hand sides of Eqs. (3.97) and (3.98), by rearranging the circle products and swapping every term of the equality we get

$$\begin{bmatrix} \omega^{\mathbb{B}}_{\mathbb{B}/S} \\ \omega^{\mathbb{S}}_{\mathbb{S}/E} \end{bmatrix} \circ \begin{bmatrix} p_{\mathbb{B}} \left(q^*_{\mathbb{B}/S}(q_{\mathbb{B}/S} - \mathbf{1})^S \right)^S + K_{\mathbb{B}} \star (\dot{\omega}^{\mathbb{B}}_{\mathbb{B}/I} - \dot{\omega}^{\mathbb{B}}_{\mathbb{S}/I}) \\ p_{\mathbb{S}} \left(q^*_{\mathbb{S}/E}(q_{\mathbb{S}/E} - \mathbf{1})^S \right)^S + K_{\mathbb{S}} \star (\dot{\omega}^{\mathbb{S}}_{\mathbb{S}/I} - \dot{\omega}^{\mathbb{S}}_{\mathbb{E}/I}) \end{bmatrix} = - \begin{bmatrix} \omega^{\mathbb{B}}_{\mathbb{B}/S} \\ \omega^{\mathbb{S}}_{\mathbb{S}/E} \end{bmatrix} \circ \begin{bmatrix} k_{\mathbb{B}}\, \omega^{\mathbb{B}}_{\mathbb{B}/S} \\ k_{\mathbb{S}}\, \omega^{\mathbb{S}}_{\mathbb{S}/E} \end{bmatrix}. \tag{3.99}$$

The vector $[\omega^{\mathbb{B}}_{\mathbb{B}/S}, \omega^{\mathbb{S}}_{\mathbb{S}/E}]^T$ can be dropped on both sides of the equation, hence the scalar equality can be written in a vector form; reminding the use of the E_{15} mapping matrix, we assemble an operator E_{all}

$$E_{\text{all}} = \begin{bmatrix} E_{15} & 0_{6\times 8} \\ 0_{6\times 8} & E_{15} \end{bmatrix} \in \mathbb{R}^{12\times 16} \tag{3.100}$$

which we apply on both sides of the vector equality. Recalling the definition of e in Eq. (3.91),

$$\begin{aligned} E_{\text{all}} \begin{bmatrix} K_{\mathbb{B}} \star (\dot{\omega}^{\mathbb{B}}_{\mathbb{B}/I} - \dot{\omega}^{\mathbb{B}}_{\mathbb{S}/I}) \\ K_{\mathbb{S}} \star (\dot{\omega}^{\mathbb{S}}_{\mathbb{S}/I} - \dot{\omega}^{\mathbb{S}}_{\mathbb{E}/I}) \end{bmatrix} &= \begin{bmatrix} \tilde{K}_{\mathbb{B}} & 0 \\ 0 & \tilde{K}_{\mathbb{S}} \end{bmatrix} \begin{bmatrix} E_{15}(\dot{\omega}^{\mathbb{B}}_{\mathbb{B}/I} - \dot{\omega}^{\mathbb{B}}_{\mathbb{S}/I}) \\ E_{15}(\dot{\omega}^{\mathbb{S}}_{\mathbb{S}/I} - \dot{\omega}^{\mathbb{S}}_{\mathbb{E}/I}) \end{bmatrix} \\ &= \begin{bmatrix} \tilde{K}_{\mathbb{B}} & 0_{6\times 6} \\ 0_{6\times 6} & \tilde{K}_{\mathbb{S}} \end{bmatrix} \dot{e} = \begin{bmatrix} \tilde{K}_{\mathbb{B}} & 0_{6\times 6} \\ 0_{6\times 6} & \tilde{K}_{\mathbb{S}} \end{bmatrix} \mu \end{aligned} \tag{3.101}$$

where $\tilde{K}_{\mathbb{B}}, \tilde{K}_{\mathbb{S}}$ are the previous diagonal gain matrices whose first and fifth rows and columns have been deleted (note that this is allowed as they match the entries of the dual velocities). Substituting

Eq. (3.101) in the vector equality, we obtain

$$\begin{bmatrix} \tilde{K}_{\mathfrak{o}_B} & 0_{6\times6} \\ 0_{6\times6} & \tilde{K}_{\mathfrak{o}_8} \end{bmatrix} \mu = E_{all} \begin{bmatrix} -k_{\mathfrak{o}_B} \omega^{\mathfrak{o}_B}_{\mathfrak{o}_B/S} - p_{\mathfrak{o}_B} \left(q^*_{\mathfrak{o}_B/S} (q_{\mathfrak{o}_B/S} - \mathbf{1})^S \right)^S \\ -k_{\mathfrak{o}_8} \omega^{\mathfrak{o}_8}_{\mathfrak{o}_8/E} - p_{\mathfrak{o}_8} \left(q^*_{\mathfrak{o}_8/E} (q_{\mathfrak{o}_8/E} - \mathbf{1})^S \right)^S \end{bmatrix}, \tag{3.102}$$

from which the linearized control input $\mu \in \mathbb{R}^{12}$ can be recovered as

$$\mu = \begin{bmatrix} -k_{\mathfrak{o}_B} \tilde{K}^{-1}_{\mathfrak{o}_B} E_{15} \omega^{\mathfrak{o}_B}_{\mathfrak{o}_B/S} - p_{\mathfrak{o}_B} \tilde{K}^{-1}_{\mathfrak{o}_B} E_{15} \left(q^*_{\mathfrak{o}_B/S} (q_{\mathfrak{o}_B/S} - \mathbf{1})^S \right)^S \\ -k_{\mathfrak{o}_8} \tilde{K}^{-1}_{\mathfrak{o}_8} E_{15} \omega^{\mathfrak{o}_8}_{\mathfrak{o}_8/E} - p_{\mathfrak{o}_8} \tilde{K}^{-1}_{\mathfrak{o}_8} E_{15} \left(q^*_{\mathfrak{o}_8/E} (q_{\mathfrak{o}_8/E} - \mathbf{1})^S \right)^S \end{bmatrix}. \tag{3.103}$$

As we now want to solve for the real control input $\tilde{u}$, we use Eq. (3.65) where, for the case under analysis,

$$E(x) = \underbrace{\begin{bmatrix} \left(\tilde{\Psi}(x)\right)_2 \\ \left(\tilde{\Psi}(x)\right)_8 \end{bmatrix} V_{\text{map,prism-arm}}}_{\mathbb{R}^{12\times7}}, \tag{3.104}$$

and

$$\Xi(x) = \underbrace{\begin{bmatrix} \left(\tilde{\Phi}(x)\right)_2 - \dot{\omega}^{\mathfrak{o}_B}_{\mathfrak{o}_S/I} \\ \left(\tilde{\Phi}(x)\right)_8 - \dot{\omega}^{\mathfrak{o}_8}_{\mathfrak{o}_E/I} \end{bmatrix}}_{\mathbb{R}^{12\times1}}. \tag{3.105}$$

As $\tilde{u} = E(x)^+ (\mu - \Xi(x))$, the nonlinear control input will be

$$\tilde{u} = E(x)^+ \left(\begin{array}{c} -\left(\tilde{\Phi}(x)\right)_2 + \dot{\omega}^{\mathfrak{o}_B}_{\mathfrak{o}_S/I} + \tilde{K}^{-1}_{\mathfrak{o}_B} \left[-k_{\mathfrak{o}_B} E_{15} \omega^{\mathfrak{o}_B}_{\mathfrak{o}_B/S} + \right. \\ -\left(\tilde{\Phi}(x)\right)_8 + \dot{\omega}^{\mathfrak{o}_8}_{\mathfrak{o}_E/I} + \tilde{K}^{-1}_{\mathfrak{o}_8} \left[-k_{\mathfrak{o}_8} E_{15} \omega^{\mathfrak{o}_8}_{\mathfrak{o}_8/E} + \right. \\ \left. -p_{\mathfrak{o}_B} E_{15} \left(q^*_{\mathfrak{o}_B/S} (q_{\mathfrak{o}_B/S} - \mathbf{1})^S \right)^S \right] \\ \left. -p_{\mathfrak{o}_8} E_{15} \left(q^*_{\mathfrak{o}_8/E} (q_{\mathfrak{o}_8/E} - \mathbf{1})^S \right)^S \right] \end{array} \right). \tag{3.106}$$

The mapping matrix $V_{\text{map,prism-arm}} \in \mathbb{R}^{64\times7} : u \in \mathbb{R}^{64} \mapsto \tilde{u} \in \mathbb{R}^7$ in

Eq. (3.104) is defined as

$$V_{\text{map,prism-arm}} = \begin{bmatrix} 0_{8\times1} & 0_{8\times1} & \cdots & \cdots & 0_{8\times1} \\ V_{\text{act,prism}} & 0_{8\times1} & & & 0_{8\times1} \\ 0_{8\times1} & V_{\text{act,rev}} & & & 0_{8\times1} \\ \vdots & & \ddots & & \vdots \\ \vdots & & & V_{\text{act,rev}} & 0_{8\times1} \\ 0_{8\times1} & \cdots & \cdots & 0_{8\times1} & V_{\text{act,rev}} \end{bmatrix}. \quad (3.107)$$

The result presented in Eq. (3.106) is meaningful; from a unique compact equation we are able to find the 7 elements of $\tilde{u}$ which correspond to the control inputs on each joint; by construction, these are able to track a reference linear and angular position of the end effector together with the corresponding linear and angular velocities, while the prismatic joint is simultaneously brought to the desired state in terms of position and velocity.

This result has been achieved without the need of any kinematic inversion; it is however crucial to point out that matrix $E(x)$ must feature full column rank in order to be pseudo-invertible. This condition on the rank suggests that the manipulator should always be in a nonsingular configuration in order to recover the vector $\tilde{u}$; as a consequence, the reference signal has to be designed so that the condition on the nonsingularity of the manipulator is respected. Moreover, even if the reference signal enables a singularity free trajectory in the joint space, the presence of disturbances could lead the manipulator close to a singularity, and therefore compromise the soundness of the solution. We will tackle these problems in a specific way in the remainder of the discussion, exploiting the idea of *Control Barrier Functions* (CBFs).

Chapter 4

Control barrier functions based singularity avoidance

4.1 Introduction

The growing complexity of modern control systems is only partially due to an increase in the difficulty of the control goal itself, while instead is often to be attributed to always more challenging operational requirements. Not only trains, planes or cars should be able to reach a certain destination without danger for the customers, but also they are supposed to do so in an autonomous way, with the minimum possible emissions, the best user experience, the most profitable performances, and so on. All these requirements clearly have an impact on the control design philosophy, meaning for example that it is often no more sufficient to grant a certain rate of convergence to a certain desired state, cause at the same time there might be other multiple conditions to be fulfilled, possibly with different levels of priority; this translates in the need of adjusting the still valid results from classical control theory to new methods, which allow wider coverage of the problem.

The same considerations hold when it comes to the problem of the spacecraft-manipulator, as the control strategy design must take into account a wide range of factors; first of all, the system should be

able to perform operations with a degree of accuracy which is often not required in ground-based applications. Moreover, the system is required an high level of autonomy, this mainly being due to the high communication latency, while at the same time it may have to cooperate with other agents to achieve its control goal; all these factors steer our research towards the implementation of a more comprehensive control strategy, in order to widen the applicability of what discussed in Chapter 3.

As already mentioned, the construction of the control input introduced in Eq. (3.106) is subject to one main condition, namely that the matrix $E(x)$ has full column rank; if this happens, we can always find a pseudoinverse $E(x)^+$ (in particular, a left inverse) s.t. $E^+E = I$. By recalling the definition given in Eq. (3.104), we can argue that the columns of $E(x)$ are linearly independent (i.e. E has full column rank) whenever a mapping $\tilde{u} \mapsto \ddot{\Gamma}$ exists, such that a target Γ_d can be achieved in a finite time with finite values of $\tilde{u}$. Given the structure of $E(x)$, such a mapping is clearly configuration-dependent, and recalling the results from classic robotics (see for example [55]), any singular configuration of the manipulator will prevent $E(x)$ from fulfilling the previously mentioned conditions on the full rank.

In the remainder of the discussion we advocate the use of control barrier functions (CBFs in the following) as a tool to provide stability and enhanced performances to our system. To do so, we will focus on singularity avoidance and robustness with respect to disturbances as two additional requirements for the control system, keeping in mind that the introduction of CBFs leaves the door open to a lot of different options in the system's design.

In the next sections we first suggest a brief introduction to the theory of control barrier functions, highlighting how they provide a good match for the control design techniques explained in Chapter 3; then, we further inquire the singular configurations of our case study. As a last step we specialize the theory to the aim of enforcing singularity avoidance, while simultaneously satisfying reference tracking requirements.

4.2 CBF mathematical preliminaries

4.2.1 Overview on control barrier functions

The main idea behind the use of control barrier functions is the one of ensuring the safety of a system through the achievement of *controlled invariance*. This means that, if we define a safe set $\mathcal{C}$ as the subset of the state space which satisfies a certain safety-related condition, we want to keep the trajectory of the state inside this set by means of an appropriate control action. We can assume $\mathcal{C}$ to be the superlevel set of a smooth function $h : \mathbb{R}^n \to \mathbb{R}$, i.e.

$$\begin{aligned} \mathcal{C} &= \{x \in \mathbb{R}^n : h(x) \geqslant 0\}, \\ \partial\mathcal{C} &= \{x \in \mathbb{R}^n : h(x) = 0\}, \\ \text{Int}(\mathcal{C}) &= \{x \in \mathbb{R}^n : h(x) > 0\}, \end{aligned} \tag{4.1}$$

where $\partial\mathcal{C}$ is the boundary of $\mathcal{C}$. According to Nagumo's theorem ([43]), if a dynamical system of the form $\dot{x} = f(x)$ is considered, the necessary and sufficient condition to obtain set invariance is

$$\mathcal{C} \text{ is invariant } \longleftrightarrow \dot{h}(x) \geqslant 0, \ \forall x \in \partial\mathcal{C}. \tag{4.2}$$

The same result can be obtained exploiting $\mathcal{C}_u$, which is the (unsafe) complement of the safe set, and a set of initial conditions $\mathcal{C}_0$. If we define a function $B : \mathbb{R}^n \to \mathbb{R}$, where $B(x) \leqslant 0$ for all $x \in \mathcal{C}_0$ and $B(x) > 0$ for all $x \in \mathcal{C}_u$, then

$$\dot{B}(x) \leqslant 0 \ \rightarrow \ \mathcal{C} \text{ is invariant.} \tag{4.3}$$

If instead we consider an affine control system in the form

$$\dot{x} = f(x) + g(x)u, \tag{4.4}$$

we can state that our aim is to design a control input $u \in \mathbb{R}^m$ which renders the set $\mathcal{C}$ *forward invariant*, i.e. for every $x_0 \in \mathcal{C}$, $x(t) \in \mathcal{C}$ for

$x(0) = x_0$ and all $t \in I(x_0)$, where $I(x_0) = [0, \tau_{max})$ is the maximum interval of existence such that $x(t)$ is the unique solution to Eq. (4.4) (see [49]).

Definition 4.1. *Let $\mathcal{C} \subset \mathbb{R}^n$ be defined by Eq. (4.1) with $h : \mathbb{R}^n \to \mathbb{R}$ continuously differentiable, then a function $B : \mathcal{C} \to \mathbb{R}$ is a **control barrier function (CBF)** if there exist class $\mathcal{K}$ functions α_1, α_2 and a constant $\gamma > 0$ such that*

$$\begin{aligned} &\frac{1}{\alpha_1(h(x))} \leqslant B(x) \leqslant \frac{1}{\alpha_1(h(x))}, \\ &\inf_{u \in \mathbb{R}^m} \left[\mathcal{L}_f B(x) + \mathcal{L}_g B(x) u - \frac{\gamma}{B(x)} \right] \leqslant 0. \end{aligned} \tag{4.5}$$

Lemma 4.1. *Given a set $\mathcal{C} \subset \mathbb{R}^n$ defined by Eq. (4.1), if a function $B(x) : \mathcal{C} \to \mathbb{R}$ for a continuously differentiable function $h(x) : \mathbb{R}^n \to \mathbb{R}$ satisfies the following conditions:*

$$\inf_{x \in \text{Int}(\mathcal{C})} B(x) \geqslant 0, \quad \lim_{x \to \partial \mathcal{C}} B(x) = \infty, \tag{4.6}$$

and $B(x) \to \infty$ if and only if $x \to \partial \mathcal{C}$, then there exist class $\mathcal{K}$ functions α_1, α_2 such that

$$\frac{1}{\alpha_1(h(x))} \leqslant B(x) \leqslant \frac{1}{\alpha_1(h(x))}. \tag{4.7}$$

Note that the use of the term "barrier" comes from the fact that the value of $B(x)$ blows up on the boundary of $\mathcal{C}$

Proof. See [56]. □

As a result, the set of control inputs we are interested in is expressed as

$$K_B(x) = \{u \in \mathbb{R}^m : \mathcal{L}_f B(x) + \mathcal{L}_g B(x) u - \frac{\gamma}{B(x)} \leqslant 0\}, \tag{4.8}$$

where $B(x)$ can be built according to Eq. (4.6). Note that if $B(x)$ is chosen such that $\mathcal{L}_g B(x) = 0$, then $K_B(x)$ is empty. Therefore, we will follow the backstepping-like procedure outlined in [49, 56] to render $\mathcal{C}$ forward invariant even when $h(x)$ has relative degree ρ higher than 1; whenever $h(x)$ expresses a constraint relative to a

robot configuration, as it happens when dealing with singularity avoidance, $\rho > 1$. In this case, we differentiate h in a recursive fashion, until we obtain

$$h^{(\rho)}(x, u) = \mathcal{L}_f^{\rho} + \mathcal{L}_g \mathcal{L}_f^{\rho-1} h(x) u, \tag{4.9}$$

with $\mathcal{L}_g \mathcal{L}_f^{\rho-1} h(x) \neq 0$, and $\mathcal{L}_g \mathcal{L}_f^{k-1} h(x) = 0$, $k = 1, \ldots, \rho - 1$. Next, we define the new coordinates

$$\begin{aligned} \zeta_1(x) &= h(x) \\ \dot{\zeta}_1(x) &= \zeta_2(x) \\ \dot{\zeta}_2(x) &= \zeta_3(x) \\ &\vdots \\ \dot{\zeta}_\rho(x) &= \mathcal{L}_f^{\rho} + \mathcal{L}_g \mathcal{L}_f^{\rho-1} h(x) u, \end{aligned} \tag{4.10}$$

whose dynamics can be described by

$$\begin{aligned} \dot{\zeta}(x) &= A\zeta(x) + B\mu, \\ h(x) &= C\zeta(x), \end{aligned} \tag{4.11}$$

where A, B, C have the form already seen in Eq. (3.23), and u has been chosen such that

$$\mathcal{L}_f^{\rho} + \mathcal{L}_g \mathcal{L}_f^{\rho-1} h(x) u = \mu. \tag{4.12}$$

Now we define a control barrier function candidate in the form

$$B_\rho(x) = B_1(x) + \sum_{i=1}^{\rho-1} E_i(h_i), \tag{4.13}$$

where $h_i = \zeta_{i+1} - \xi_i$, and

$$\xi_1 = 0,$$

$$
\begin{aligned}
\xi_2 &= \frac{-1}{\frac{dE_1}{dh_1}} \frac{dB_1}{dh} h_1, \\
&\vdots \\
\xi_i &= \dot{\xi}_{i-1} - \frac{1}{\frac{dE_{i-1}}{dh_{i-1}}} \frac{dE_{i-2}}{dh_{i-2}} h_{i-1}.
\end{aligned}
\tag{4.14}
$$

Moreover, $B_1(x)$ is picked such that the first inequality in Eq. (4.5) is respected, while each $E_i(h_i)$ has the following properties:

$$
\begin{aligned}
&\inf_{x \in \mathrm{Int}(\mathcal{C})} E_i(h_i) > 0, \\
&\sup_{x \in \mathrm{Int}(\mathcal{C})} E_i(h_i) \leqslant E_{\max,i}, \\
&\frac{dE_i(h_i)}{d\dot{h}_i} = 0 \text{ if and only if } \dot{h}_i = 0,
\end{aligned}
\tag{4.15}
$$

where $E_{\max,i}$ is a positive constant dependent on the choice of $E_i(h_i)$. The derivative of $B_\rho(x)$ can be computed therefore as

$$
\dot{B}_\rho(x) = \frac{dE_{\rho-2}}{dh_{\rho-2}} h_{\rho-1} + \frac{dE_{\rho-1}}{dh_{\rho-1}} \left(\mathcal{L}_f^\rho h(x) + \mathcal{L}_g \mathcal{L}_f^{\rho-1} h(x) u - \dot{\xi}_{\rho-1} \right)
\tag{4.16}
$$

If $\frac{dE_{\rho-1}}{dh_{\rho-1}} = 0$, then $\dot{B}_\rho(x) = 0$, which is still compliant with the condition expressed in the second inequality of Eq. (4.5), equivalent to $\dot{B}_\rho(x) \leqslant \frac{\gamma}{B_\rho(x)}$. If instead $\frac{dE_{\rho-1}}{dh_{\rho-1}} \neq 0$, depending on the sign of $\frac{dE_{\rho-1}}{dh_{\rho-1}} \mathcal{L}_g \mathcal{L}_f^{\rho-1} h(x)$, the controller will either be

$$
u \leqslant \frac{1}{\frac{dE_{\rho-1}}{dh_{\rho-1}} \mathcal{L}_g \mathcal{L}_f^{\rho-1} h(x)} \left(\frac{\gamma}{B_\rho(x)} - \frac{dE_{\rho-2}}{dh_{\rho-2}} h_{\rho-1} \right) - \frac{\mathcal{L}_f^\rho h(x) - \dot{\xi}_{\rho-1}}{\mathcal{L}_g \mathcal{L}_f^{\rho-1} h(x)}
\tag{4.17}
$$

if $\frac{dE_{\rho-1}}{dh_{\rho-1}} \mathcal{L}_g \mathcal{L}_f^{\rho-1} h(x) > 0$, or

$$u \geqslant \frac{1}{\frac{dE_{\rho-1}}{dh_{\rho-1}} \mathcal{L}_g \mathcal{L}_f^{\rho-1} h(x)} \left(\frac{\gamma}{B_\rho(x)} - \frac{dE_{\rho-2}}{dh_{\rho-2}} h_{\rho-1} \right) - \frac{\mathcal{L}_f^{\rho} h(x) - \dot{\xi}_{\rho-1}}{\mathcal{L}_g \mathcal{L}_f^{\rho-1} h(x)} \tag{4.18}$$

if $\frac{dE_{\rho-1}}{dh_{\rho-1}} \mathcal{L}_g \mathcal{L}_f^{\rho-1} h(x) < 0$, where $\mathcal{L}_g \mathcal{L}_f^{\rho-1} h(x) \neq 0$ because of the assumption on the relative degree of h.

Theorem 4.1. *Given a set $\mathcal{C} \subset \mathbb{R}^n$ defined by Eq. (4.1), if $h(x)$ has a relative degree ρ, then $B_\rho(x)$ as defined in Eq. (4.13) is a control barrier function and any Lipschitz continuous controller $u(x) \in K_{B_\rho}(x)$ for the system Eq. (4.4) renders the set $\mathcal{C}$ forward invariant.*

Proof. See [56]. □

4.2.2 Combining CLFs and CBFs via quadratic programs (QPs)

The previously outlined CBF framework provides a solution to the problem of designing a control u which renders the set $\mathcal{C}$ in Eq. (4.1) controlled forward invariant. This means that whenever the control input fulfills the conditions in Eqs. (4.17) and (4.18), the trajectory $x(t)$ which is the unique solution to Eq. (4.4) will never leave the safe set; from a more practical viewpoint, this means that, for example, the state will be kept away from a certain set of undesired values of the position and velocity, hence evolving in a constraint-admissible region. It is however clear that, while we want to enforce a constraint-admissible state evolution, the system should also be driven towards its control objectives, which in our framework are specified through the use of a control Lyapunov function (CLF) (see Eqs. (3.75) and (3.92)).

In order to pursue control objectives (represented by CLFs) which must be achieved through a state evolution inside a desired set (as stated by CBFs), as suggested by a number of previous applications

[47, 48, 56], we advocate the use of a single controller built upon the combination of CLFs and CBFs through quadratic programming (QP). Hence the controller can be synthesized in the form

$$
\begin{aligned}
u^*(x) = \quad & \underset{\mathbf{u}=\begin{bmatrix} u \\ \delta \end{bmatrix} \in \mathbb{R}^{m+1}}{\arg\min} \quad \frac{1}{2}\mathbf{u}^T H(x)\mathbf{u} + F^T(x)\mathbf{u} \\
\text{s.t.} \quad & \psi_0(x) + \psi_1^T(x)u \leqslant \delta, \\
& \mathcal{L}_f B(x) + \mathcal{L}_g B(x)u \leqslant \frac{\gamma}{B(x)},
\end{aligned}
\tag{4.19}
$$

where $\psi_0(x) = \mathcal{L}_f B(x) + W(x)$, $\psi_1(x) = \mathcal{L}_g V(x)^T$, and $W(x)$ is a continuous positive definite function on $\mathbb{R}^n$. $H(x) \in \mathbb{R}^{m+1 \times m+1}$, $F(x) \in \mathbb{R}^{m+1}$ are arbitrarily smooth cost functions that can be chosen to assign a different (state-based) cost to each control input. As it will become clear in the following, depending on the choice of H, F, the objective function can be defined either to give a simple condition on the controller (e.g. to yield a minimum-norm controller), or to provide a parameter whose minimization drives the system closer to the control objective.

The scalar δ, known as *relaxation factor*, plays a key role in the formulation of the problem; by relaxing the condition dictated by the CLF, it allows the optimization in Eq. (4.19) (CLF-CBF-QP) to always have a solution. This means that whenever the conditions expressed by the CLF and the CBFs are in conflict, the system will enforce respect of the constraints expressed by the CBFs, while temporarily losing sight of the control objective; when instead the two conditions do not conflict, they will be achieved simultaneously.

4.3 CBF application to singularity avoidance

4.3.1 Singular configurations

In order to design the robot controller, it is required to know which are the specific singular configurations of the manipulator of interest, as these may lead to dangerous arm behaviors. This is of utmost importance when the control is formulated in the task space (as it is in our case), and therefore no explicit inversion of the kinematics is carried out; an expression of the error in the task space is directly mapped to a force input, as in Eq. (3.106), hence resulting in possibly uncontrolled and large force inputs, which may damage the actuators and pose a threat to human operators.

When dealing with our case study, we rely on an already available description of the kinematic singularities for the Universal Robot 6R arms, which is discussed in detail in [57]. The UR10e has three types of kinematic singularities, corresponding to the different configurations in which $\det(\boldsymbol{J}(\mathbf{q}, \zeta)) = 0$. Exploiting the Denavit-

Joint	θ [rad]	**a** [m]	**d** [m]	α [rad]
Joint 1	0	0	0.1807	$-\pi/2$
Joint 2	0	-0.6127	0	0
Joint 3	0	-0.5716	0	0
Joint 4	0	0	0.17415	$\pi/2$
Joint 5	0	0	0.11985	$-\pi/2$
Joint 6	0	0	0.1165	0

Table 4.1: DH parameters of the UR10e.

Hartenberg parameters of the UR10e (see [58] and Table 4.1), we can first perform the Weierstrass substitution in order to write the

angles as algebraic values, as in

$$\begin{aligned} \sin\theta_i &= \frac{2v_i}{1+v_i^2}, \quad \cos\theta_i = \frac{1-v_i^2}{1+v_i^2}, \\ \sin\alpha_i &= \frac{2t_i}{1+t_i^2}, \quad \cos\alpha_i = \frac{1-t_i^2}{1+t_i^2}, \end{aligned} \tag{4.20}$$

where

$$v_i = \tan\frac{\theta_i}{2}, \quad t_i = \tan\frac{\alpha_i}{2}. \tag{4.21}$$

Exploiting Eqs. (4.20) and (4.21), $\det(\boldsymbol{J}(\mathbf{q},\zeta)) = 0$ can be rearranged as

$$\begin{aligned} \det(\boldsymbol{J}(\mathbf{q},\zeta)) = v_3 v_5 \Big[&(v_4^2+1)(v_3^2+1)(v_2-1)(v_2+1)a_2 + \\ &-(v_4^2+1)(v_2v_3+v_2+v_3-1)(v_2v_3-v_2-v_3-1)a_3 + \\ &-2(v_2v_3+v_2v_4+v_3v_4-1)(v_2v_3v_4-v_2-v_3-v_4)d_5 \Big] = 0. \end{aligned} \tag{4.22}$$

From inspection of Eq. (4.22) it is possible to reconstruct the three different types of singularities. The first is characterized by $v_3 = 0$ (elbow singularity) and takes place when the arm is stretched out; the second, known as wrist singularity, corresponds to $v_5 = 0$, the condition in which the fourth and the sixth axis are coplanar. The third expression describes the shoulder singularity, and only contains v_2, v_3 and v_4; when two of these parameters are set, the third can be recovered with the remaining quadratic equation. Rather than focusing on the exact algebraic conditions of this last singularity, whose definition can be pretty cumbersome, we accept the operative definition which states that the shoulder singularity occurs whenever the intersection point of the axes of joints 5 and 6 lies in one plane with the axes of joints 1 and 2; this definition will allow a simple way to avoid its occurrence, as it will become clear in the following.

Wrist and elbow singularities can be avoided if the conditions on the correspondent $v_i \neq 0$ are turned into constraints on the admissi-

ble values of the joint coordinates θ_3 and θ_5; this will be the starting point for the creation of the CBFs.

4.3.2 Numerical benchmark

Before going forward with the discussion regarding the application of CBFs to the problem of avoiding kinematic singularities, we find it useful to briefly introduce a numerical technique for singularity avoidance, which will be tested against our CBFs-based method, in order to get some insights regarding the pros and cons of each of them. This method, first suggested in [59] and whose efficiency has been repeatedly proven (see for example [40]), was developed to overcome problems deriving from close-to-singular configurations of clusters of single-gimbal control moment gyros (SGCMGs).

We recall that the steering equation for a set of SGCMGs can be cast in the form

$$A\dot{\gamma} = b, \tag{4.23}$$

where the unknown $\dot{\gamma} \in \mathbb{R}^n$ is the gimbal rate, $A \in \mathbb{R}^{3\times n}$, $b \in \mathbb{R}^3$ is the torque that must be generated by the CMGs, and the contribution $J\ddot{\gamma}$ associated to the inertia of the wheels has been dropped, as often done in the literature. In order to compute the gimbal rates, keeping in mind that usually $n > 3$, Eq. (4.23) can be solved as

$$\dot{\gamma} = A^T(AA^T)^{-1}b, \tag{4.24}$$

which is known as the Moore-Penrose (MP) solution. However, when $\text{rank}(A) < 3$, matrix AA^T is not invertible, and therefore Eq. (4.24) fails to retrieve a solution. Besides, it can be proven [60] that Eq. (4.24) causes the gimbal angles to move towards singular configuration, hence the necessity of adding an additional steering logic to the MP solution. As anticipated, we exploit one of these steering logic, known as Singular Direction Avoidance (SDA), to set a benchmark to test the validity of our novel CBFs-based approach. From a practical standpoint, we adapt the SDA method to the solu-

tion of equation Eq. (3.106), which if rewritten as

$$E\tilde{u} = b, \tag{4.25}$$

with

$$b = \begin{pmatrix} -\left(\tilde{\Phi}(x)\right)_2 + \dot{\omega}^{\mathfrak{o}_B}_{\mathfrak{o}_S/I} + \tilde{K}^{-1}_{\mathfrak{o}_B}\left[-k_{\mathfrak{o}_B} E_{15}\omega^{\mathfrak{o}_B}_{\mathfrak{o}_B/S} + \right. \\ -\left(\tilde{\Phi}(x)\right)_8 + \dot{\omega}^{\mathfrak{o}_8}_{\mathfrak{o}_E/I} + \tilde{K}^{-1}_{\mathfrak{o}_8}\left[-k_{\mathfrak{o}_8} E_{15}\omega^{\mathfrak{o}_8}_{\mathfrak{o}_8/E} + \right. \\ \left. -p_{\mathfrak{o}_B} E_{15}\left(q^*_{\mathfrak{o}_B/S}(q_{\mathfrak{o}_B/S} - \mathbf{1})^S\right)^S\right] \\ \left. -p_{\mathfrak{o}_8} E_{15}\left(q^*_{\mathfrak{o}_8/E}(q_{\mathfrak{o}_8/E} - \mathbf{1})^S\right)^S\right] \end{pmatrix}, \tag{4.26}$$

closely resembles Eq. (4.23).

The SDA method, applied to our case $E\tilde{u} = b$, starts from the singular value decomposition (SVD) of matrix $E \in \mathbb{R}^{m\times n}$, where m, n depend on the type of control strategy we want to realize (see Chapter 3); we will consider the scenario described in Eq. (3.106), in which we want to actuate all the seven joints, hence $E \in \mathbb{R}^{12\times 7}$. The SVD yields

$$E = USV^T, \tag{4.27}$$

with $U \in \mathbb{R}^{12\times 12}$, $S \in \mathbb{R}^{12\times 7}$ and $V \in \mathbb{R}^{7\times 7}$. Recall that the only nonzero elements of S are the S_{ii}, $i = 1, \ldots, 7$; these are known as the *singular values* of E. From linear algebra theory [61], we know that the S_{ii} are arranged in descending order such that $S_{11} \geqslant S_{22} \geqslant \ldots \geqslant S_{77}$; hence, when the manipulator is close to a singular configuration, $S_{77} \to 0$. The method developed in [59] exploits this property by suitably modifying the smallest singular value, in order to recover a full rank modified version of E; when matrix E is rank-deficient, its pseudoinverse is computed as

$$E^+_{SDA} = VS^+_{SDA}U^T, \tag{4.28}$$

where

$$S^{+}_{SDA} = \left[\begin{array}{cccc|c} \frac{1}{S_{11}} & 0 & \cdots & 0 & \\ 0 & \frac{1}{S_{22}} & \cdots & 0 & \\ \vdots & \vdots & \ddots & \vdots & 0_{7\times 5} \\ 0 & 0 & \cdots & \frac{S_{77}}{S_{77}^2+\alpha} & \end{array}\right]. \tag{4.29}$$

The scalar α is known as the singularity avoidance parameter, and it increases as the system approaches to a singularity; following the considerations on its choice in [59], we define it as

$$\alpha = \alpha_0 e^{-k_\sigma \sigma^2}, \tag{4.30}$$

where α_0, k_σ may be selected as desired, while $\sigma = \sqrt{\frac{n}{m}} S_{77}$, m, n being the dimensions of E. Note also that when the manipulator is far from a singular configuration S_{77} becomes larger, hence

$$\frac{S_{77}}{S_{77}^2 + \alpha} \to \frac{1}{S_{77}}, \tag{4.31}$$

thus retrieving the original expression of E^{+}.

4.3.3 CBF-based singularity avoidance

Combining the ideas introduced in the previous sections, we are interested in implementing a singularity avoidance method, by adding some constraints on the admissible value of the trajectory of the state $x(t)$. Of the three possible types of singularity illustrated in Sec. 4.3.1 we will encode wrist and elbow singularity avoidance into the CBFs formulation, while the shoulder singularity will be prevented through the regulation of the position of the base of the arm with respect to the intersection of axes 5 and 6. More details on this are reported in Chapter 5.

Specifically, the constraints will define a set of admissible values for θ_3 and θ_5; in order to have $\det(\boldsymbol{J}) \neq 0$, a necessary condition is that $v_3, v_5 \neq 0$. Moreover, we suggest an additional condition on the

value of θ_3 in order to avoid self-collision of the arm. Translating this in terms of joint coordinates yields

$$\begin{cases} \theta_3 \neq 0 + k\pi, \\ \theta_5 \neq 0 + 2k\pi, \quad k \in \mathbb{Z}. \end{cases} \tag{4.32}$$

Remembering Eq. (4.1), the safe sets associated with the conditions on the elbow and on wrist are defined as

$$\begin{aligned} \mathcal{C}_e &= \{\theta_3 \in \mathbb{R} \,:\, \theta_3 \neq 0 + k\pi\}, \\ \mathcal{C}_w &= \{\theta_5 \in \mathbb{R} \,:\, \theta_5 \neq 0 + 2k\pi\}. \end{aligned} \tag{4.33}$$

We now wish to define two smooth (continuously differentiable) functions, which assume positive nonzero values only in the constraint-admissible region of the state, and become zero on $\partial\mathcal{C}_e$, $\partial\mathcal{C}_w$. Hence,

$$\begin{aligned} h_e(\theta_3) &= \sin^2\theta_3, \\ h_w(\theta_5) &= \sin^2(\theta_5/2). \end{aligned} \tag{4.34}$$

The functions in Eq. (4.34) provide the foundation for the creation of the actual barrier functions; the constraints on the values of θ_3, θ_5 represent configuration constraints, and it is easy to verify that they have relative degree $\rho = 2$. Knowing this and using Eq. (4.13) as a driver for our choice, we suggest a general form for both the barrier functions,

$$B_2(x) = B_1(x) + E(\dot{h}(x)). \tag{4.35}$$

The first element $B_1(x)$ must be compliant with what introduced in Eq. (4.7); exploiting the result of Lemma 4.1, a valid candidate is

$$B_1(x) = -\log\left(\frac{h(x)}{1 + h(x)}\right). \tag{4.36}$$

The term $E(\dot{h}(x))$ on its turn must fulfill the conditions in Eq. (4.15);

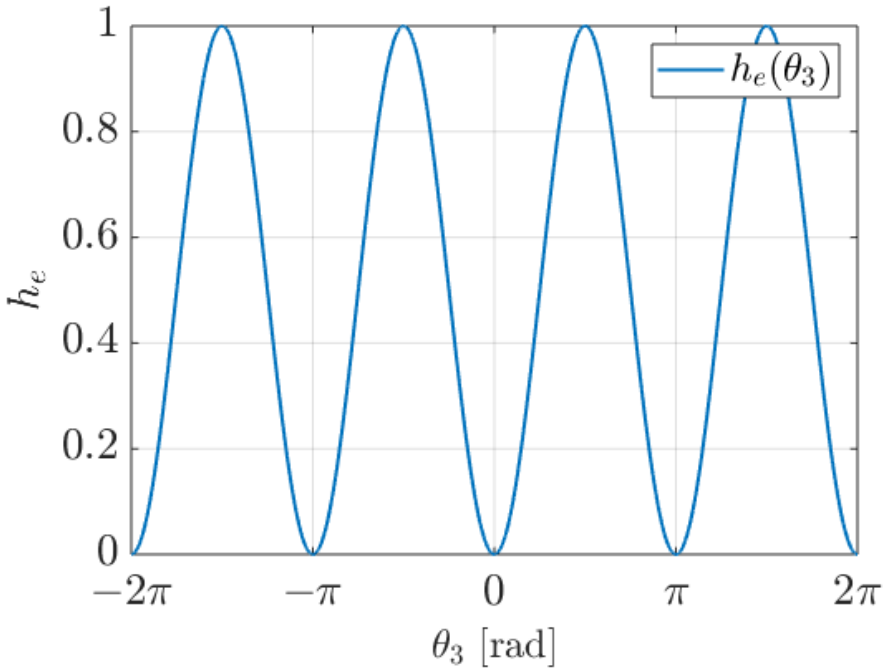

(a) h_e function in $(-2\pi : 2\pi)$. Note that $h_e(0 \pm k\pi) = 0$

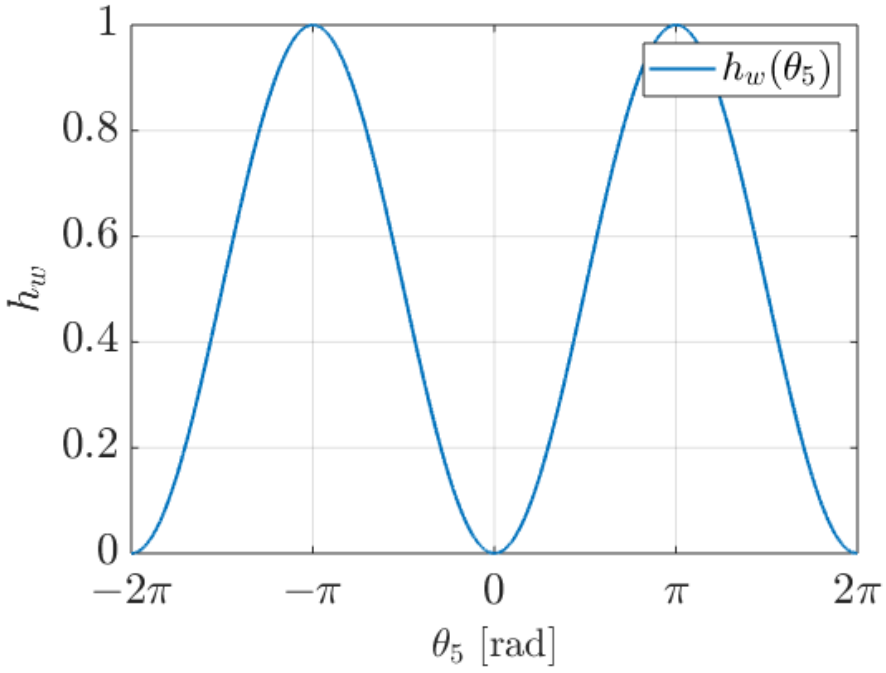

(b) h_w function in $(-2\pi : 2\pi)$. Note that $h_w(0 \pm 2k\pi) = 0$

Figure 4.1: Functions $h_e(\theta_3)$, $h_w(\theta_5)$

we choose

$$E(\dot{h}(x)) = a\frac{b\dot{h}^2(x)}{1 + b\dot{h}^2(x)}, \tag{4.37}$$

where a, b are tunable positive scalars. Using Eqs. (4.35) to (4.37) as suggested in Eq. (4.13),

$$B_2(x) = -\log\left(\frac{h(x)}{1 + h(x)}\right) + a\frac{b\dot{h}^2(x)}{1 + b\dot{h}^2(x)} \tag{4.38}$$

Note that the presence of the square elements and of the logarithm in Eq. (4.38) justifies the overall choice as per Eq. (4.6). Once the general formulation is laid out, it can be specialized for the two different cases using h_e and h_w; this yields the two specific expressions of the barrier functions, respectively

$$B_e(\theta_3, \dot{\theta}_3) = -\log\left(\frac{\sin^2\theta_3}{1 + \sin^2\theta_3}\right) + a_e\frac{b_e(2\sin\theta_3\cos\theta_3\dot{\theta}_3)^2}{1 + b_e(2\sin\theta_3\cos\theta_3\dot{\theta}_3)^2} \tag{4.39}$$

and

$$B_w(\theta_5, \dot{\theta}_5) = -\log\left(\frac{\sin^2(\theta_5/2)}{1 + \sin^2(\theta_5/2)}\right) + a_w\frac{b_w\left(\sin(\theta_5/2)\cos(\theta_5/2)\dot{\theta}_5\right)^2}{1 + b_w\left(\sin(\theta_5/2)\cos(\theta_5/2)\dot{\theta}_5\right)^2}. \tag{4.40}$$

It is straightforward to check that

$$\inf_{\theta_3 \in \mathrm{Int}(\mathcal{C}_e)} B_e(\theta_3, \dot{\theta}_3) \geqslant 0, \quad \lim_{\theta_3 \to \partial\mathcal{C}_e} B_e(\theta_3, \dot{\theta}_3) = \infty \tag{4.41}$$

and

$$\inf_{\theta_5 \in \mathrm{Int}(\mathcal{C}_w)} B_w(\theta_5, \dot{\theta}_5) \geqslant 0, \quad \lim_{\theta_5 \to \partial\mathcal{C}_w} B_w(\theta_5, \dot{\theta}_5) = \infty. \tag{4.42}$$

Once the two CBFs are defined, they both must be differentiated in order to make the control input u appear; exploiting the Lie

derivatives, this step leads to

$$\begin{aligned}\dot{B}_e(\theta_3, \dot{\theta}_3, u) &= \mathcal{L}_{f_e} B_e(\theta_3, \dot{\theta}_3) + \mathcal{L}_{g_e} B_e(\theta_3, \dot{\theta}_3) u, \\ \dot{B}_w(\theta_5, \dot{\theta}_5, u) &= \mathcal{L}_{f_w} B_w(\theta_5, \dot{\theta}_5) + \mathcal{L}_{g_w} B_w(\theta_5, \dot{\theta}_5) u.\end{aligned} \tag{4.43}$$

The expressions of $\dot{B}_e(\theta_3, \dot{\theta}_3, u)$ and $\dot{B}_e(\theta_5, \dot{\theta}_5, u)$ will not be explicitly reported for the sake of brevity; their computation is however straightforward taking Eqs. (4.39) and (4.40) as a starting point, and then using Eq. (3.49) to express $\ddot{\theta}_3$, $\ddot{\theta}_5$ as a nonlinear function of the input.

The next step is to specialize the constraint in Eq. (4.8) for the case under study, to obtain two constraints on the admissible value of u; this yields

$$\begin{aligned}\mathcal{L}_{g_e} B_e(\theta_3, \dot{\theta}_3) u &< \frac{\gamma_e}{B_e(\theta_3)} - \mathcal{L}_{f_e} B_e(\theta_3, \dot{\theta}_3), \\ \mathcal{L}_{g_w} B_w(\theta_5, \dot{\theta}_5) u &< \frac{\gamma_w}{B_w(\theta_5)} - \mathcal{L}_{f_w} B_w(\theta_5, \dot{\theta}_5).\end{aligned} \tag{4.44}$$

Enforcing respect of Eq. (4.44) will make the state controlled forward invariant in $\mathcal{C}_e$ and $\mathcal{C}_w$.

Once the formulation of the CBFs is available, these must be plugged into the CLF-CBF-QP described in Eq. (4.19) to enable a unified resolution of the nonlinear constrained control problem. The control objective (expressed through a CLF) provides a *soft constraint*, while the CBFs add *hard constraints*; the concept of different tasks which must be achieved according to a well defined hierarchy is clearly borrowed from safety applications. If we consider the reference tracking problem formulated in Chapter 3, we can rearrange the condition on $\dot{V}$ to obtain a scalar inequality; the terms $\mathcal{L}_f V(x)$ and $\mathcal{L}_g V(x) u$ can be retrieved by suitably rearranging Eq. (3.97), while we define

$$W(x) = -k_{\mathfrak{o}_B} (\omega^{\mathfrak{o}_B}_{\mathfrak{o}_B/S})^S \circ (\omega^{\mathfrak{o}_B}_{\mathfrak{o}_B/S})^S - k_{\mathfrak{o}_8} (\omega^{\mathfrak{o}_8}_{\mathfrak{o}_8/E})^S \circ (\omega^{\mathfrak{o}_8}_{\mathfrak{o}_8/E})^S. \tag{4.45}$$

Therefore, the inequality

$$\dot{V}(x) \leqslant -W(x) \tag{4.46}$$

becomes

$$\psi_0(x) + \psi_1^T(x)u \leqslant 0, \tag{4.47}$$

where $\psi_0(x) = \mathcal{L}_f V(x) + W(x)$ and $\psi_1(x) = \mathcal{L}_g V(x)^T$. The CLF-CBF-QP in Eq. (4.19) can be specialized for the problem at hand, assuming the form

$$\begin{aligned} u^*(x) = \; & \underset{\mathbf{u}=\begin{bmatrix}\tilde{u}\\ \delta\end{bmatrix}\in\mathbb{R}^8}{\arg\min} \; \frac{1}{2}\mathbf{u}^T H(x)\mathbf{u} + F^T(x)\mathbf{u} \\ \text{s.t.} \quad & \psi_0(x) + \psi_1^T(x)\tilde{u} \leqslant \delta, \\ & \mathcal{L}_{f_e} B_e(\theta_3, \dot{\theta}_3) + \mathcal{L}_{g_e} B_e(\theta_3, \dot{\theta}_3)\tilde{u} \leqslant \frac{\gamma_e}{B_e(\theta_3, \dot{\theta}_3)}, \\ & \mathcal{L}_{f_w} B_w(\theta_5, \dot{\theta}_5) + \mathcal{L}_{g_w} B_w(\theta_5, \dot{\theta}_5)\tilde{u} \leqslant \frac{\gamma_w}{B_w(\theta_5, \dot{\theta}_5)}. \end{aligned} \tag{4.48}$$

Matrices $H(x)$ and $F(x)$ define the meaning of the quadratic objective cost function; among the many possibilities we choose to minimize the quantity $Eu - b$, which describes the deviation from the nominal control law. Thus

$$\begin{aligned} \mathcal{J} &= \frac{1}{2}\left(E\tilde{u} - b\right)^T \left(E\tilde{u} - b\right) \\ &= \frac{1}{2}\tilde{u}^T \underbrace{\left(E^T E\right)}_{H_1} \tilde{u} \underbrace{-b^T E}_{F_1^T} \tilde{u}. \end{aligned} \tag{4.49}$$

Note that $H_1 \in \mathbb{R}^{m\times m}$ and $F_1 \in \mathbb{R}^m$; these must be augmented to match the size of $\mathbf{u} \in \mathbb{R}^{m+1}$, which also includes the relaxation factor δ. Hence,

$$H = \begin{bmatrix} H_1 & 0_{m\times 1} \\ 0_{1\times m} & p_\delta \end{bmatrix} \text{ and } F = \begin{bmatrix} F_1^T & 0 \end{bmatrix}^T, \tag{4.50}$$

where p_δ is the weight associated with the relaxation factor.

The three constraint equations can be rearranged in a unique vector inequality in the form

$$A\mathbf{u} \leqslant b, \tag{4.51}$$

with A, b defined as

$$\begin{aligned} A &= \begin{bmatrix} \psi_1^T & -1 \\ \mathcal{L}_{g_e} B_e & 0 \\ \mathcal{L}_{g_w} B_w & 0 \end{bmatrix} \in \mathbb{R}^{3\times 8}, \\ b &= \begin{bmatrix} -\psi_0 \\ \gamma_e / B_e - \mathcal{L}_{f_e} B_e \\ \gamma_w / B_w - \mathcal{L}_{f_w} B_w \end{bmatrix} \in \mathbb{R}^{3\times 1}. \end{aligned} \tag{4.52}$$

Eq. (4.48) can therefore be rewritten in the compact familiar form

$$\begin{aligned} u^*(x) = \underset{\mathbf{u}=\begin{bmatrix}\tilde{u}\\ \delta\end{bmatrix}\in\mathbb{R}^8}{\arg\min}\ & \frac{1}{2}\mathbf{u}^T H \mathbf{u} + F^T \mathbf{u} \\ \text{s.t.}\quad & A\mathbf{u} \leqslant b; \end{aligned} \tag{4.53}$$

which represents a quadratic optimization problem with linear constraints. Using one of the many dedicated algorithms (see [62] for some hints), Eq. (4.53) can be easily solved.

Chapter 5

Simulations and results

5.1 Introduction

Different simulations have been developed to reproduce the experimental platform recently installed at the *Dynamics and Control System Laboratory* (DCSL) of the Georgia Institute of Technology, whose testbed consists in a 6R universal robotic manipulator (UR10e) attached to the wall via a prismatic joint. Matlab and Simulink have been used to create a simulation environment able to reproduce accurately the experimental platform, with the aim of testing and evaluating the feasibility, validity and suitability of the control algorithm, before actually performing the real tests in the lab environment.
This chapter analyzes in detail the physical properties of the Universal Robot manipulator; technical details such as masses, inertial properties, geometrical description and orientation of the different frames are described in Sec. 5.2, while Sec. 5.3 presents the different techniques used to verify the model and collect the results, proving the validity and accuracy of the model. Once the correctness of the model is verified, Sec. 5.4 describes the different reference trajectories and their numeric generation; these will be used in Sec. 5.5, where three different approaches are discussed to perform pose tracking. A comparison of the results obtained using the algorithm

which appeared to be the best choice is reported in Sec. 5.6; its effectiveness and performances are assessed in the context of the overall solution strategy.

5.2 UR10e: robot configuration and features

The UR10e installed in the DCSL features six revolute joints, whose base is linked via a prismatic joint to a guide fixed on a wall, which provides an additional translational degree of freedom to the whole platform. The key feature of the UR10e is its ability to perform a 360° rotation around all the wrist joints, and an infinite rotation about the end effector axis; with a radius reach of up to 1300 mm, the UR10 is effective for tasks that are performed across a large area. The addition of the prismatic DOF to the base of the arm allows the platform to move and extend both the reachability and the radius reach in the direction of the first joint axis.
The physical description of the UR10e is based on the original CAD files provided by the manufacturing company and, as described in Sec. 2.3, some assumptions are made in the transition from the real system to the physical one. Assuming constant density, the masses of the different component lumped in the link masses are stated in Table 5.1.
As shown in Table 5.1, the lab wall is modeled as a free floating base, with high mass and moments of inertia, in order to keep it practically fixed in the inertial space, but at the same time to retain the mathematical description explained in Sec. 2.4.2; in this way the UR10e is treated as a manipulator mounted on a spacecraft of elevate dimensions, as it could be for a robot on the International Space Station.
In order to describe the different bodies within the DQ framework, we have developed a system of reference frames adopting some conventions to make the process more intuitive. As a first consideration, the axis describing the degree of freedom of each joint must be along its local Z direction; moreover, the reference frame of each

child body is always oriented as the one of the parent joint, as illustrated in Sec. 2.3.2.
Quaternion rotations are referred to using $q_{\bar{n}}(\theta)$:

$$q_{\bar{n}}(\theta) = [\cos(\theta/2), \bar{n}\sin(\theta/2)]^T, \tag{5.1}$$

where $\bar{n}$ is the Euler axis and θ is the Euler angle.

Body	**Mass** [kg]
Base	$102180.978 \cdot 10^7$
Link 1	2.611
Link 2	7.369
Link 3	13.051
Link 4	3.989
Link 5	2.100
Link 6	1.980
Link 7	0.615

Table 5.1: Masses of the different bodies composing the UR10e

The inertial reference frame, which is the starting point for the orientation of every other frame, is centered in the center of mass (CoM) of the guide, and has its Y axis pointed outwards with respect to the wall; the Z axis is in the upward direction and X descends from the first two, as shown in Fig. 5.1. Hence, the orientation of every other frame can be expressed with respect to the inertial one using the property of consecutive rotation presented in Eq. (2.26).

Quaternion rotations		
$q_{\mathbf{e}_1/I}$		$[1,0,0,0]^T$
$q_{1/\mathbf{e}_1}$	$q_y\left(\frac{\pi}{2}\right)$	$[0.7071,0,0.7071,0]^T$
$q_{\mathbf{e}_2/1}$		$[1,0,0,0]^T$
$q_{2/\mathbf{e}_2}$	$q_z\left(-\frac{\pi}{2}\right) q_y\left(-\frac{\pi}{2}\right)$	$[0.5,-0.5,-0.5,-0.5]^T$
$q_{\mathbf{e}_3/2}$		$[1,0,0,0]^T$
$q_{3/\mathbf{e}_3}$	$q_z\left(\frac{\pi}{2}\right) q_x\left(\frac{\pi}{2}\right)$	$[0.5,0.5,0.5,0.5]^T$
$q_{\mathbf{e}_4/3}$		$[1,0,0,0]^T$
$q_{4/\mathbf{e}_4}$	$q_y(\pi)$	$[0,0,1,0]^T$
$q_{\mathbf{e}_5/4}$		$[1,0,0,0]^T$
$q_{5/\mathbf{e}_5}$	$q_y(-\pi)$	$[0,0,-1,0]^T$
$q_{\mathbf{e}_6/5}$		$[1,0,0,0]^T$
$q_{6/\mathbf{e}_6}$	$q_x\left(-\frac{\pi}{2}\right) q_z\left(-\frac{\pi}{2}\right)$	$[0.5,-0.5,-0.5,-0.5]^T$
$q_{\mathbf{e}_7/6}$		$[1,0,0,0]^T$
$q_{7/\mathbf{e}_7}$	$q_z\left(-\frac{\pi}{2}\right) q_x\left(\frac{\pi}{2}\right)$	$[0.5,0.5,-0.5,-0.5]^T$
$q_{\mathbf{e}_8/7}$		$[1,0,0,0]^T$

Table 5.2: Relative orientations of the frames of each child body with respect to its parent joint ($q_{\mathbf{e}_{i+1}/i}$) and between each joint and its proximal body ($q_{i/\mathbf{e}_i}$).

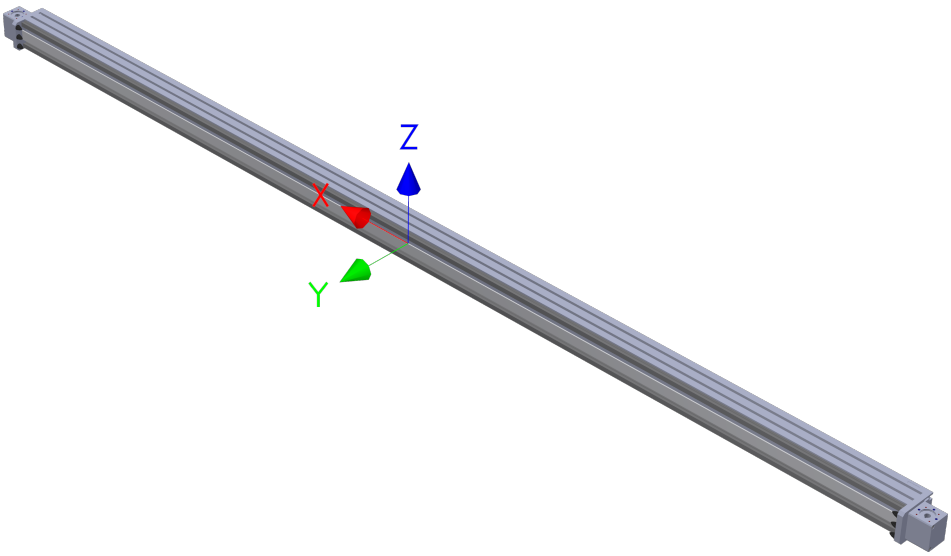

Figure 5.1: Inertial reference frame centered in the center of mass of the guide

Quaternion rotations		
$q_{1/I}$	$q_y\left(\frac{\pi}{2}\right)$	$[0.7071, 0, 0.7071, 0]^T$
$q_{\mathfrak{B}_2/I}$	$q_y\left(\frac{\pi}{2}\right)$	$[0.7071, 0, 0.7071, 0]^T$
$q_{2/I}$	$q_x\left(-\frac{\pi}{2}\right)$	$[0.7071, -0.7071, 0, 0]^T$
$q_{\mathfrak{B}_3/I}$	$q_x\left(-\frac{\pi}{2}\right)$	$[0.7071, -0.7071, 0, 0]^T$
$q_{3/I}$	$q_y\left(\frac{\pi}{2}\right)$	$[0.7071, 0, 0.7071, 0]^T$
$q_{\mathfrak{B}_4/I}$	$q_y\left(\frac{\pi}{2}\right)$	$[0.7071, 0, 0.7071, 0]^T$
$q_{4/I}$	$q_y\left(\frac{3\pi}{2}\right)$	$[-0.7071, 0, 0.7071, 0]^T$
$q_{\mathfrak{B}_5/I}$	$q_y\left(\frac{3\pi}{2}\right)$	$[-0.7071, 0, 0.7071, 0]^T$
$q_{5/I}$	$q_y\left(\frac{\pi}{2}\right)$	$[0.7071, 0, 0.7071, 0]^T$
$q_{\mathfrak{B}_6/I}$	$q_y\left(\frac{\pi}{2}\right)$	$[0.7071, 0, 0.7071, 0]^T$
$q_{6/I}$	$q_x\left(-\frac{\pi}{2}\right)$	$[0.7071, -0.7071, 0, 0]^T$
$q_{\mathfrak{B}_7/I}$	$q_x\left(-\frac{\pi}{2}\right)$	$[0.7071, -0.7071, 0, 0]^T$
$q_{7/I}$	$q_y\left(-\frac{\pi}{2}\right)$	$[0.7071, 0, -0.7071, 0]^T$
$q_{\mathfrak{B}_8/I}$	$q_y\left(-\frac{\pi}{2}\right)$	$[0.7071, 0, -0.7071, 0]^T$

Table 5.3: Orientation of joint and body frames with respect to the inertial reference frame I

It is important to underline that only the choice of each local Z axis is constrained, while the definition of X and Y is made on a convenience basis. With regard to the inertia matrices of the UR10e, the values presented in Tables 5.6 and 5.7 are expressed in the body frames defined within the CAD files. Once the reference frames of the robotic arm have been stated, the relation between them and the CAD frames is used in order to rotate the inertia matrix of each body from CAD coordinates to the actual body ones, that have been used all throughout the study.

Quaternion rotations		
$q_{\mathfrak{o}_1/\mathrm{CAD}}$	$q_y\left(\frac{\pi}{2}\right)$	$[0.7071, 0, 0.7071, 0]^T$
$q_{\mathfrak{o}_2/\mathrm{CAD}}$	$q_y\left(\frac{\pi}{2}\right)$	$[0.7071, 0, 0.7071, 0]^T$
$q_{\mathfrak{o}_3/\mathrm{CAD}}$	$q_z\left(-\frac{\pi}{2}\right) q_y\left(-\frac{\pi}{2}\right)$	$[0.5, -0.5, -0.5, -0.5]^T$
$q_{\mathfrak{o}_4/\mathrm{CAD}}$		$[1, 0, 0, 0]^T$
$q_{\mathfrak{o}_5/\mathrm{CAD}}$	$q_y(\pi)$	$[0, 0, 1, 0]^T$
$q_{\mathfrak{o}_6/\mathrm{CAD}}$	$q_x\left(-\frac{\pi}{2}\right) q_z\left(\frac{\pi}{2}\right)$	$[0.5, -0.5, 0.5, 0.5]^T$
$q_{\mathfrak{o}_7/\mathrm{CAD}}$	$q_y\left(-\frac{\pi}{2}\right) q_z\left(-\frac{\pi}{2}\right)$	$[0.5, 0.5, -0.5, -0.5]^T$
$q_{\mathfrak{o}_8/\mathrm{CAD}}$	$q_x\left(-\frac{\pi}{2}\right) q_z(\pi)$	$[0, 0, 0.7071, 0.7071]^T$

Table 5.4: Orientation of the body frames with respect to the CAD reference frames

Initial value	$[^\circ]$
$\Gamma_{0,1}$	0
$\Gamma_{0,2}$	90
$\Gamma_{0,3}$	100
$\Gamma_{0,4}$	120
$\Gamma_{0,5}$	0
$\Gamma_{0,6}$	90
$\Gamma_{0,7}$	0

Table 5.5: Initial condition for the joint generalized coordinates

INERTIA MATRICES $[kg \cdot m^2]$
Base
$\begin{bmatrix} 213135784.988 & -186942.766 & -80579.944 \\ -186942.766 & 1.51998373290580e+11 & -1506.148 \\ -80579.944 & -1506.148 & 1.51990880260658e+11 \end{bmatrix} \cdot 10^{1}$
Link 1
$\begin{bmatrix} 6850773.395 & -5462.497 & -1695.059 \\ -5462.497 & 10529508.773 & -175150.623 \\ -1695.059 & -175150.623 & 7676083.313 \end{bmatrix} \cdot 10^{-9}$
Link 2
$\begin{bmatrix} 30386820.773 & 69.517 & -47.448 \\ 69.517 & 25285600.458 & 375162.314 \\ -47.448 & 375162.314 & 27005662.240 \end{bmatrix} \cdot 10^{-9}$
Link 3
$\begin{bmatrix} 40965189.356 & -1080.604 & -2059799.950 \\ -1080.604 & 940590466.152 & -52.740 \\ -2059799.950 & -52.740 & 934098437.783 \end{bmatrix} \cdot 10^{-9}$

Table 5.6: Inertia of the first four bodies composing the UR10e, expressed in CAD axes

Inertia matrices $[kg \cdot m^2]$
Link 4
$\begin{bmatrix} 7158190.253 & 230.383 & -8608217.225 \\ 230.383 & 261520871.736 & 25.134 \\ -8608217.225 & 25.134 & 260278725.126 \end{bmatrix} \cdot 10^{-9}$
Link 5
$\begin{bmatrix} 3319148.978 & 14.130 & 102938.858 \\ 14.130 & 4013926.432 & 8.261 \\ 102938.858 & 8.261 & 2922878.203 \end{bmatrix} \cdot 10^{-9}$
Link 6
$\begin{bmatrix} 2840676.432 & 3.155 & -86420.121 \\ 3.155 & 3336079.265 & 3.738 \\ -86420.121 & 3.738 & 2606249.760 \end{bmatrix} \cdot 10^{-9}$
Link 7
$\begin{bmatrix} 463145.925 & 0 & 0 \\ 0 & 465712.590 & -15.021 \\ 0 & -15.021 & 609165.320 \end{bmatrix} \cdot 10^{-9}$

Table 5.7: Inertia of the last four bodies composing the UR10e, expressed in CAD axes

The rotation expressed in quaternion in Table 5.4 is converted into a matrix representation with the following formula:

$$A_{\clubsuit_i/CAD} = I_3 - 2q_{0,i} \cdot [\bar{q}_i]^\times + 2[\bar{q}_i]^\times [\bar{q}_i]^\times \tag{5.2}$$

where $q_{0,i}$ is the scalar part of $q_{\clubsuit_i/CAD}$ and $\bar{q}_i$ the vector part.
Hence, the inertia matrices express in body frame can be found using Eq. (5.3),

$$I_\clubsuit = A^T_{\clubsuit/CAD} I_{CAD} A_{\clubsuit/CAD}. \tag{5.3}$$

The initial conditions (see Table 5.5) are selected in order to avoid proximity to singularity in the initial configuration; this can be proved by a sufficiently high value of the manipulability index, which is defined as

$$w = \sqrt{\det\left(\tilde{J}\tilde{J}^T\right)}, \tag{5.4}$$

where $\tilde{J}$ is the Jacobian introduced in Eq. (2.53) whose first and fifth rows have been eliminated as they are always associated with the zero entries of vector DQ velocities. In this way, we assure that the initial condition is coherent with the idea of safe set as illustrated in Chapter 4, and that the robotic arm is placed in an optimal starting position to perform the pose tracking maneuver. Moreover, the initial joint angles result in a folded position of the arm (see Fig. 5.2), which is meant to occupy less space in the DCSL facility.

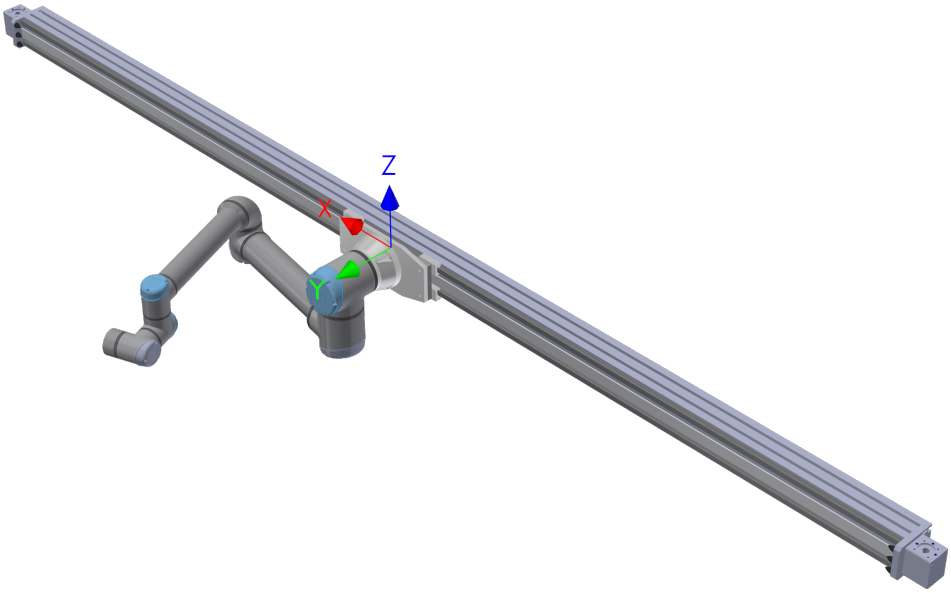

Figure 5.2: Initial condition for the UR10e

Using the initial values of the joint coordinates and the product of consecutive rotation for quaternions, it is possible to evaluate the initial $q_{i/I}$ for each joint; once this is done, by exploiting the measurements in inertial reference frame taken from the CAD, we can obtain the same dimensions but expressed in body frame.

Quaternion distances	
Symbol	**Value** $[\mathrm{m}]$
$r^{I}_{1/\mathfrak{o}_1}$	$[0, 190.045, 59.235, 45.001]^T \cdot 10^{-3}$
$r^{I}_{\mathfrak{o}_2/1}$	$[0, -180.079, 104.3, -51.592]^T \cdot 10^{-3}$
$r^{I}_{2/\mathfrak{o}_2}$	$[0, 0.079, 39.947, 1.592]^T \cdot 10^{-3}$
$r^{I}_{\mathfrak{o}_3/2}$	$[0, 0, 83.39, -12.894]^T \cdot 10^{-3}$
$r^{I}_{3/\mathfrak{o}_3}$	$[0, 0, -1.99, -81.706]^T \cdot 10^{-3}$
$r^{I}_{\mathfrak{o}_4/3}$	$[0, 208.04, -36.683, -82.392]^T \cdot 10^{-3}$
$r^{I}_{4/\mathfrak{o}_4}$	$[0, 395.327, -69.896, 65.975]^T \cdot 10^{-3}$
$r^{I}_{\mathfrak{o}_5/4}$	$[0, -83.06, 228.206, 62.011]^T \cdot 10^{-3}$
$r^{I}_{5/\mathfrak{o}_5}$	$[0, -112.421, 308.875, -46.494]^T \cdot 10^{-3}$
$r^{I}_{\mathfrak{o}_6/5}$	$[0, -0.542, 1.487, -62.698]^T \cdot 10^{-3}$
$r^{I}_{6/\mathfrak{o}_6}$	$[0, -19.097, 52.47, -15.952]^T \cdot 10^{-3}$
$r^{I}_{\mathfrak{o}_7/6}$	$[0, -16.398, 50.235, 0]^T \cdot 10^{-3}$
$r^{I}_{7/\mathfrak{o}_7}$	$[0, 49.002, 28.069, 0]^T \cdot 10^{-3}$
$r^{I}_{\mathfrak{o}_8/7}$	$[0, 25.602, 9.318, 0.111]^T \cdot 10^{-3}$

Table 5.8: Quaternion expressions of the distances from parent body to child joint, and viceversa, expressed in inertial frame

Using the quantities expressed in inertial frame, which are obtained from the CAD files (see Table 5.8), all the measurements are subsequently rotated in body frames according to Eq. (2.11),

$$\begin{aligned} r^{\mathfrak{o}_{i+1}}_{\mathfrak{o}_{i+1}/i} &= q^{*}_{\mathfrak{o}_{i+1}/I} r^{I}_{\mathfrak{o}_{i+1}/i} q_{\mathfrak{o}_{i+1}/I}, \\ r^{\mathfrak{o}_k}_{i/\mathfrak{o}_k} &= q^{*}_{\mathfrak{o}_k/I} r^{I}_{i/\mathfrak{o}_k} q_{\mathfrak{o}_k/I}. \end{aligned} \tag{5.5}$$

The last necessary step to fully characterize the UR10e is the creation of the mapping matrices described in Sec. 2.3.4. In the end, all the parameters necessary to start the simulation are collected in a data struct, whose content can be summed up as:

- The dual pose of each node of the system, i.e. all the joint and body frames, which is found using Eq. (2.40) in order to characterize the initial forward kinematics.
- The mapping matrices according to each joint type (see Table 5.9).

Joint type	V	Λ	V_{act}	L
P	E^T_{145}	E_{158}	$E^T_{1235678}$	$[0,0,0,0,0,0,0,1]$
R	E^T_{158}	E_{145}	$E^T_{1234567}$	$[0,0,0,1,0,0,0,0]$

Table 5.9: Mapping matrices.

- The dual mass and inertia matrices expressed in Sec. 2.4.2.
- The initial state vector as described in Eq. (2.97).

5.3 Model simulation and verification

It is vital to ensure the proper functioning of the simulated dynamics of the UR10e, before starting with more complex simulations involving the control laws; this process, also known as *model verification*, is defined as "ensuring that the computer program of the computerized model and its implementation are correct" [63].
In order to ensure the correct implementation, two simulations are performed with different initial velocities and no external wrenches or disturbances applied; hence, the system is isolated and the results can be checked in terms of conservation of dual momentum and kinetic energy.

5.3.1 Initial conditions

As per Eq. (2.97), the initial dual velocities in the state vector are expressed in body reference frames, with respect to a steady inertial frame. Therefore, to help the creation of consistent initial conditions that satisfy the constraints given by each joint, a computer routine has been used to retrieve the initial conditions from the generalized joint velocities, which were written with respect to the parent bodies, in the form $\boldsymbol{\omega}^{i}_{i/\mathfrak{o}_k}$. Note that the $\boldsymbol{\omega}^{i}_{i/\mathfrak{o}_k}$ must be defined in compliance with the constraints exerted by the joints; for example, a revolute joint shall have its unique nonzero entry in the position corresponding with an angular velocity on its local Z axis (see Table 5.10). After defining the relative joint velocities, the forward kinematics express in Sec. 2.3.4 is used to find the joint velocities in the inertial reference frame, by rearranging Eq. (2.76) in the form

$$\boldsymbol{\omega}^{\mathfrak{o}_{i+1}}_{\mathfrak{o}_{i+1}/I} = \mathbf{q}^{*}_{\mathfrak{o}_{i+1}/i}(\boldsymbol{\omega}^{i}_{i/\mathfrak{o}_k} + \mathbf{q}^{*}_{i/\mathfrak{o}_k}\boldsymbol{\omega}^{\mathfrak{o}_k}_{\mathfrak{o}_k/I}\mathbf{q}_{i/\mathfrak{o}_k})\mathbf{q}_{\mathfrak{o}_{i+1}/i}, \quad k = N[C(i,:)], \quad i = \{1,\dots,J\}. \tag{5.6}$$

Starting from the initial velocity of the first body, which is always null, and from the relative velocity of each joint, it is possible to convert the initial conditions into the ones needed by the state vector.

5.3.2 Free response of the system

Once the initial conditions are stated, an analysis on the physical quantities which must be conserved is carried out, in order to check consistency of the model. The system, in absence of applied wrenches and dissipation, can be considered isolated; therefore, its kinetic energy E_k, dual momentum $\mathbf{H}^{I}_{S}(O_I)$ and overall center of mass remain constant. Table 5.10 reports the set of initial conditions which have been used in the first case of the system free response, while Table 5.11 describes the second set.

First case

Initial relative velocity	$[m \cdot s^{-1}]$ or $[rad \cdot s^{-1}]$
$\omega^1_{1/\mathfrak{o}_1}$	$[0,0,0,0,0,0,0,0]^T$
$\omega^2_{2/\mathfrak{o}_2}$	$[0,0,0,0.3,0,0,0,0]^T$
$\omega^3_{3/\mathfrak{o}_3}$	$[0,0,0,0,0,0,0,0]^T$
$\omega^4_{4/\mathfrak{o}_4}$	$[0,0,0,0,0,0,0,0]^T$
$\omega^5_{5/\mathfrak{o}_5}$	$[0,0,0,0,0,0,0,0]^T$
$\omega^6_{6/\mathfrak{o}_6}$	$[0,0,0,0,0,0,0,0]^T$
$\omega^7_{7/\mathfrak{o}_7}$	$[0,0,0,0,0,0,0,0]^T$

Table 5.10: First set of initial joint relative velocities expressed in the parent body's reference frame

As it is shown in Figs. 5.3 to 5.6, the conserved quantities do not display significant variations; the data in Figs. 5.4 and 5.5 have been extracted from the overall dual momentum vector. The variation in the value of the kinetic energy in Fig. 5.3, in the order of 10^{-5}, is due to the limits in the accuracy of the numerical solution.

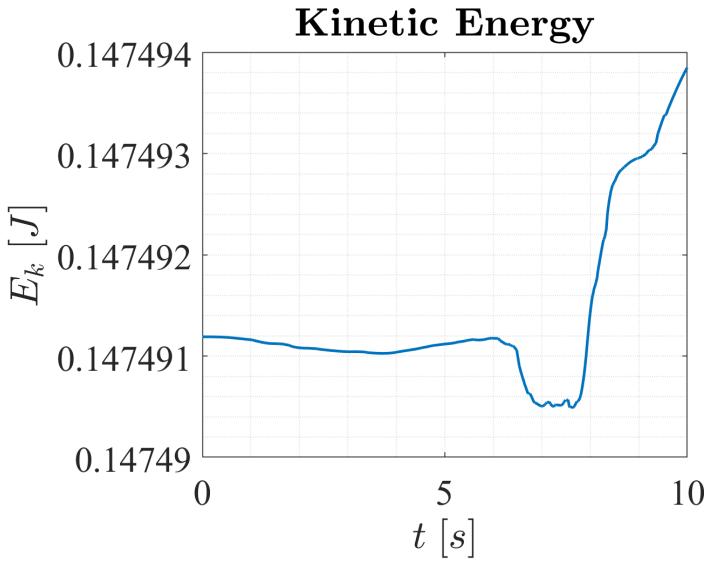

Figure 5.3: Overall system kinetic energy, first case

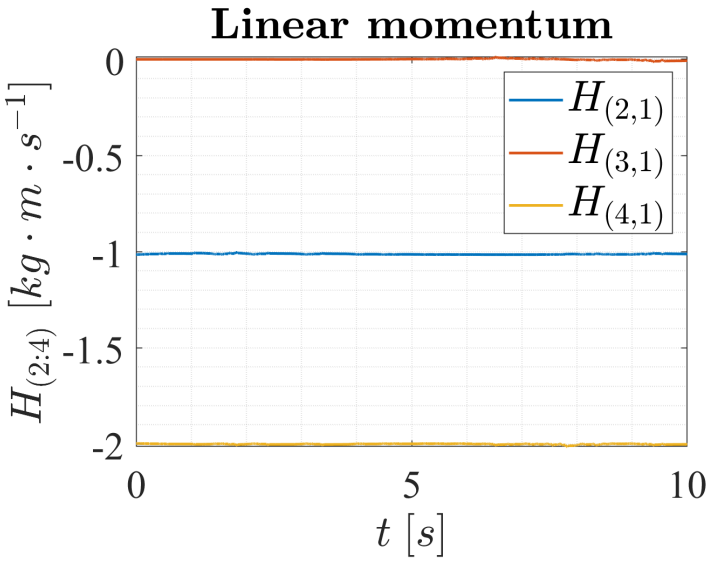

Figure 5.4: Overall system linear momentum, first case

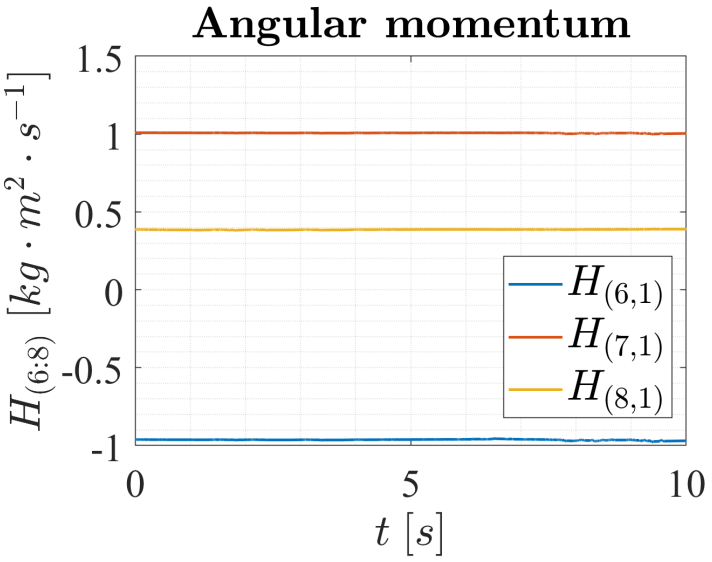

Figure 5.5: Overall system angular momentum, first case

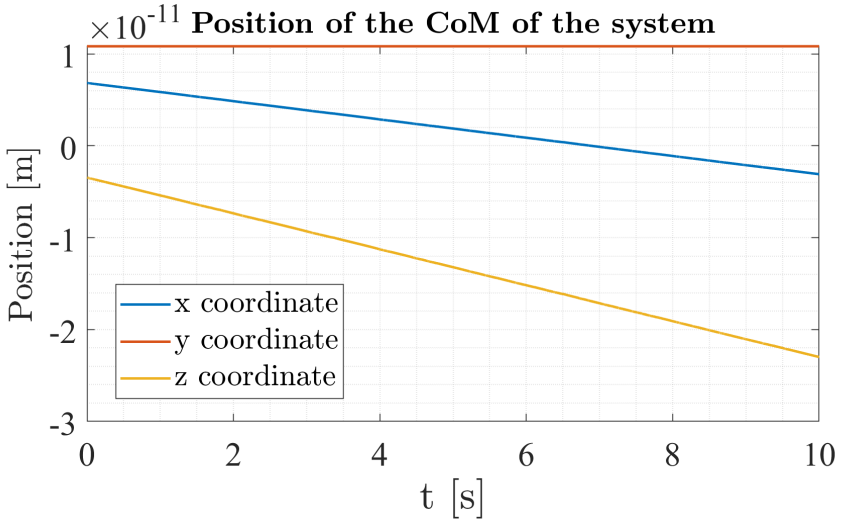

Figure 5.6: Overall system center of mass expressed in inertial reference frame, first case

When analyzing the overall motion of the robotic manipulator, it is important to underline that, due to momentum conservation, the rotations around the six revolute joints also cause a motion of

the prismatic joint, as shown in Fig. 5.7. In order to increase the performance of the control, it will be critical to keep this motion at a minimum. Fig. 5.9 describes the reaction wrenches generated by the first joint on its parent body, which are due to the rotation of the UR10e around the second joint; looking at the values of $\boldsymbol{W}^{1}_{\mathrm{B_2/B_1}}$ it is possible to have an initial estimate of the order of magnitude of the actuation which will be needed to move the robotic arm.

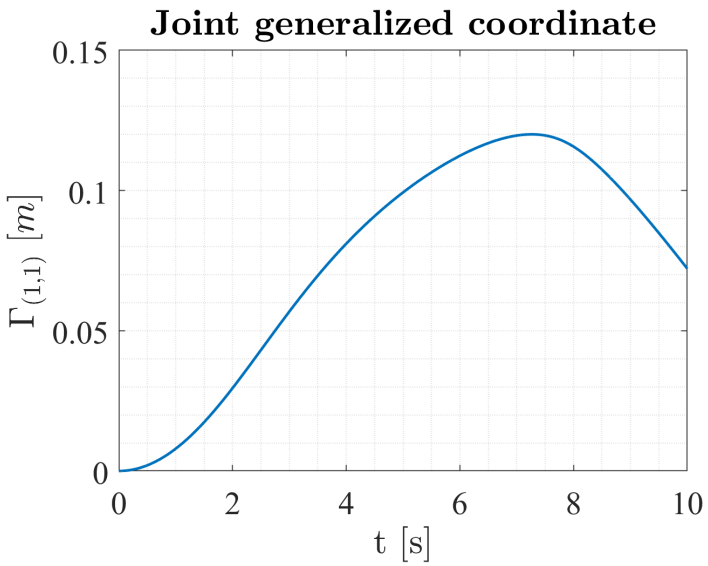

Figure 5.7: Prismatic joint displacement, first case

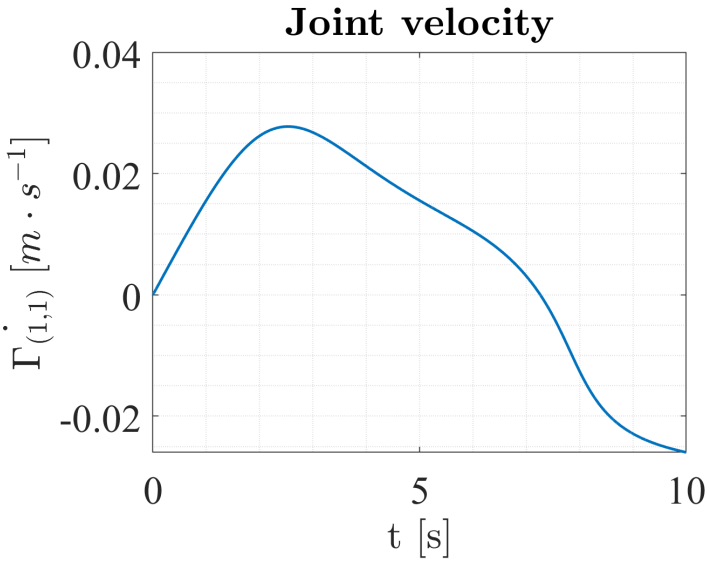

Figure 5.8: Prismatic joint velocity, first case

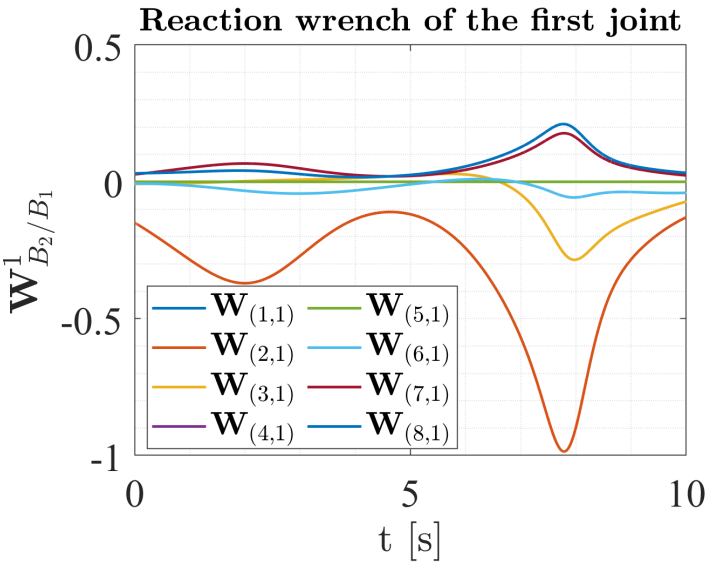

Figure 5.9: Reaction wrench exerted by the prismatic joint on its adjacent bodies, first case

Second case

A second set of initial conditions is hereby used in order to further verify the model; this set is more demanding as it implies more nonzero entries with respect to the case in Table 5.11. Nonetheless, invariance of the mechanical constants is still preserved.

Initial relative velocity	$[m \cdot s^{-1}]$ or $[rad \cdot s^{-1}]$
$\omega^1_{1/\circ_1}$	$[0,0,0,0,0,0,0,0]^T$
$\omega^2_{2/\circ_2}$	$[0,0,0,0.3,0,0,0,0]^T$
$\omega^3_{3/\circ_3}$	$[0,0,0,0,0,0,0,0]^T$
$\omega^4_{4/\circ_4}$	$[0,0,0,0.3,0,0,0,0]^T$
$\omega^5_{5/\circ_5}$	$[0,0,0,-0.1,0,0,0,0]^T$
$\omega^6_{6/\circ_6}$	$[0,0,0,-0.2,0,0,0,0]^T$
$\omega^7_{7/\circ_7}$	$[0,0,0,0,0,0,0,0]^T$

Table 5.11: Second set of initial joint relative velocities expressed in the parent body's reference frame

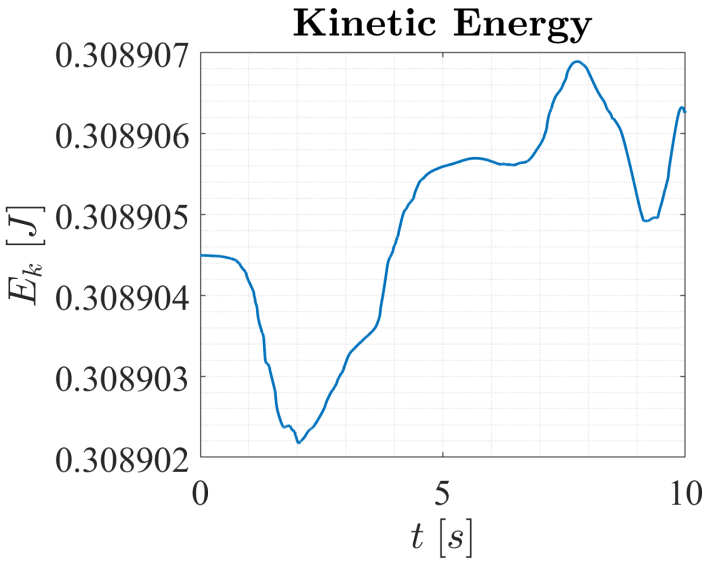

Figure 5.10: Overall system kinetic energy, second case

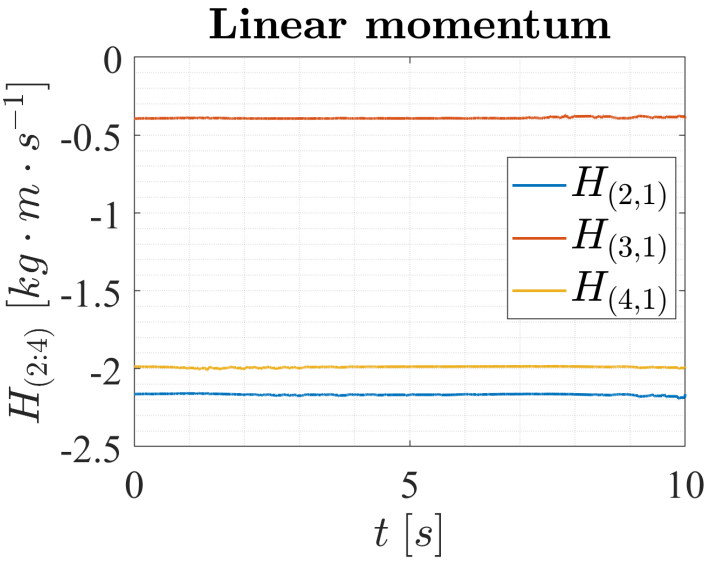

Figure 5.11: Overall system linear momentum, second case

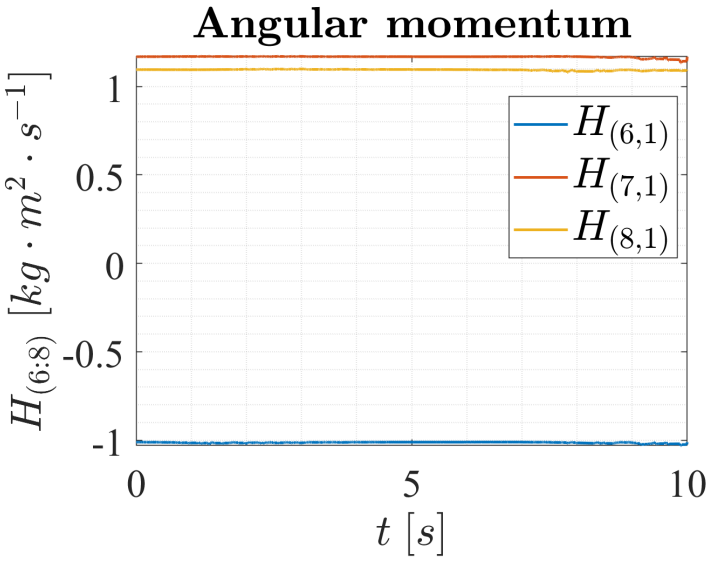

Figure 5.12: Overall system angular momentum, second case

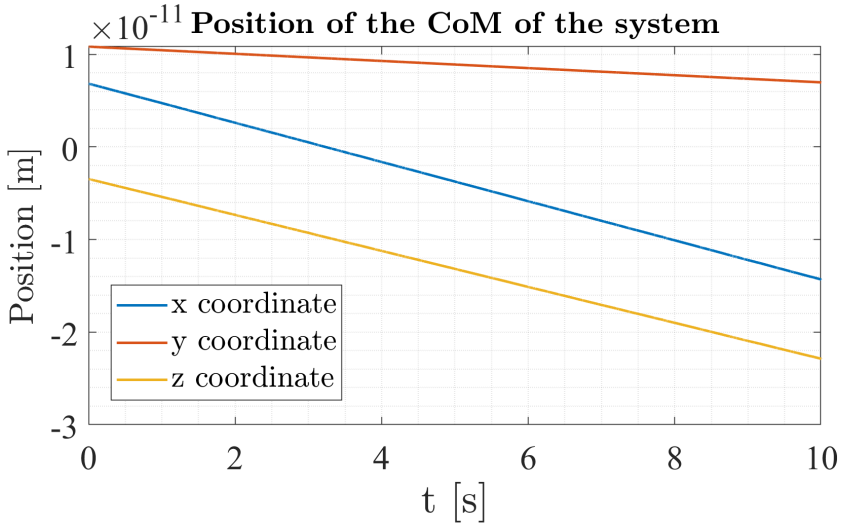

Figure 5.13: Overall system center of mass expressed in inertial reference frame, second case

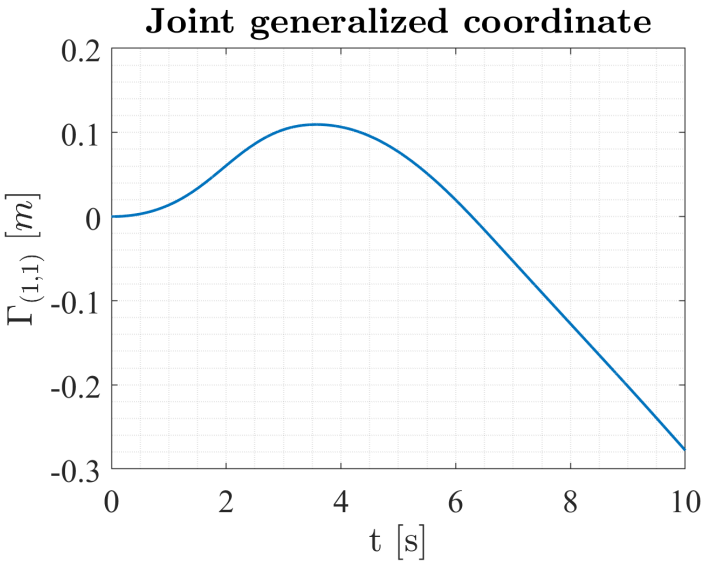

Figure 5.14: Prismatic joint displacement, second case

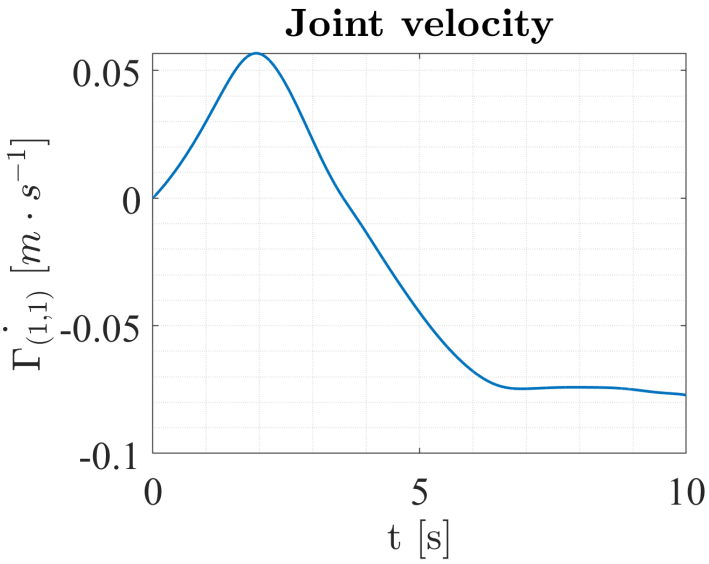

Figure 5.15: Prismatic joint velocity, second case

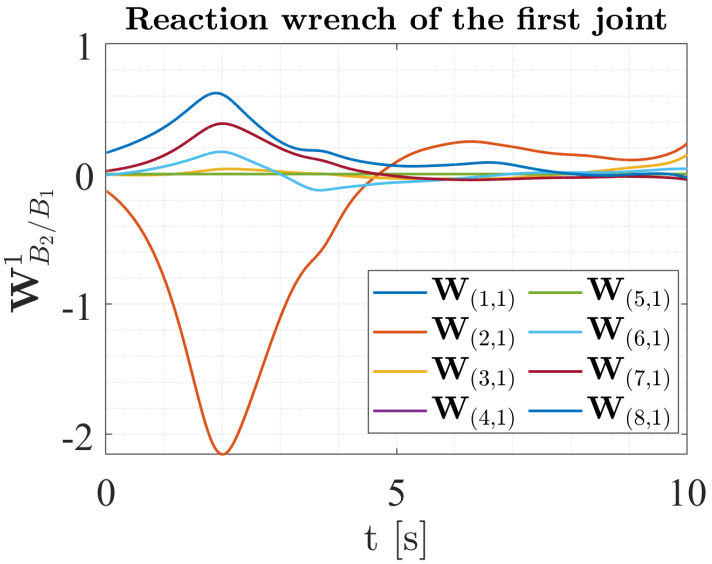

Figure 5.16: Reaction wrench exerted by the prismatic joint on its adjacent bodies, secind case

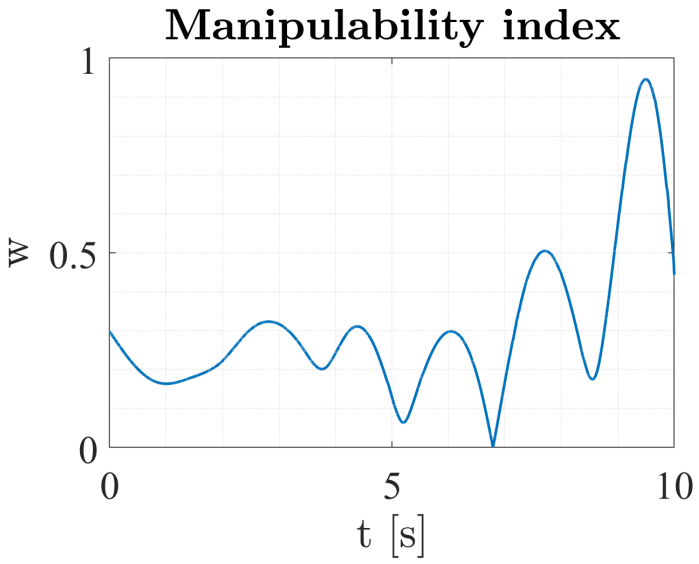

Figure 5.17: Manipulability index for the UR10e, second example.

The relative motion of the links around the different joint axes may lead the UR10e close to singularity, so $w \to 0$, as shown in

Fig. 5.17; this introduces a problem that will be discussed in depth in Sec. 5.5

5.4 DQ reference pose generation

A unique reference trajectory has been chosen to simulate pose tracking; this was done to better compare the performances of the different types of controller. The position trajectory is given by a circular motion in the XY inertial plane, while the reference attitude of the end effector is constant and equal to the orientation of inertial frame. The circle in the XY plane is expressed in Cartesian coordinate and is defined by three different quantities; $\bar{r}_0$ is the vector that defines the position of the center of the circle in the inertial reference frame, r is the radius of the circle and ω is its angular frequency expressed in $[rad \cdot s^{-1}]$. These values are combined to obtain the path, which is parametrized with respect to time t, as in

$$\begin{aligned} \bar{r}^I_{E/I,x} &= \bar{r}_{0,x} + r\cos(\omega t), \\ \bar{r}^I_{E/I,y} &= \bar{r}_{0,y} + r\sin(\omega t), \\ \bar{r}^I_{E_I,z} &= \bar{r}_{0,z}, \end{aligned} \tag{5.7}$$

where the quaternion position vector has been defined as: $r^I_{E/I} = [0, \bar{r}_{E/I}]^T$. The desired attitude is oriented as the inertial reference frame, hence $q_{E/I} = [1,0,0,0]^T$; the reference dual pose trajectory is therefore obtained as in Eq. (2.25):

$$q_{E/I} = q_{E/I} + \epsilon\left(\frac{1}{2} r^I_{E/I} q_{E/I}\right). \tag{5.8}$$

The desired end effector orientation does not change in time - so $q_{E/I}$ is constant. In this way both $\omega^I_{E/I}$ and $\dot{\omega}^I_{E/I}$ are equal to $\mathbf{0}$. On the contrary, the

reference linear velocity and acceleration are

$$\begin{aligned} \bar{v}^{I}_{E/I,x} &= -r\omega \sin(\omega t), \\ \bar{v}^{I}_{E/I,y} &= r\omega \cos(\omega t), \\ \bar{v}^{I}_{E/I,z} &= 0 \end{aligned} \tag{5.9}$$

and

$$\begin{aligned} \dot{\bar{v}}^{I}_{E/I,x} &= -r\omega^2 \sin(\omega t), \\ \dot{\bar{v}}^{I}_{E/I,y} &= -r\omega^2 \cos(\omega t), \\ \dot{\bar{v}}^{I}_{E/I,z} &= 0. \end{aligned} \tag{5.10}$$

Eqs. (5.9) and (5.10) are used to create the quaternion form of the velocities and accelerations, $\nu^{I}_{E/I} = [0, \bar{v}^{I}_{E/I}]$ and $\dot{\nu}^{I}_{E/I} = [0, \dot{\bar{v}}^{I}_{E/I}]$; this leads to the reference dual velocity and acceleration, which evolve as

$$\begin{aligned} \boldsymbol{\omega}^{I}_{E/I} &= \omega^{I}_{E/I} + \epsilon(\nu^{I}_{E/I} + r^{I}_{E/I} \times \omega^{I}_{E/I}), \\ \dot{\boldsymbol{\omega}}^{I}_{E/I} &= \dot{\omega}^{I}_{E/I} + \epsilon(\dot{\nu}^{I}_{E/I} + r^{I}_{E/I} \times \dot{\omega}^{I}_{E/I} - \omega^{I}_{E/I} \times \nu^{I}_{E/I}). \end{aligned} \tag{5.11}$$

These dual reference quantities will be used to compute the error between the actual and the desired state, following the procedure outlined in Chapter 3.

5.5 Reference pose tracking: 3 different approaches

There are different ways to tackle Eq. (3.106); three different methods (see details in Secs. 5.5.1 to 5.5.3) are proposed in the following as a way to construct the control input. All the initial inertial velocities are null for every simulation; moreover, in order to compare the results, a unique pose trajectory is used, whose parameters are reported in Table 5.12.

Parameter	Value	Measurement unit
$\bar{r}_0$	$[0.5, 1, -0.08]^T$	$[m]$
ω	0.2	$[rad \cdot s^{-1}]$
r	0.2	$[m]$

Table 5.12: Reference pose parameters

The control proposed is the one illustrated in detail in Sec. 3.4.2, which is used to simultaneously stabilize the position of the base and follow the prescribed position and attitude with the end-effector. All the scalar and matrix gain of Eq. (3.106) are reported in Table 5.13:

Control gains			
Base		**End effector**	
$\tilde{K}_{\mathcal{B}}$	$\begin{bmatrix} 1 & 0 & 0 \\ 0 & 1 & 0 \\ 0 & 0 & 1 \end{bmatrix}$	$\tilde{K}_{\mathcal{E}_8}$	$\begin{bmatrix} 1 & 0 & 0 \\ 0 & 1 & 0 \\ 0 & 0 & 1 \end{bmatrix}$
$k_{\mathcal{B}}$	1	$k_{\mathcal{E}_8}$	3
$p_{\mathcal{B}}$	1	$p_{\mathcal{E}_8}$	3

Table 5.13: Control parameter for base and end effector pose tracking.

5.5.1 Pseudoinverse-based solution

The first way to find the nonlinear control input is the straight solution of equation $\tilde{u} = E(x)^+ b$, whose result is shown in Fig. 5.18. From $t = 5$ to $t = 10$, two different spikes can be detected. These are caused by a close-to-singular configuration, as described by Fig. 5.19: as expected, in correspondence with the spikes the manipulability index w approaches 0, give the close-to-singular value $\Gamma_6 = 0.0107$ [rad] (see Fig. 5.20).

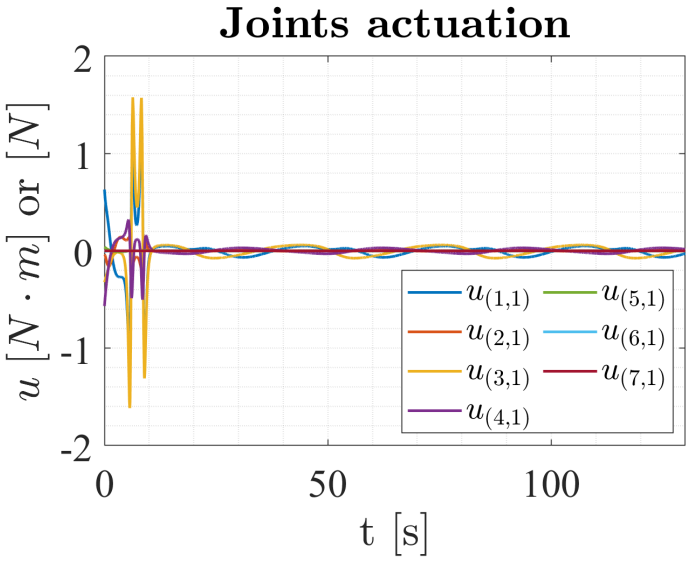

Figure 5.18: Control input

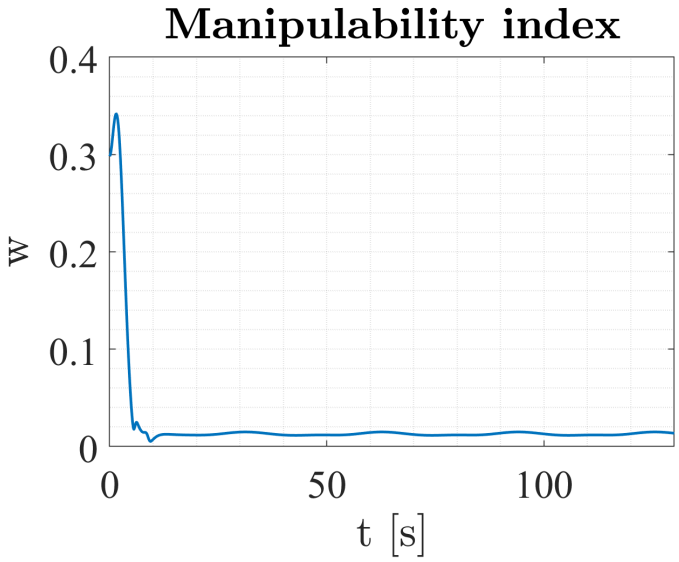

Figure 5.19: Manipulability index

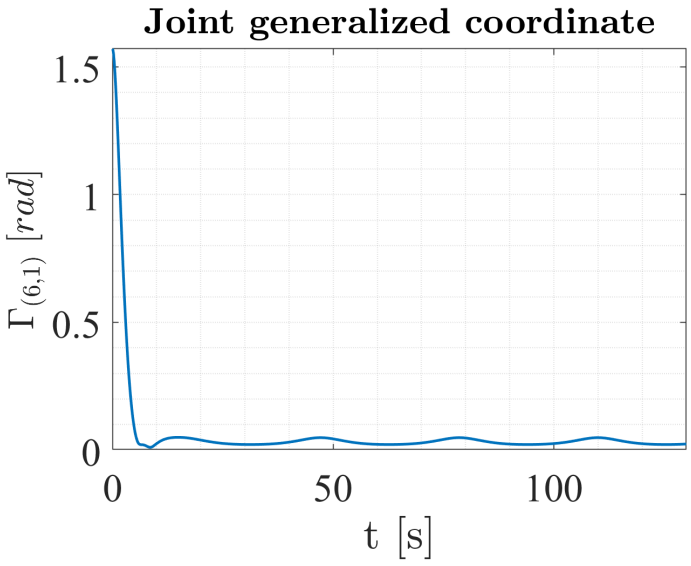

Figure 5.20: Evolution of the sixth joint angle

The pose tracking result is presented in Fig. 5.21, where it is possible to compare the reference trajectory to the one achieved by the control. The error in the pose tracking for this first method is also reported; dual quaternion pose and velocity error are plotted in Figs. 5.22 and 5.23, while position and attitude error are depicted Figs. 5.24 and 5.25.

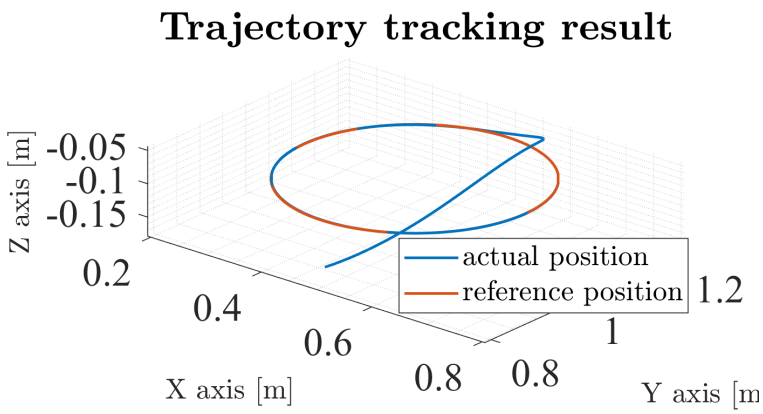

Figure 5.21: Pose tracking result

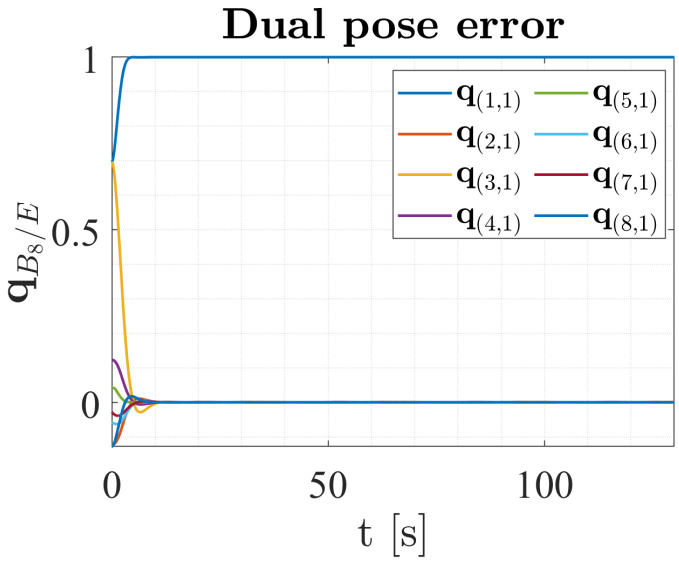

Figure 5.22: Dual pose error

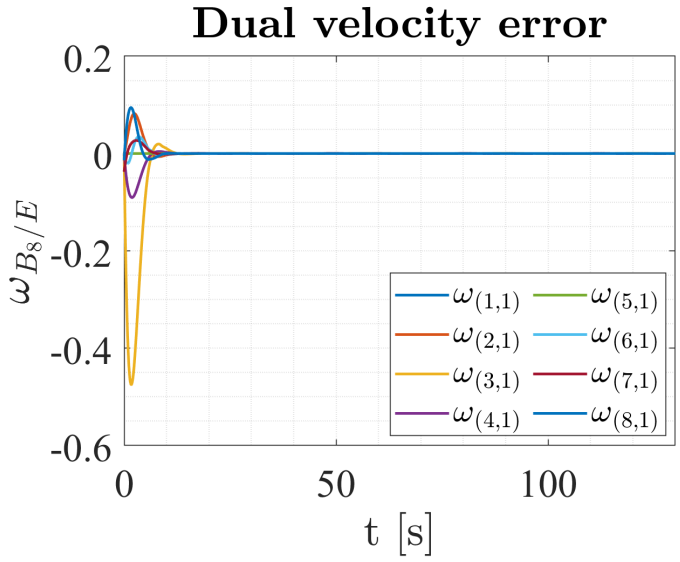

Figure 5.23: Dual velocity error

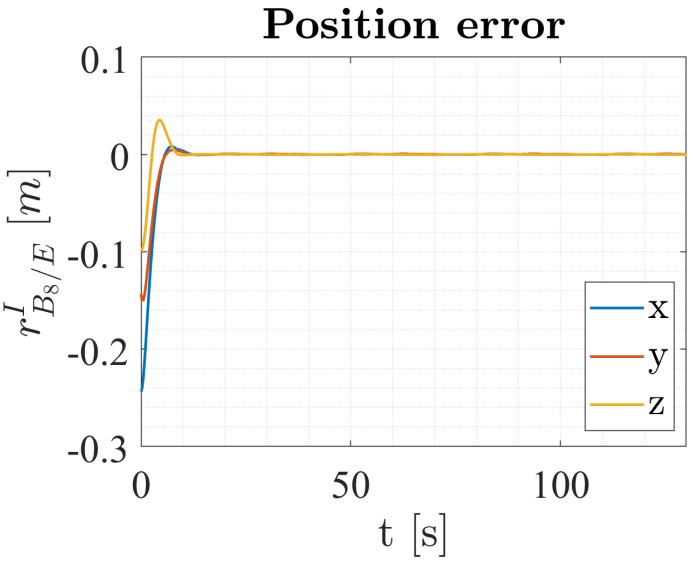

Figure 5.24: Position Error

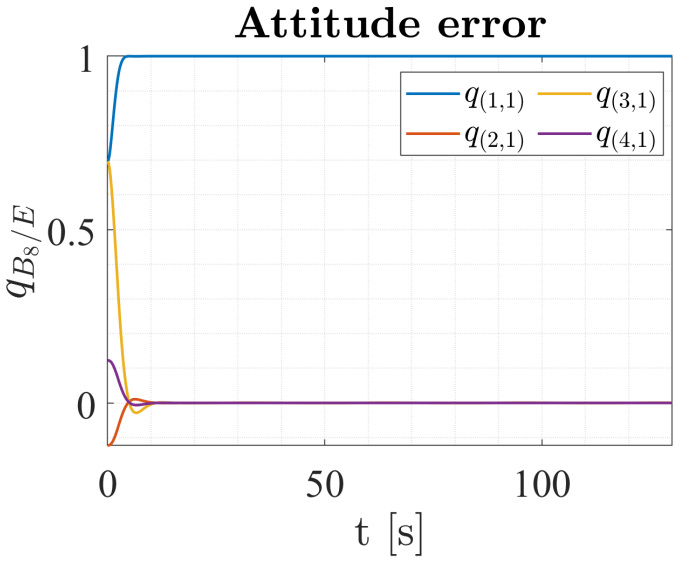

Figure 5.25: Attitude error

This first solution strategy features some problems when approaching to singularity, which result in an unsatisfactory profile of the input $\tilde{u}$. This happens when the joint angle Γ_6 moves from the initial folded position to the one needed to follow the reference input; on the other hand, Γ_4 is far from the singular condition $\Gamma_4 = 0$ and its evolution does not influence the quality of the solution.

5.5.2 Singular Direction Avoidance (SDA)

In order to better deal with singularities, a second way of solving the control equation is presented; this method is known as Singular Direction Avoidance (SDA).
As specified in Sec. 4.3.1, the SDA method is principally used to deal with near singular configurations of control moment gyros, and has therefore been adapted to our case; in order to solve Eq. (4.28) some parameters must be defined:

SDA parameters	
α_0	0.001
k_σ	10

Table 5.14: Parameter for singular direction avoidance control

The solution obtained using the SDA method is displayed in Fig. 5.26. Between t = 8.6 and t = 9.2 a single spike can be observed, in correspondence of the end of the singular zone of the pure pseudoinverse solution. The differences with respect to the previous solution can be found in comparison with Figs. 5.27 and 5.28. This time, the value of Γ_6 crosses the singular condition at 0° and the joint angle reaches negative values, as shown in Fig. 5.28. The condition $\Gamma_6 = 0$ and the subsequent trend, which consists in the repeated approach to 0° from the negative half-plane, brings the manipulability index close to 0 (Fig. 5.27) and yields an increase in the value of the joints actuation.

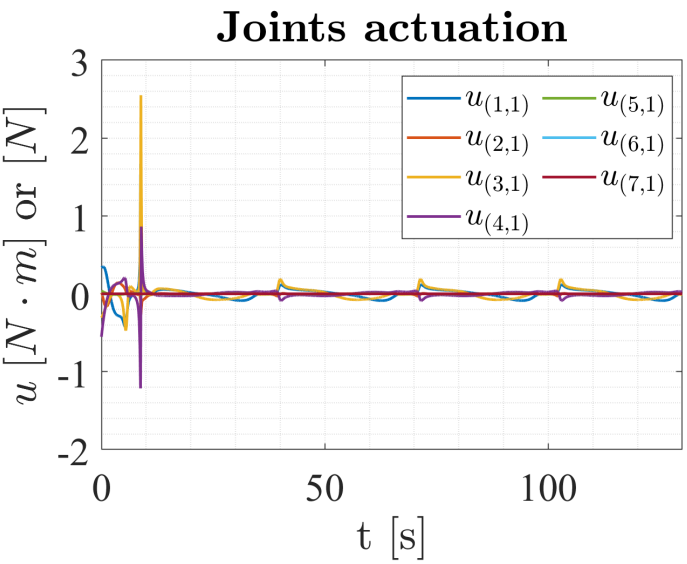

Figure 5.26: Control input with SDA

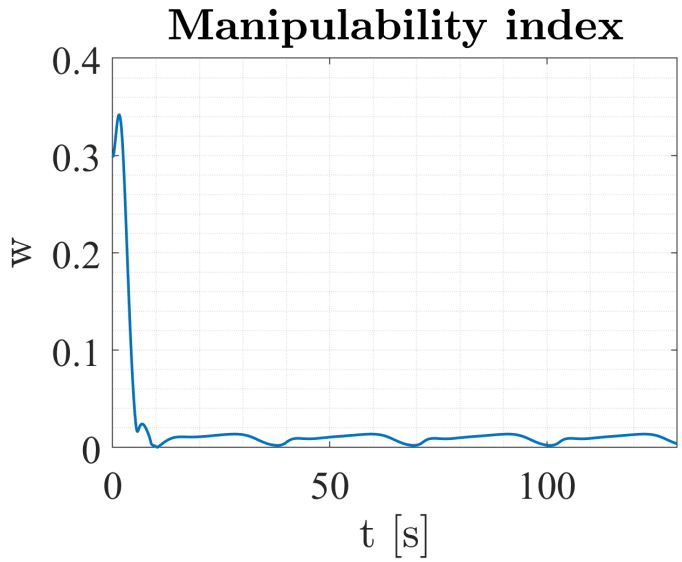

Figure 5.27: Manipulability index with SDA

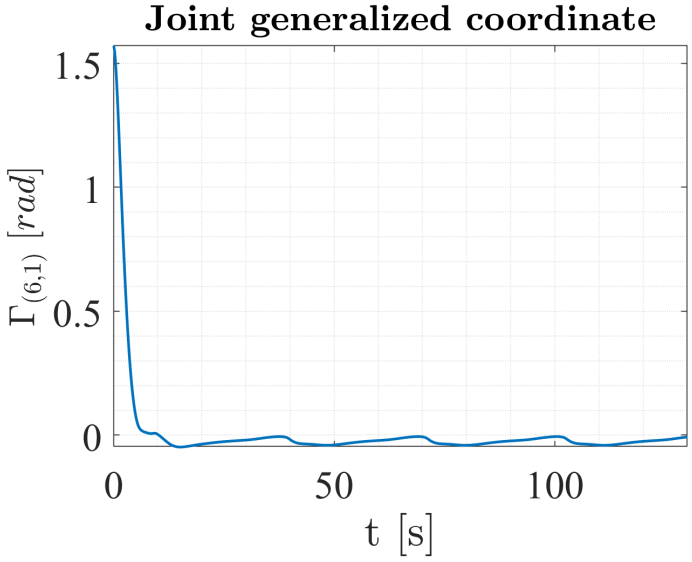

Figure 5.28: Evolution of the sixth joint angle with SDA

The pose tracking result can be observed in Fig. 5.29, while the dual quaternion error is described in Figs. 5.30 and 5.31. Fig. 5.32 shows a less satisfactory behavior of the position error obtained by

the SDA, in relation to the first method. An increase in the deviation from the reference trajectory is observed when there is a reduction in the manipulability index; this happens because, in order to pass through the singularity, the algorithm performs a variation of the singular values in matrix Σ, hence decreasing tracking accuracy. This mainly happens for the position, as it is can be observed comparing Fig. 5.32 and Fig. 5.33.

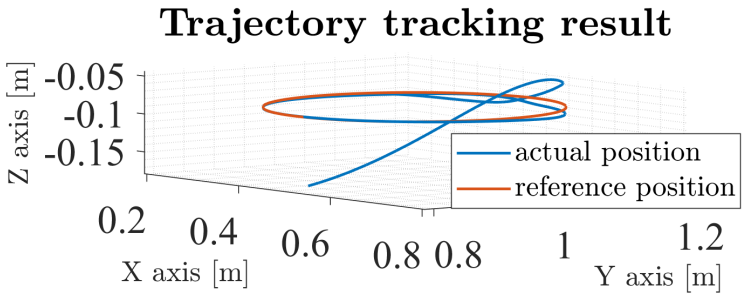

Figure 5.29: Pose tracking with SDA

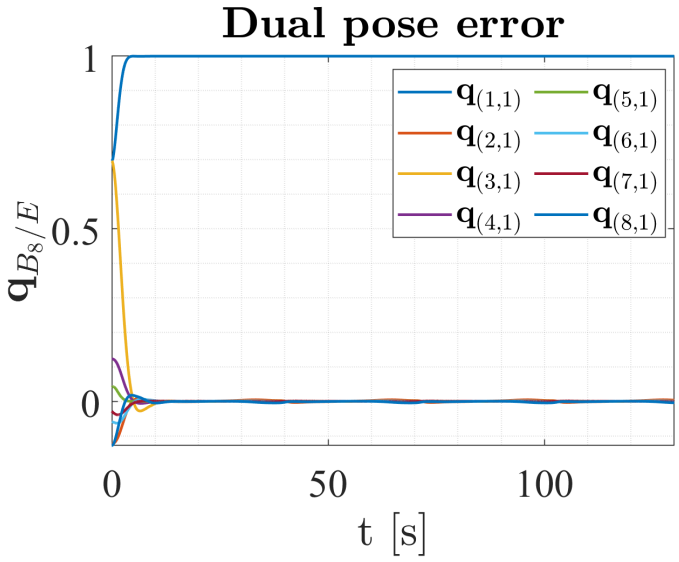

Figure 5.30: Dual pose error with SDA

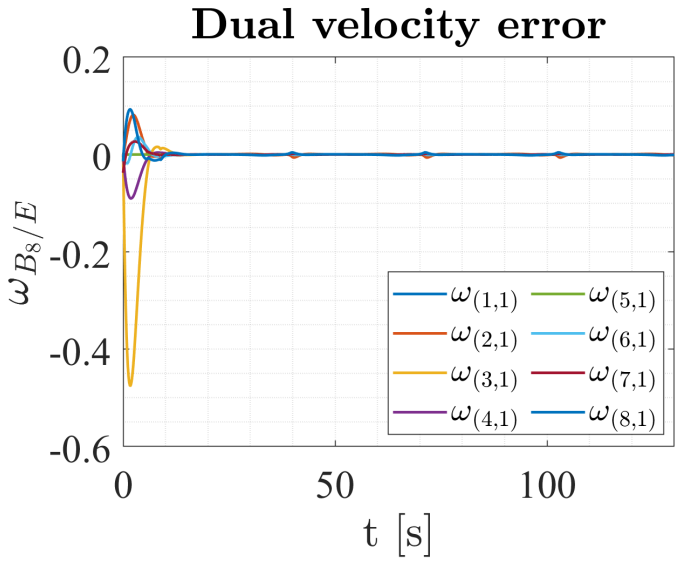

Figure 5.31: Dual velocity error with SDA

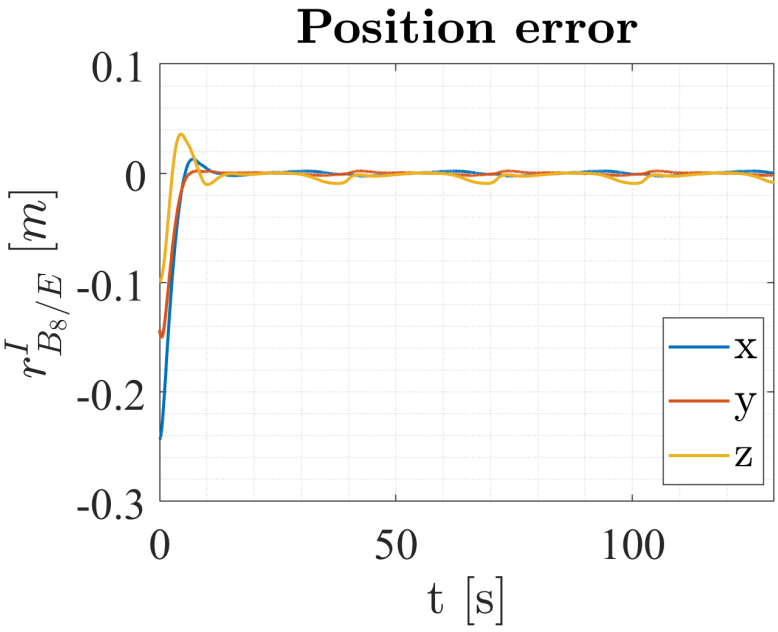

Figure 5.32: Position error with SDA

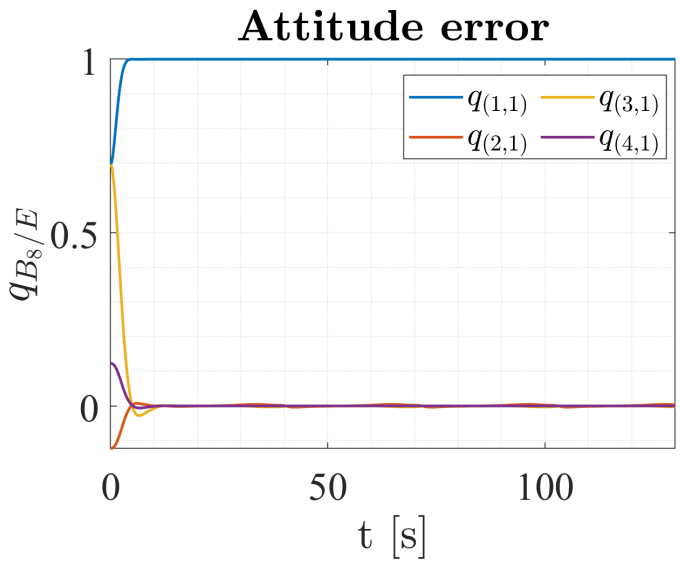

Figure 5.33: Attitude error with SDA

In conclusion, the solution achieved by the SDA method is able

to cross singular configurations, but in doing so it loses tracking accuracy, hence resulting in a larger errors.

5.5.3 Control Barrier Functions (CBFs)

The last solution, which has been explained in Sec. 4.3.3, is focused on singularity avoidance through the use of control barrier functions. In this way it is possible to prevent the spikes in Figs. 5.18 and 5.26 by avoiding singular conditions; the parameters present in the CBFs formulation are described in Table 5.15, while the results coming from the solution of the CLF-CBF-QP are expressed in Fig. 5.34.

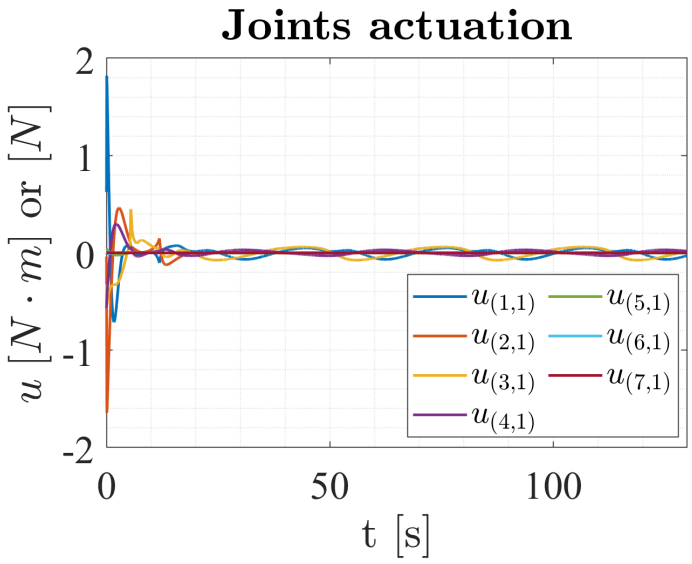

Figure 5.34: Control input with CBFs

CBF PARAMETERS			
Wrist		**Elbow**	
$H_\delta = 10^{-5}$			
a_w	150	a_e	1
b_w	50	b_e	1
c_w	10	c_e	1

Table 5.15: Control barrier function parameters

As we can see from Fig. 5.34, no spikes are present in the profile of the control input. In the first part of the simulation, when the manipulator moves from the initial folded position, higher values of the input torques are needed in order to reach the desired angle Γ_6 without crossing the singular condition. This variation in the overall movement of the arm can be observed in the path of the end effector in Fig. 5.35, and it clearly has a counterpart in the evolution of Γ_2 in Fig. 5.36. This leads to a slower variation of Γ_6 in Fig. 5.38, and to a minimum value of the manipulability index that is higher (Fig. 5.42) than the ones in the previous examples.

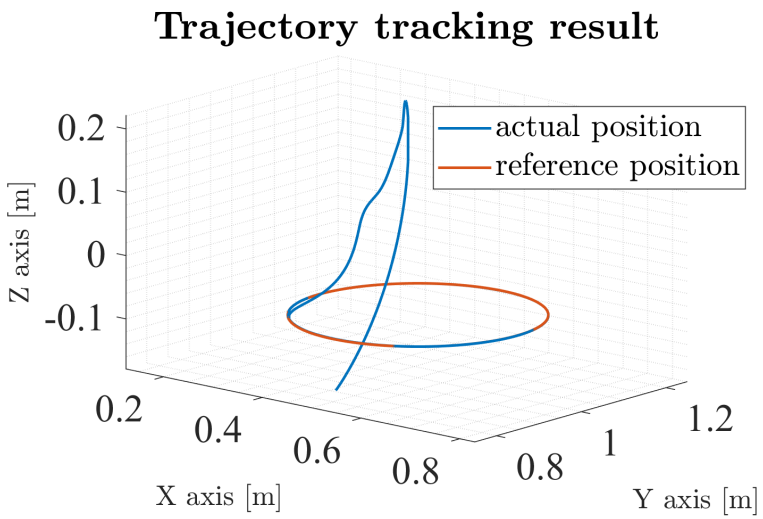

Figure 5.35: Pose tracking with CBFs

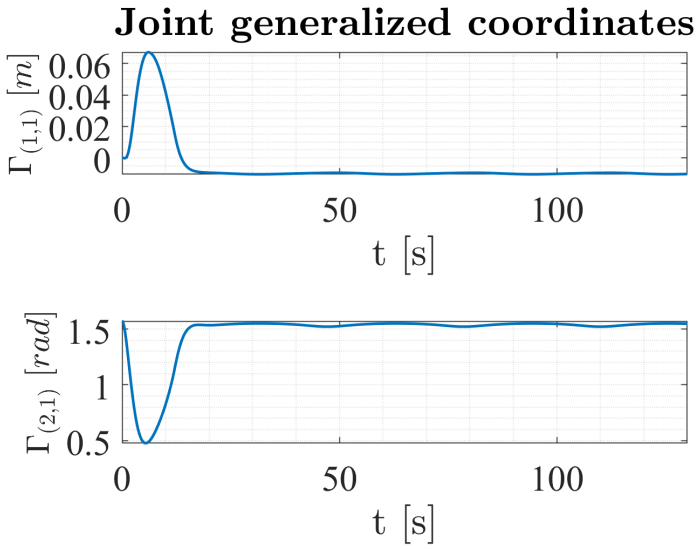

Figure 5.36: Joints coordinates with CBFs

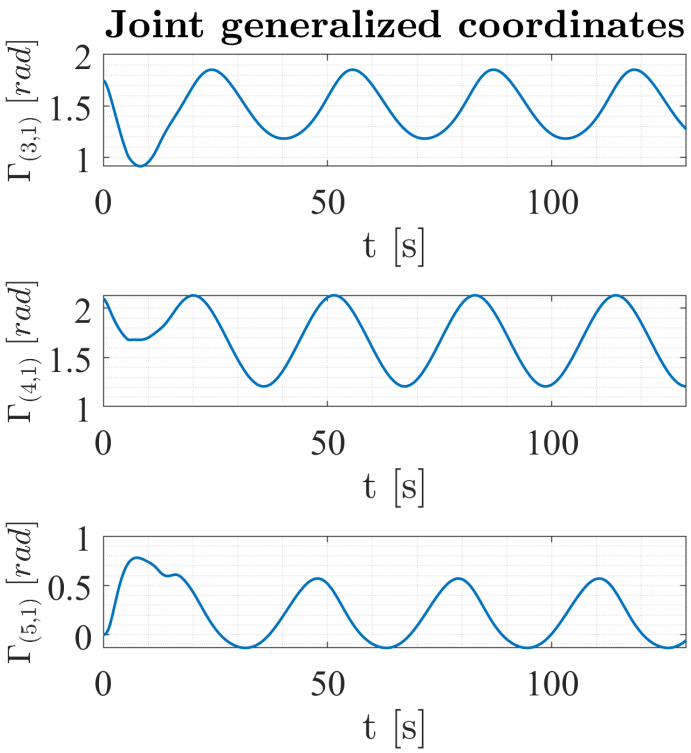

Figure 5.37: Joints coordinates with CBFs

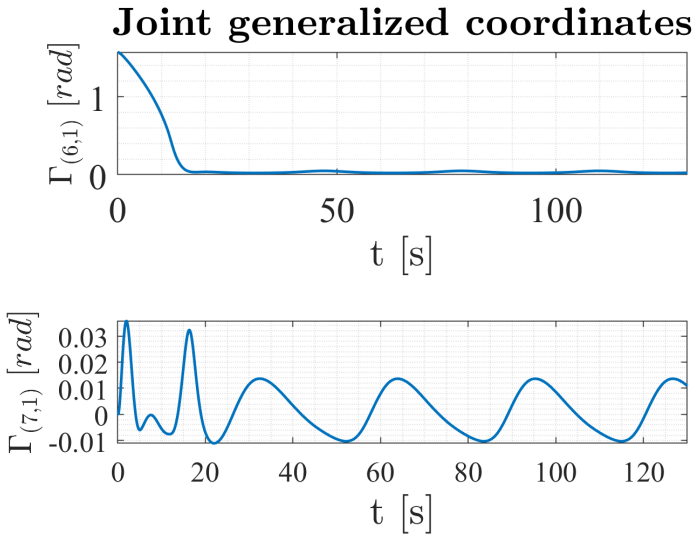

Figure 5.38: Joints coordinates with CBFs

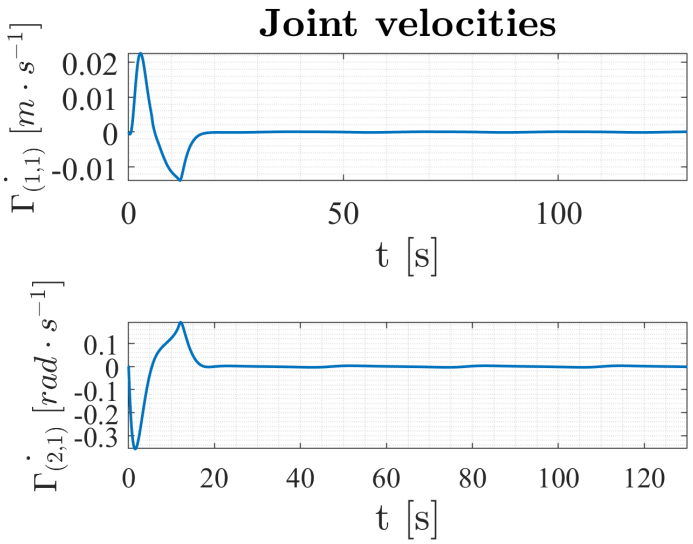

Figure 5.39: Joint velocities with CBFs

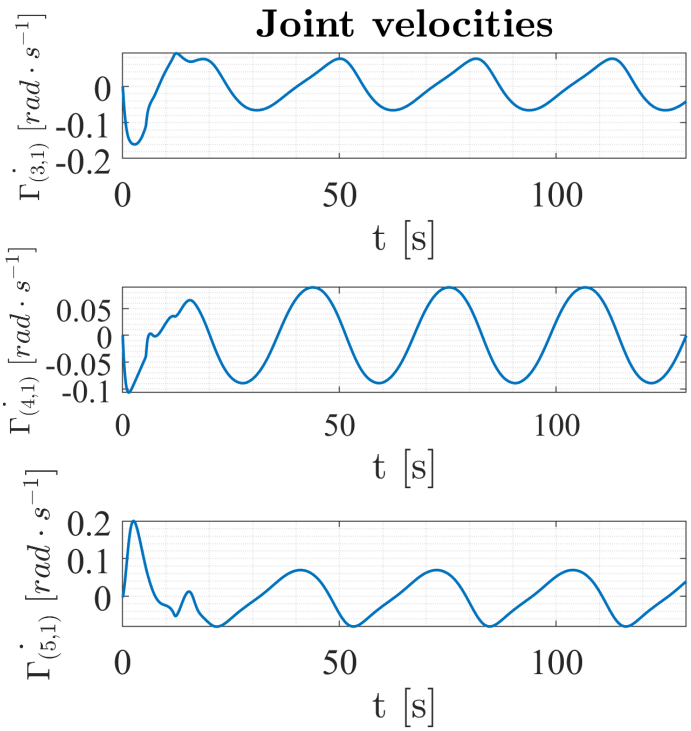

Figure 5.40: Joint velocities with CBFs

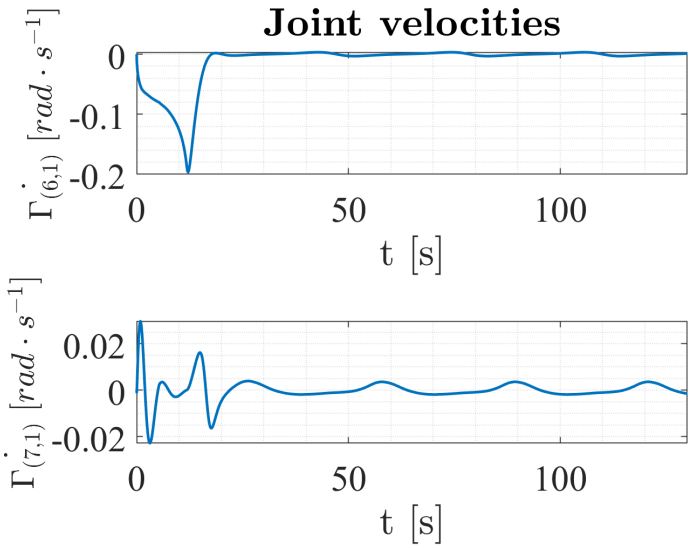

Figure 5.41: Joint velocities with CBFs

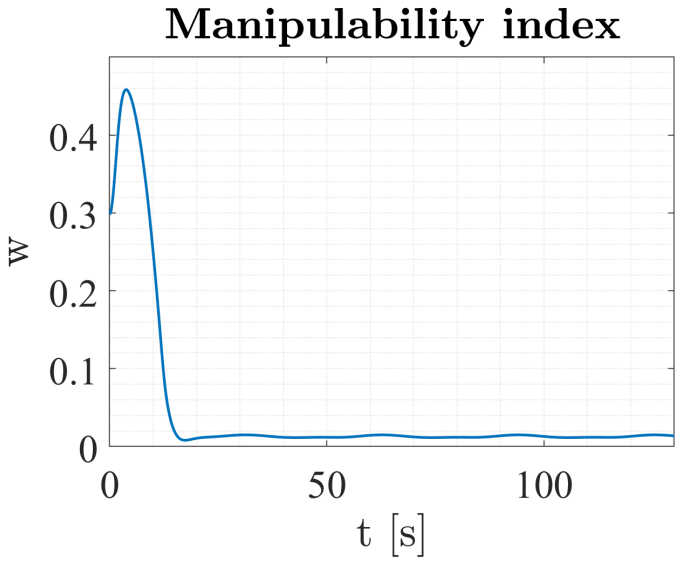

Figure 5.42: Manipulabity index with CBFs

The error is hereby reported in dual form (Figs. 5.43 and 5.44); for the sake of clarity, it can be also decomposed in attitude and position error (Figs. 5.45 and 5.46).

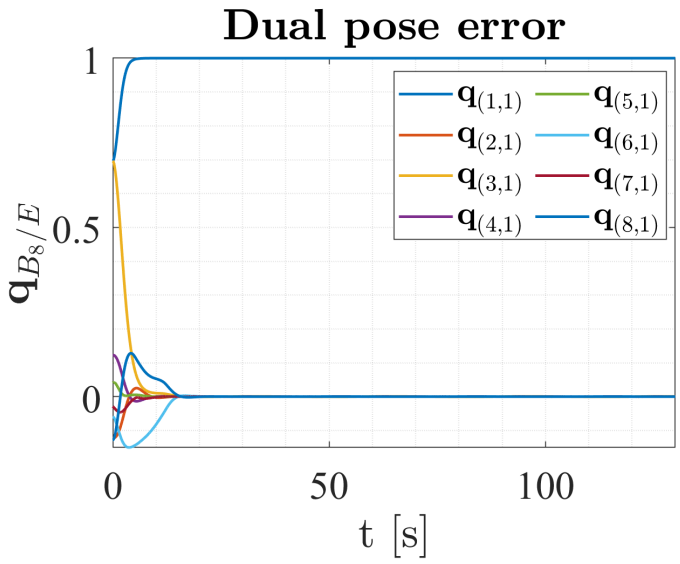

Figure 5.43: Dual pose error with CBFs

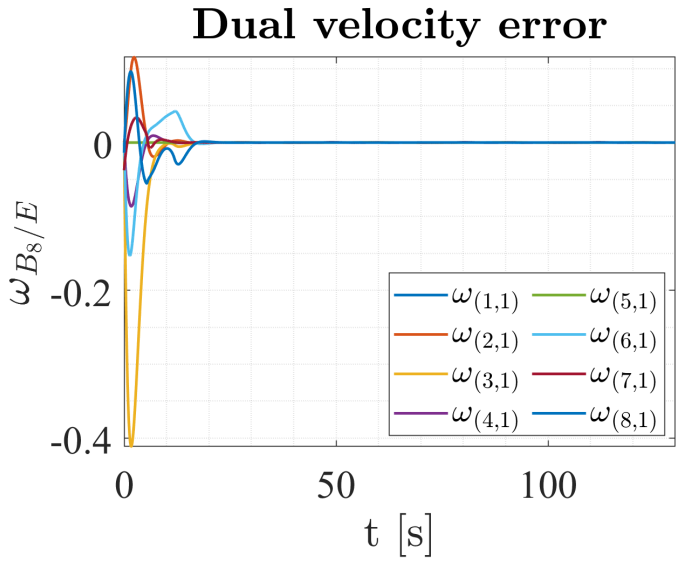

Figure 5.44: Dual velocity error with CBFs

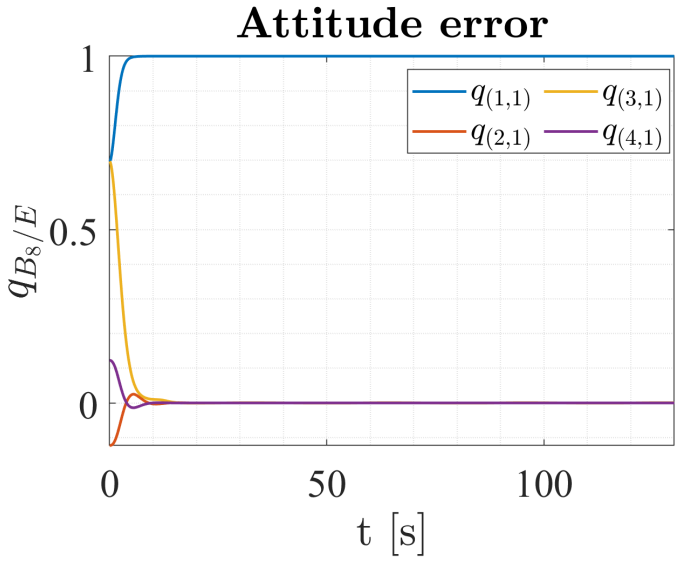

Figure 5.45: Attitude error with CBFs

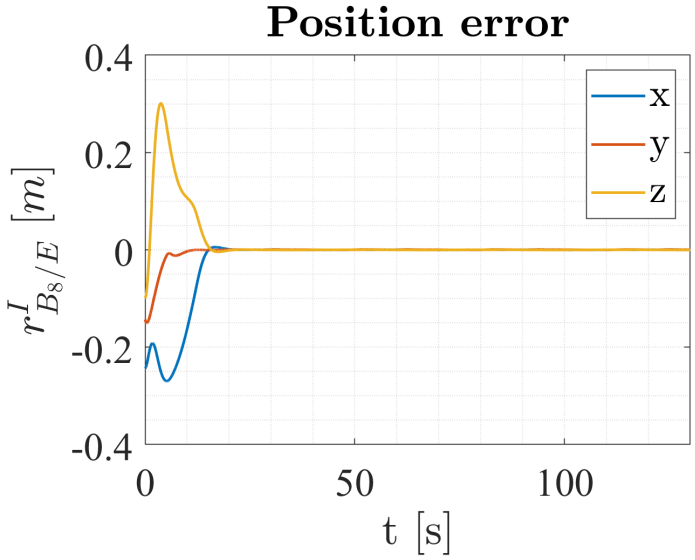

Figure 5.46: Position error with CBFs

It is possible to compare the motion generated by the nonlinear controller with the CBFs based method to the other simulations in Fig. 5.47; as explained before, the manipulator exploits a larger

variation of Γ_2 to obtain the same orientation of the end effector, as shown in Figs. 5.48 and 5.49. A significant variation of Γ_2 can be noticed, along with a slower decrease of Γ_6. This coordinated movement prevents the manipulabitity index from reaching the value of the first two simulations (Fig. 5.50), thus proving to be effective in avoiding the singular condition. In order to compare the different strategies in terms of accuracy, the norm of the different position errors are reported in Fig. 5.54; a clear discrepancy between SDA and the other simulations can be noticed.

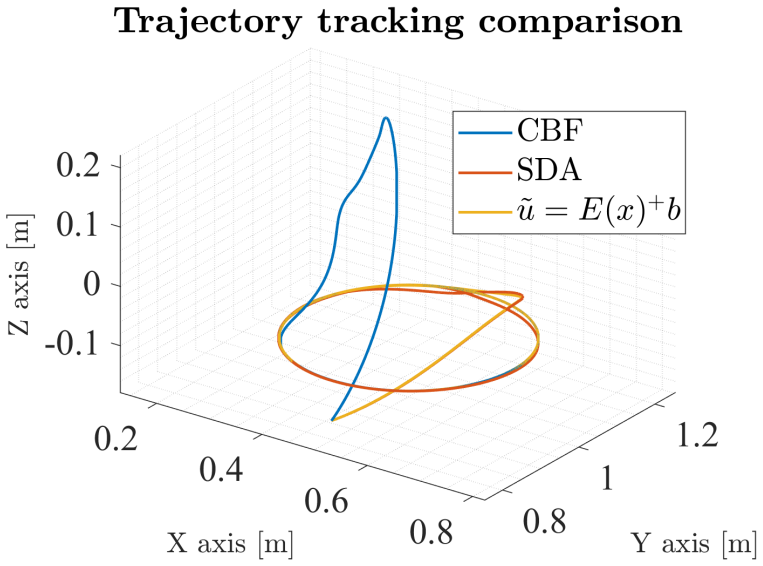

Figure 5.47: Comparison of the pose tracking results

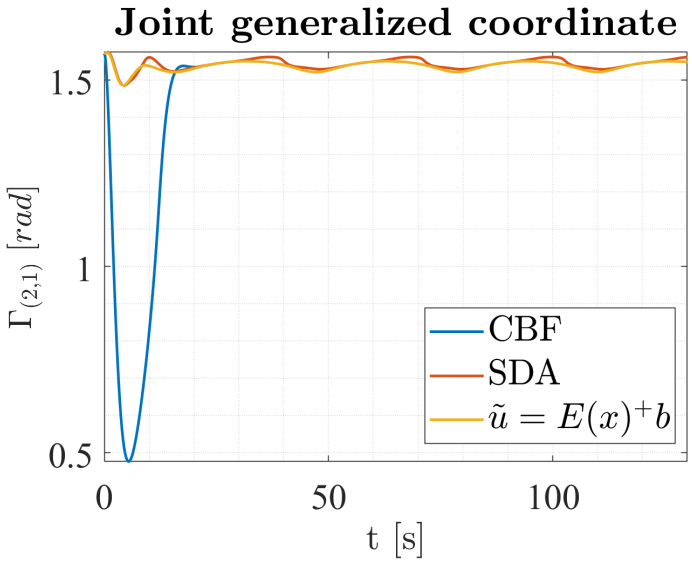

Figure 5.48: Comparison of the evolution of the second joint coordinate

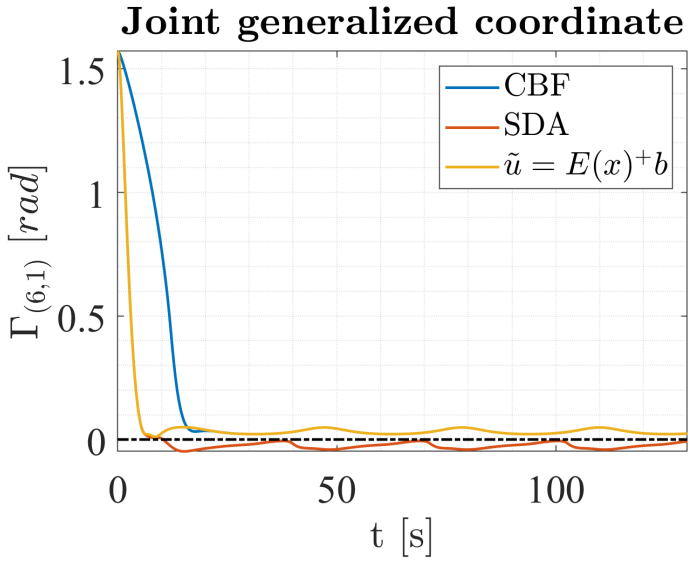

Figure 5.49: Comparison of the evolution of the sixth joint coordinate

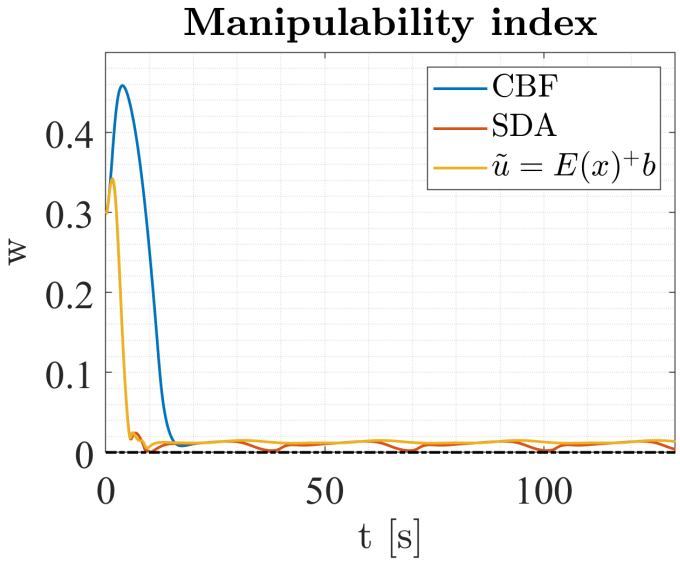

Figure 5.50: Comparison of the manipulability indices

It can be concluded that the control input does not fall into the initial singularity, which was always present when using the previous methods; the control effort is featured by higher initial values that are necessary to create the different path of the end-effector. It is important to notice that the solution originated by $\tilde{u} = E(x)^{+}b$ differs from the CBFs solution only in the first part of the simulation; after the singular condition is passed, the two solutions become equal.

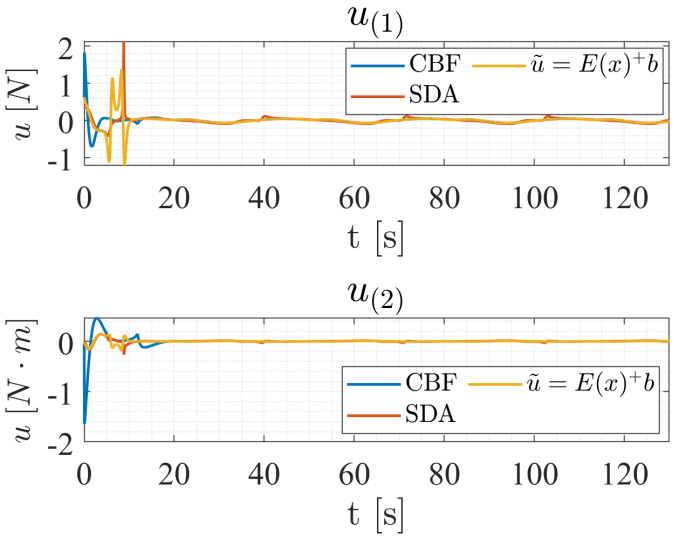

Figure 5.51: Comparison of the control inputs for the first two joints

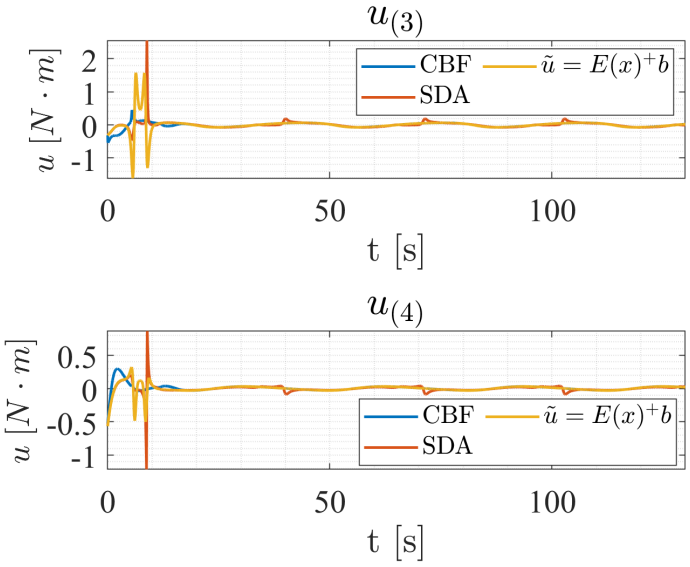

Figure 5.52: Comparison of the control inputs for the third and fourth joints

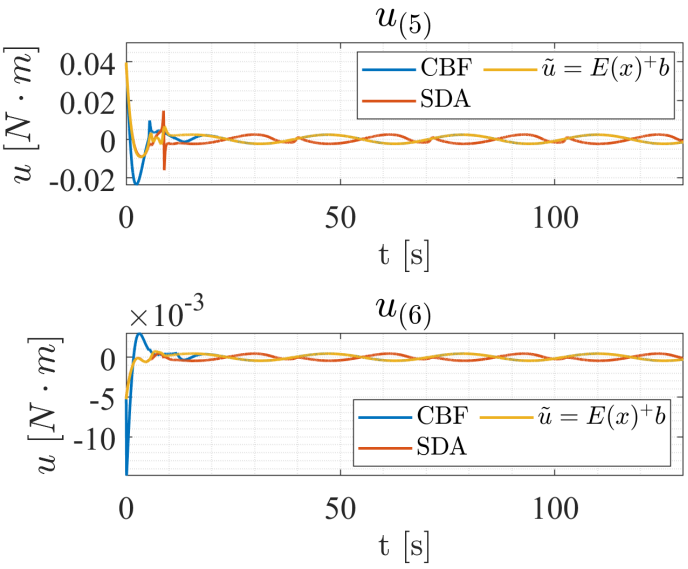

Figure 5.53: Comparison of the control inputs for the fifth and sixth joints

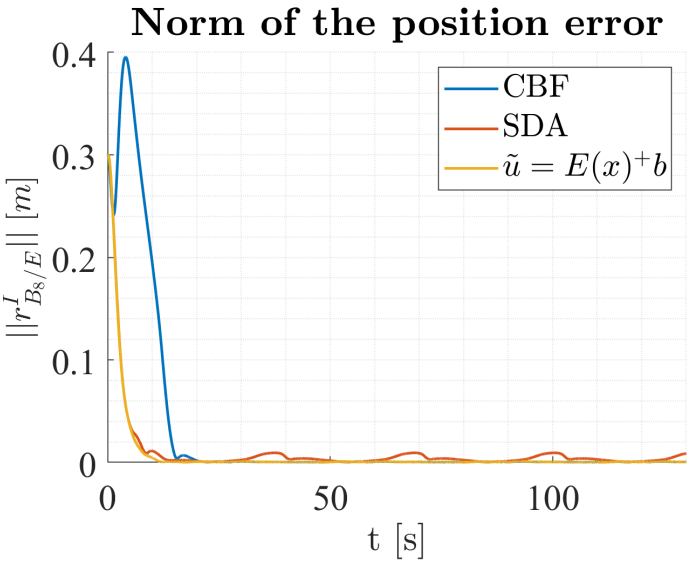

Figure 5.54: Comparison of the norm of the position error

5.6 CLF-CBF-QP: a comparison between different cases

The addition of control barrier functions to the nonlinear controller leads to a solution that keeps the evolution of the state in a safe set, thus avoiding singularities. For this reason, we will exploit the benefits illustrated in Sec. 5.5 by applying this type of control to different cases; in the last part we will introduce a disturbance to prove robustness of the proposed approach. In order to add complexity to the simulation, the circular reference trajectory is moved out of the reachability of the UR10e; therefore, in order to preserve tracking capability, a new logic for the manipulator control has been developed.

Parameter	Value	Measurement unit
$\bar{r}_0$	$[2, 1, -0.08]^T$	$[m]$
ω	0.2	$[rad \cdot s^{-1}]$
r	0.2	$[m]$

Table 5.16: Reference pose parameters

The main idea is that the control related to the end effector pose tracking should be enabled when the base of the arm is at a distance $\frac{\delta}{2}$ from the center of the desired path; thus, at the beginning of the simulation, the model evaluates the distance which the manipulator has to cover along the X-axis. The quantity Δx is defined in order to reach the desired X coordinate, which corresponds to a $\frac{\delta}{2}$ distance of the base from the center of the target trajectory. Hence,

$$\Delta x = -\left(\left\| r^I_{e_2/I,x} - \bar{r}_{0,x} \right\| - \frac{\delta}{2}\right) \text{sign}(r^I_{e_2/I,x} - \bar{r}_{0,x}), \tag{5.12}$$

where $\left\| r^I_{e_2/I,x} - \bar{r}_{0,x} \right\| = \|\Delta x\| + \frac{\delta}{2}$; by adding Δx to $r^I_{e_2/I}$, a new value

of $\mathbf{q}_{S/I}$ is obtained and can be plugged into Eq. (3.106), as in

$$\begin{aligned} r^I_{S/I} &= r^I_{\bullet_2/I} + [0, \Delta x, 0, 0]^T, \\ \mathbf{q}_{S/I} &= q_{S/I} + \epsilon \left(\frac{1}{2} r^I_{s/i} q_{S/I} \right). \end{aligned} \tag{5.13}$$

Using these quantities in the Lyapunov function, we obtain that the new position of the base is a stable equilibrium solution of the controlled system. When the base is moving, the arm is actively kept in the initial configuration described in Table 5.5, through the control illustrated in Sec. 3.4.1. In this way even if the base is moving, the initial folded configuration of the manipulator is conserved.

If the base of the arm is further than $\frac{\delta}{2}$ plus a tunable tolerance factor from the desired position, it will start moving to the aforementioned optimal position; the rationale behind the margin factor is to allow a minimal motion of the base during the tracking phase. In order to initialize the end effector pose tracking when the manipulator is in a rest condition, a check on the velocity of the joints coordinates is added; when $\dot{\Gamma} \cdot \dot{\Gamma} < 10^{-5}$, the controller start moving the end effector to track the desired trajectory.

Adding a constraint on the residual velocities means also being sure that the initial position is exactly the one desired ($r^I_{\bullet_2/I} = r^I_{S/I}$); this happens because the condition on the velocities is more conservative, while the term $\delta/2 + \text{margin}$ allows the base to move during the pose tracking phase. The parameters describing the control in Sec. 3.4.1 are:

Arm stabilization parameters	
K_ν	5
K_s	5
K_p	5
$k_{\bullet_B}$	1
$p_{\bullet_B}$	0.3

Table 5.17: Parameters of the arm/base stabilization control

$k_{\bullet_B}$ and $p_{\bullet_B}$ have been modified with respect to the values reported in Table 5.13 in order to reduce the force acting on the prismatic joint, even when its position error is large; as a side effect, also the torques needed to stabilize the arm are lower.

A first example is hereby displayed using the CBFs based control. The discontinuity at $t = 25$ shows the switch between the control in charge of moving the UR10e to the desired $r^I_{S/I}$ and the pose tracking control (Fig. 5.56). As in the example in Sec. 5.5, the manipulabity index shows no singularity even if Γ_6 tends to 0° (see Fig. 5.60); the end effector follows a path which, thanks to the variation of Γ_2, is able to avoid the singularity (Fig. 5.58).

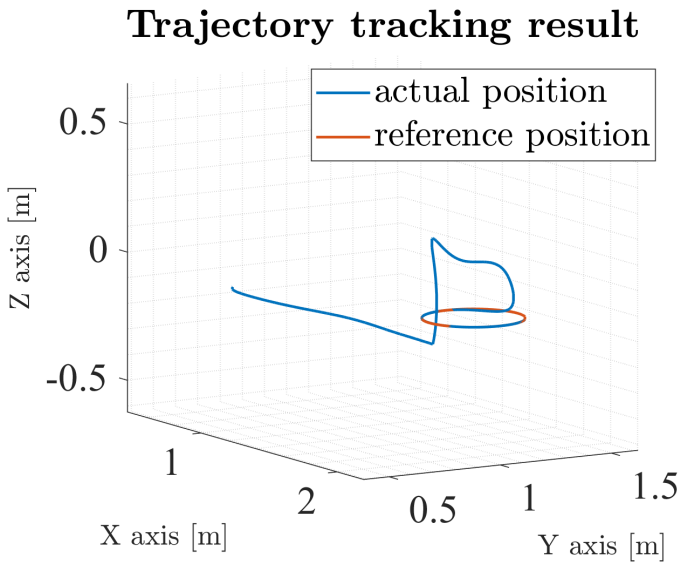

Figure 5.55: Pose tracking with CBFs

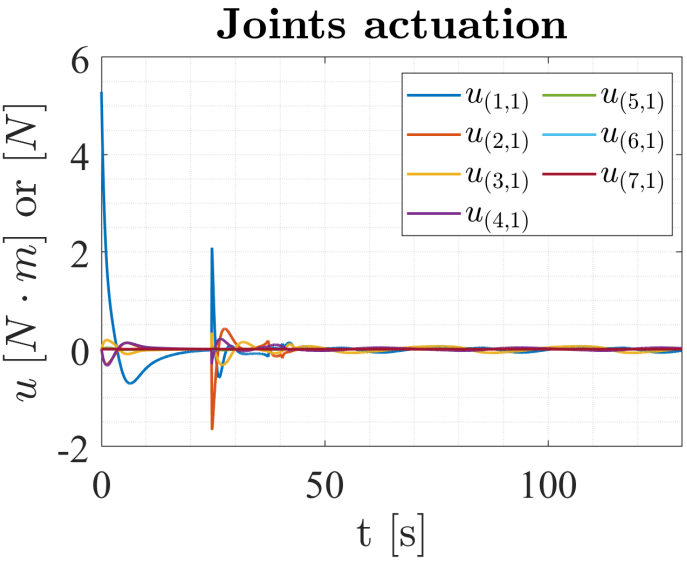

Figure 5.56: Joints actuation with CBFs

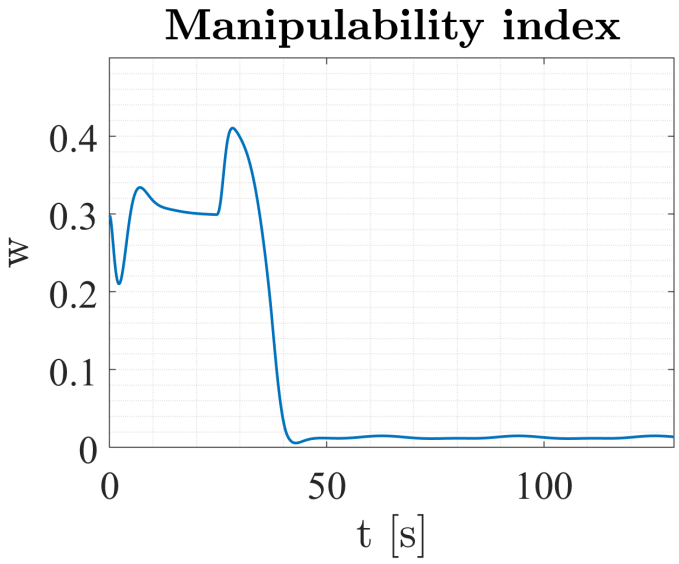

Figure 5.57: Manipulability index with CBFs

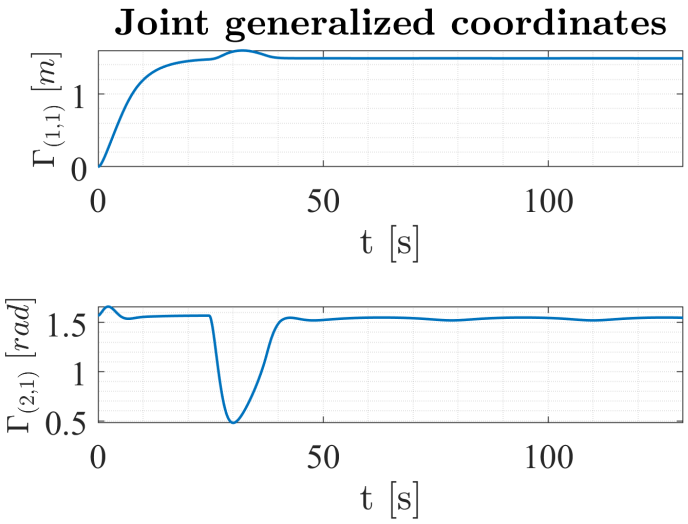

Figure 5.58: Joints generalized coordinates with CBFs

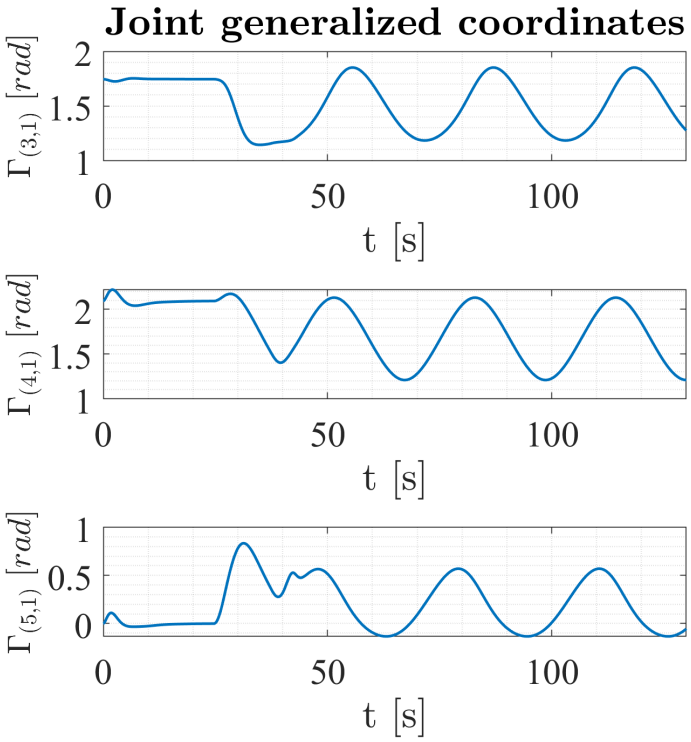

Figure 5.59: Joints generalized coordinates with CBFs

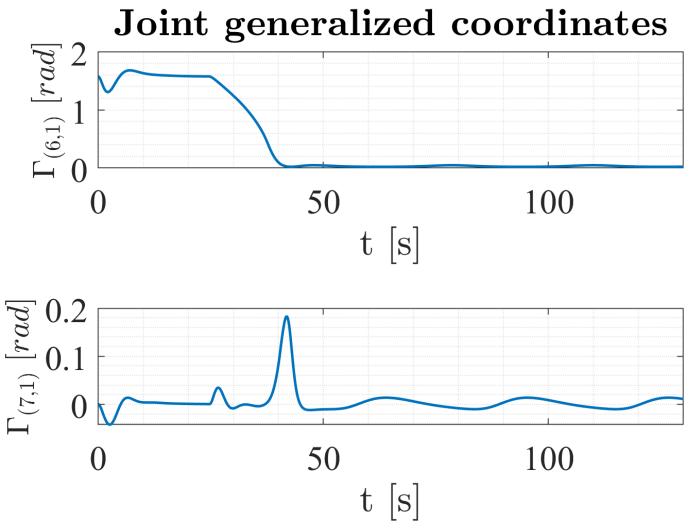

Figure 5.60: Joints generalized coordinates with CBFs

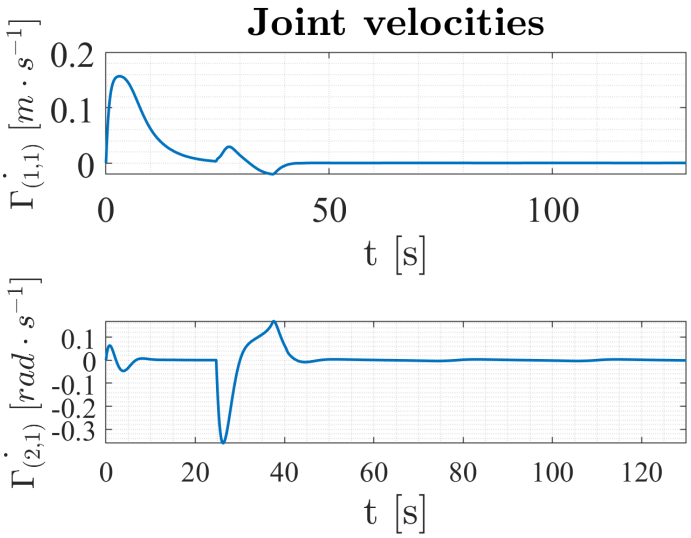

Figure 5.61: Joints velocities with CBFs

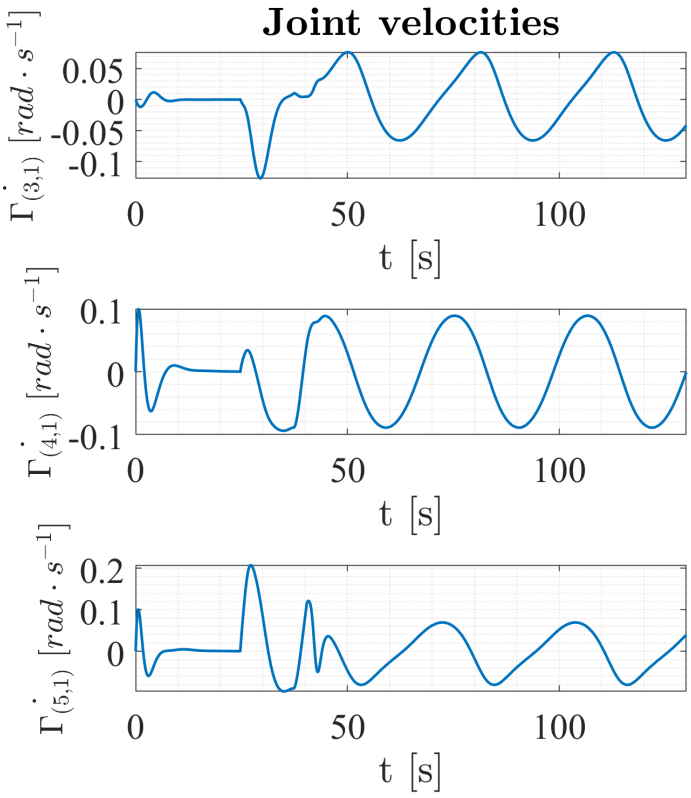

Figure 5.62: Joints velocities with CBFs

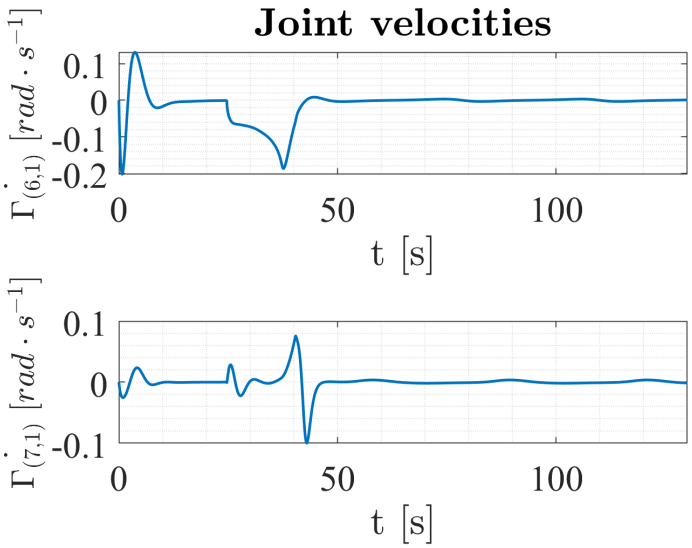

Figure 5.63: Joints velocities with CBFs

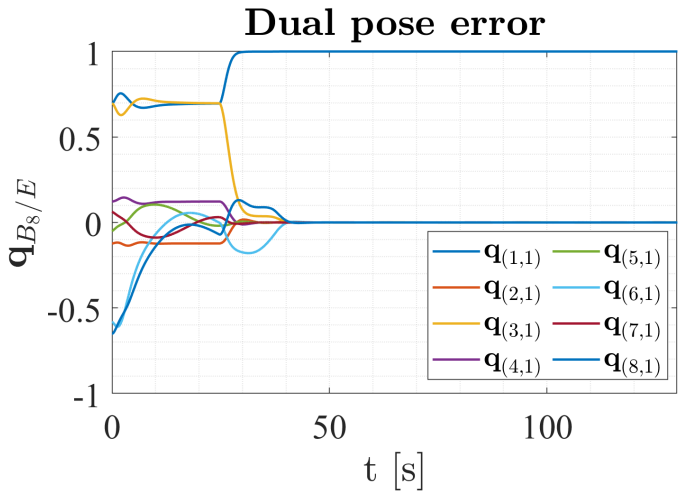

Figure 5.64: Dual pose error with CBFs

With regards to the error in the pose tracking, after the initial part in which the base is being moved to its target position, it converges to the prescribed path as shown in Fig. 5.64

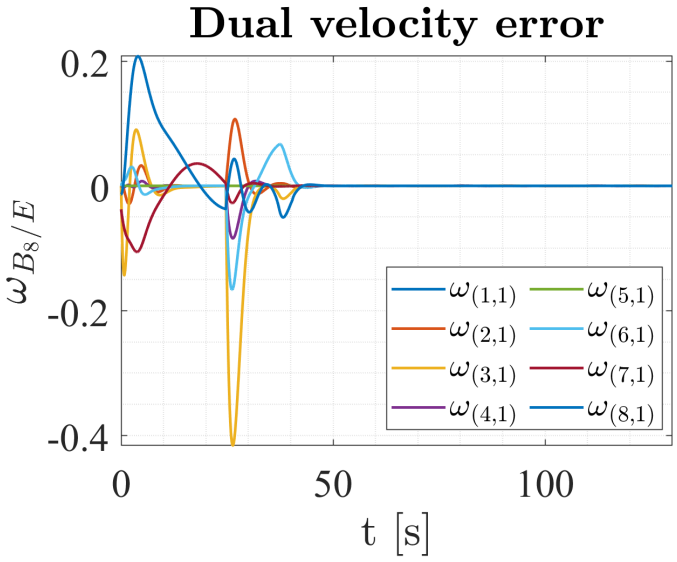

Figure 5.65: Dual velocity error with CBFs

Once again, the dual pose error is divided into attitude and position error to better understand the convergence of the two different quantities.

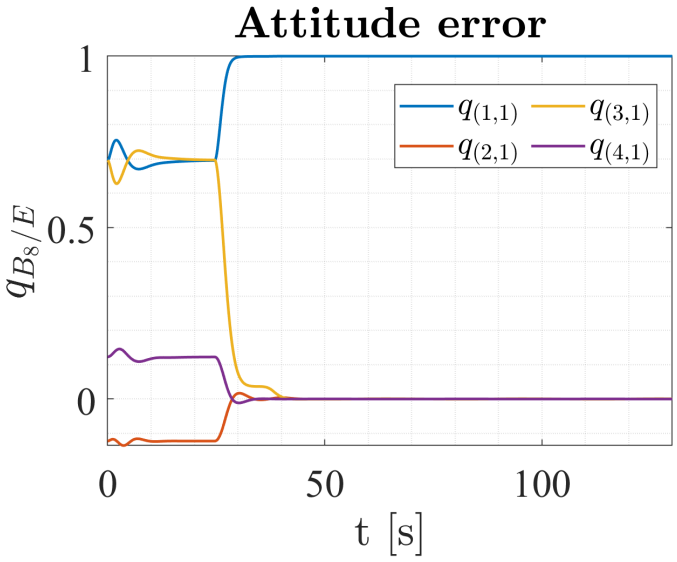

Figure 5.66: Attitude error with CBFs

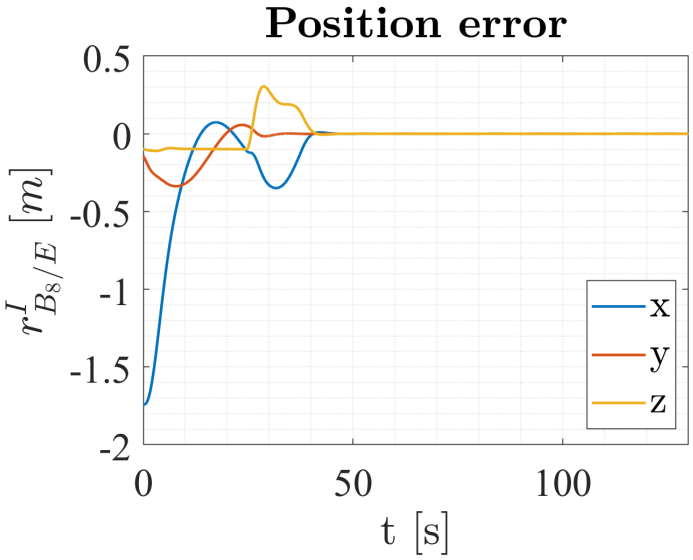

Figure 5.67: Position error with CBFs

5.6.1 Disturbances

In order to prove the robustness of the control algorithm, a disturbance is applied on the base of the UR10e. The disturbance force acts on the second body, which is the child body of the prismatic joint. The disturbance is modeled as a sinusoidal force acting in the X inertial direction; the amplitude of the disturbance and the frequency of the excitation are reported in Table 5.18.

$$W^{\mathcal{F}_2}_{\mathcal{F}_2,x} = A \sin(\omega_{dis} t) \tag{5.14}$$

Disturbance characterization	
ω_{dis}	10 [rad · s^{-1}]
A	0.25 [N]

Table 5.18: Parameters characterizing the disturbance force

The disturbance applied to the second body leads to a higher

control effort on the prismatic joint (Fig. 5.69), which is in charge of counteracting the external solicitation; the control is however able to avoid singularity and track the trajectory, with an evolution of the joint coordinates which is similar to the one already shown.

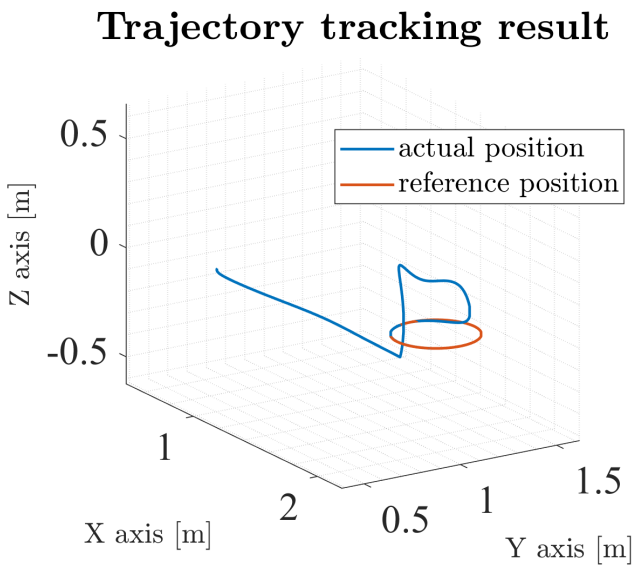

Figure 5.68: Disturbed pose tracking with CBFs

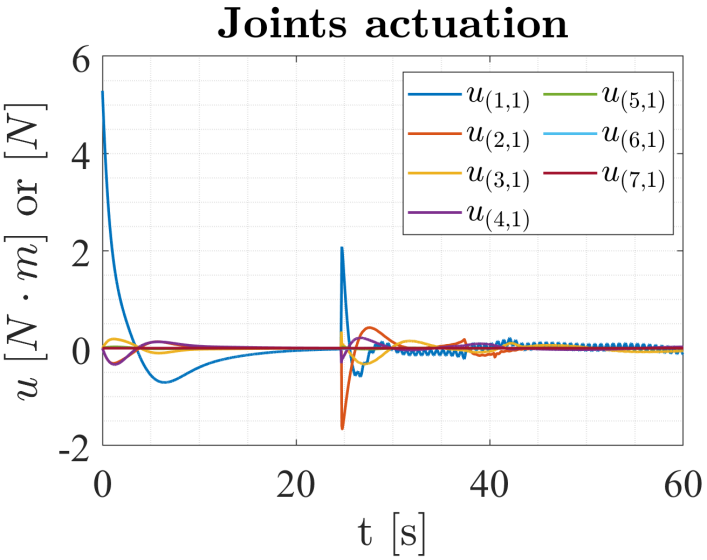

Figure 5.69: Joint actuation with CBFs in the disturbed case

The pose tracking accuracy is not influenced by the disturbance; the errors in terms of pose and velocity are also reported.

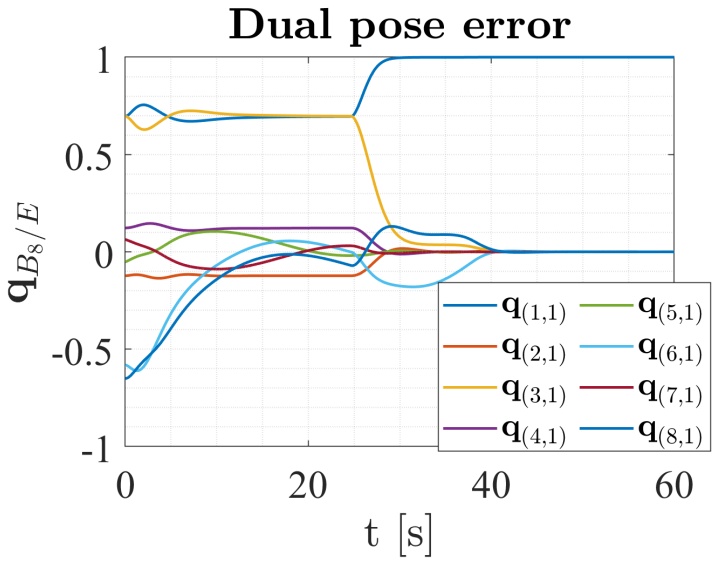

Figure 5.70: Dual pose error with CBFs and disturbance

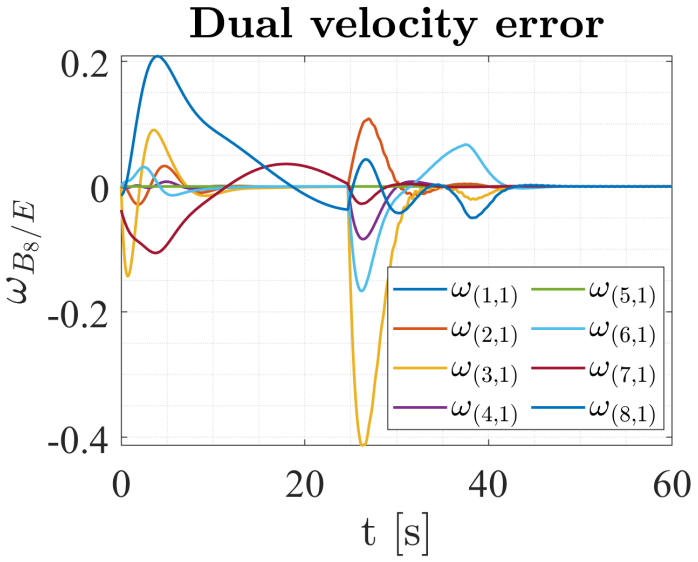

Figure 5.71: Dual velocity error with CBFs and disturbance

If the same pose tracking is required and no control barrier function are used, the joints actuation profile features the presence of spikes during in first part of the trajectory, when the UR10e has to move from the folded position to the reference one Fig. 5.73.

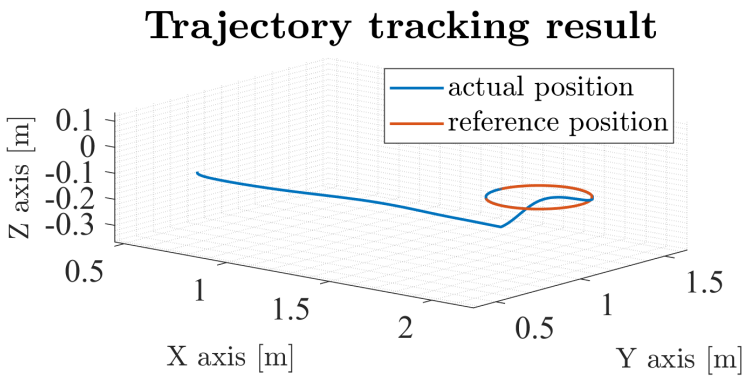

Figure 5.72: Disturbed pose tracking without CBFs

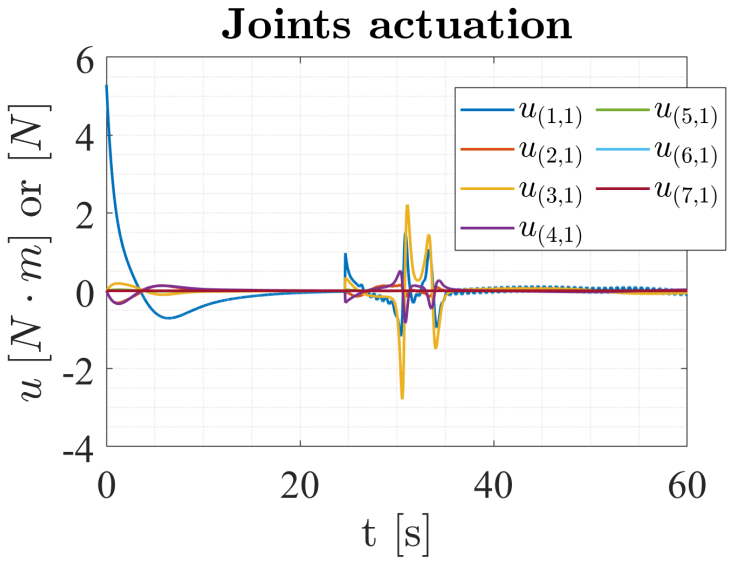

Figure 5.73: Disturbed joints actuation without CBFs

Even if the singularity occurs, it does not influence the pose tracking capability in terms of pose and velocities.

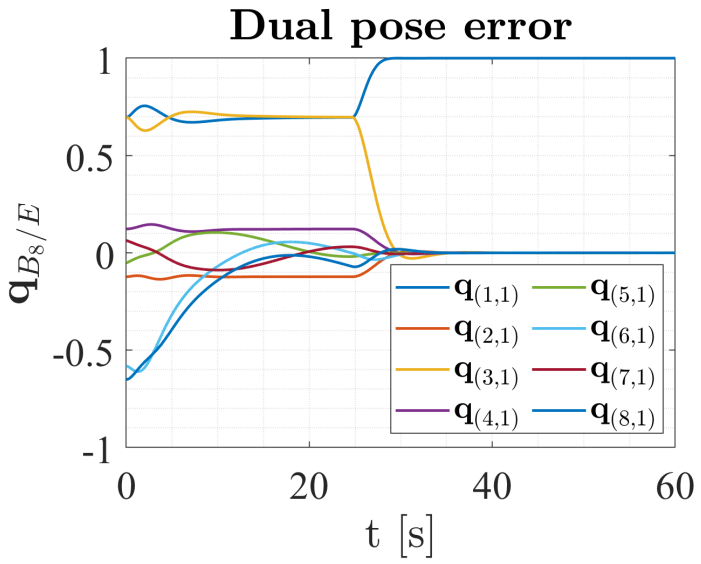

Figure 5.74: Dual pose error without CBFs, with disturbance

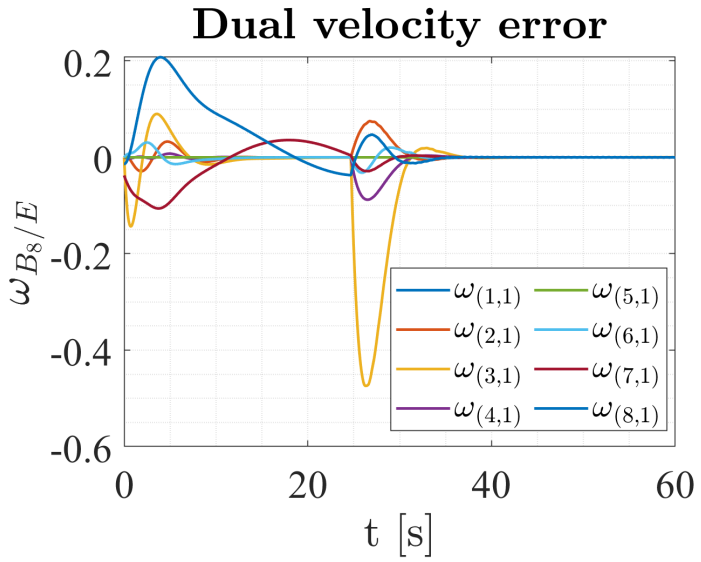

Figure 5.75: Dual velocity error without CBFs, with disturbance

Chapter 6

Conclusion

6.1 Final remarks

A dual quaternion (DQ) framework has been developed in the body of the work to provide a comprehensive description of the kinematics and dynamics of a spacecraft mounted manipulator. Exploiting the unified translational-rotational nature of the equations arising from this mathematical framework, a unique nonlinear controller has been developed to enable coordinated control of both the position and the attitude (i.e. pose) of the satellite base and of the end effector. In order to grant robustness and accuracy to the solution, a novel control barrier functions (CBFs) based singularity avoidance strategy has been suggested; this allowed to save the results coming from the Lyapunov stability analysis and to make them applicable in a wider range of cases, thanks to the achievement of controlled forward invariance of the solution with respect to a singularity-free state subset. The validity of the aforementioned ideas has been proved by the numerical results reported in Chapter 5, which also features a comparison with a more traditional singularity avoidance method.

Although more complex from the algebraic point of view, the DQ formulation was able to provide a physically sound formulation to describe both the satellite and robot dynamics; in fact, more than

highlighting the differences between the fields of space engineering and robotics, the mathematical framework was able to grasp the common concepts which stand at the basis of the multibody kinematics and dynamics, hence allowing a straightforward physical interpretation of the equations. On the other hand, it has been proved [64] that traditional point-based spatial transformations, such as the homogeneous transform, are still more effective from the computational point of view; no evidence of the contrary has been found within this study. To the authors' view, a DQ based approach is therefore to be preferred whenever a unitary algebraic description is required for the coupled satellite-manipulator problem; for example, this may be the case when it comes to the design of a coordinated controller for a free-flying spacecraft mounted manipulator system.

As an evidence to support this last consideration, the implementation of a coordinated base-manipulator pose-tracking strategy revealed to be a good match for the dual form of the equations of motion. In fact, the form of the controller was derived in a natural way from an attitude-only quaternion law, but it extended its results achieving also satisfactory results in terms of position-tracking. However, as the controller has been formulated in the task space, its feasibility is tightly related to the absence of kinematic singularities, and this constitutes a limit in the types of trajectory that can be tracked. This became evident when dealing with the numerical solution of the nominal control equation, which was extremely unstable and highly dependent from the definition of the reference trajectory; therefore, the only nominal control law was not considered sufficient to our purposes. As the work did not focus on the generation of *a priori* singularity-free trajectories, the choice was made to recover safety *a posteriori*, exploiting the CBFs as a way to impose constraints on the values of the state and therefore avoid known singular configuration. This choice, although being a quite unusual one in the context of singularity avoidance methods literature, turned out to be effective; rearranging the controller as a constrained optimization problem allowed to fully exploit the

results of the original Lyapunov-based approach, otherwise weak; on the other hand, the computational burden became significant, as each integration step involves the solution of a quadratic programming problem. The computational aspect, although not strictly of interest to the extent of this thesis, would necessary need further investigation if a method like the proposed one had to be implemented for a real application.

6.2 Further developments

As already stated, some assumptions were made during the modeling phase of the work; as a consequence, possible further developments would imply more accurate treatment of some aspects that have been voluntarily neglected. Among them, it would be interesting to exploit the simulation environment to model a real manipulation problem, hence involving contact forces, additional bodies with unknown inertia, ... This would provide a deeper insight into the coupled manipulator-base dynamics and would probably make the DQ framework even more worthwhile. Moreover, the actuator dynamics (both the base and the arm ones) has not been examined, hence not taking into account possible limits in the control action due to saturations, fuel consumption, accuracy thresholds, etc.; this analysis is necessary to predict the behavior of any experimental platform in a faithful way.

When it comes to experimental activity, it would be crucial to study the interaction of the model with the information coming from the sensors; these would allow dealing with uncertainties in the definition of the physical properties of the model, hence providing enhanced performances to the real system. Besides, the control system could use inertial and vision sensors to simulate a realistic operational scenario.

As a last remark, the introduction of CBFs into the problem leaves the door open to a number of additional applications; in particular, these could be used to increase autonomy of the system and exploit

the platform in a deeper way; the same maneuver could be given a set of tasks with different priorities, for example to maximize sun exposure, while also following a reference trajectory and respecting a line of sight constraint.

Bibliography

[1] Morgan Stanley. *Space: Investing in the Final Frontier*. 2019. URL: https://www.morganstanley.com/ideas/investing-in-space.

[2] F. Tran et al. *To Infinity and Beyond - Global Space Primer, Thematic Investing, Bank of America Merrill Lynch*. 2017. URL: https://api.guidants.com/db/a2/1e1ffc185c1d44bd.pdf.

[3] Goddard Space Flight Center NASA. *On-Orbit Satellite Servicing Study, Project Report*. 2010. URL: https://nexis.gsfc.nasa.gov/images/NASA_Satellite%20Servicing_Project_Report_0511.pdf.

[4] Donald J. Kessler and Burton G. Cour-Palais. "Collision frequency of artificial satellites: The creation of a debris belt". In: *Journal of Geophysical Research: Space Physics* 83.A6 (1978), pp. 2637–2646. DOI: 10.1029/JA083iA06p02637. eprint: https://agupubs.onlinelibrary.wiley.com/doi/pdf/10.1029/JA083iA06p02637. URL: https://agupubs.onlinelibrary.wiley.com/doi/abs/10.1029/JA083iA06p02637.

[5] Max E. Simpson. *Collision Probability of the Apollo Spacecraft with Objects in Earth Orbit*. NASA, Manned Spacecraft Center, 1967.

[6] ESA Space Debris Office. *ESA's Annual Space Environment Report*. 2019. URL: https://www.sdo.esoc.esa.int/environment_report/Space_Environment_Report_latest.pdf.

[7] Franco Davoli et al. "Small satellites and CubeSats: Survey of structures, architectures, and protocols". In: *International Journal of Satellite Communications and Networking* 37.4 (2019), pp. 343–359. DOI: 10.1002/sat.1277. eprint: https://onlinelibrary.wiley.com/doi/pdf/10.1002/sat.1277. URL: https://onlinelibrary.wiley.com/doi/abs/10.1002/sat.1277.

[8] Manlio Bacco et al. "A Survey on Network Architectures and Applications for Nanosat and UAV Swarms". In: *Wireless and Satellite Systems*. Ed. by Prashant Pillai et al. Cham: Springer International Publishing, 2018, pp. 75–85. ISBN: 978-3-319-76571-6.

[9] Keith Morris and Christopher Tamanini. "Geosynchronous Orbit CubeSat Operating Guidelines to Help the Space Situational Awareness Community". In: *Proceedings of the Advanced Maui Optical and Space Surveillance Technologies Conference*. Sept. 2019, p. 45.

[10] Bryan L. Benedict. "Rationale for Need of In-Orbit Servicing Capabilities for GEO Spacecraft". In: *AIAA SPACE 2013 Conference and Exposition*. DOI: 10.2514/6.2013-5444. eprint: https://arc.aiaa.org/doi/pdf/10.2514/6.2013-5444. URL: https://arc.aiaa.org/doi/abs/10.2514/6.2013-5444.

[11] K. Wormnes et al. "Esa technologies for space debris remediation". In: *Proceedings of the 6th IAASS Conference: Safety is Not An Option* (Jan. 2013), pp. 3–4.

[12] NASA Satellite Servicing Projects Division. *OSAM-1: On-Orbit Servicing, Assembly and Manufacturing Mission*. 2020. URL: https://nexis.gsfc.nasa.gov/OSAM-1.html.

[13] DARPA. *Robotic Servicing of Geosynchronous Satellites (RSGS)*. 2019. URL: https://www.darpa.mil/program/robotic-servicing-of-geosynchronous-satellites.

[14] Gilles Clément. *Fundamentals of Space Medicine*. Jan. 2011. DOI: 10.1007/978-1-4419-9905-4.

[15] Richard Rembala and Cameron Ower. "Robotic assembly and maintenance of future space stations based on the ISS mission operations experience". In: *Acta Astronautica* 65.7 (2009), pp. 912 –920. ISSN: 0094-5765. DOI: https://doi.org/10.1016/j.actaastro.2009.03.064. URL: http://www.sciencedirect.com/science/article/pii/S0094576509001830.

[16] Gerd Hirzinger et al. "DLR's robotics technologies for on-orbit servicing". In: *Advanced Robotics* 18.2 (2004), pp. 139–174. DOI: 10.1163/156855304322758006. eprint: https://doi.org/10.1163/156855304322758006. URL: https://doi.org/10.1163/156855304322758006.

[17] M. Oda, K. Kibe, and F. Yamagata. "ETS-VII, space robot in-orbit experiment satellite". In: *Proceedings of IEEE International Conference on Robotics and Automation*. Vol. 1. 1996, 739–744 vol.1.

[18] NASA. *NASA's Robotic Refueling Mission*. 2013. URL: https://www.nasa.gov/mission_pages/station/research/news/rrm_practice.html.

[19] Tom Mulder. "Orbital Express Autonomous Rendezvous and Capture Flight Operations, Part 2 of 2: AR&C Exercise 4,5, and End-Of-Life". In: *AIAA/AAS Astrodynamics Specialist Conference and Exhibit*. DOI: 10.2514/6.2008-6768. eprint: https://arc.aiaa.org/doi/pdf/10.2514/6.2008-6768. URL: https://arc.aiaa.org/doi/abs/10.2514/6.2008-6768.

[20] V. Brodsky and M. Shoham. "Dual numbers representation of rigid body dynamics". In: *Mechanism and Machine Theory* 34.5 (1999), pp. 693 –718. ISSN: 0094-114X. DOI: https://doi.org/10.1016/S0094-114X(98)00049-4. URL: http://www.sciencedirect.com/science/article/pii/S0094114X98000494.

[21] J. R. Dooley and J. M. McCarthy. "Spatial rigid body dynamics using dual quaternion components". In: *Proceedings. 1991 IEEE International Conference on Robotics and Automation*. 1991, 90–95 vol.1.

[22] X. Wang and C. Yu. "Unit-Dual-Quaternion-Based PID Control Scheme for Rigid-Body Transformation*". In: *IFAC Proceedings Volumes* 44.1 (2011). 18th IFAC World Congress, pp. 9296 –9301. ISSN: 1474-6670. DOI: https://doi.org/10.3182/20110828-6-IT-1002.02284. URL: http://www.sciencedirect.com/science/article/pii/S1474667016451050.

[23] N. Filipe and P. Tsiotras. "Rigid body motion tracking without linear and angular velocity feedback using dual quaternions". In: *2013 European Control Conference (ECC)*. 2013, pp. 329–334.

[24] Nuno Filipe and Panagiotis Tsiotras. "Adaptive Model Independent Tracking of Rigid Body Position and Attitude Motion with Mass and Inertia Matrix Identification using Dual Quaternions". In: *AIAA Guidance, Navigation, and Control (GNC) Conference*. DOI: 10.2514/6.2013-5173. eprint: https://arc.aiaa.org/doi/pdf/10.2514/6.2013-5173. URL: https://arc.aiaa.org/doi/abs/10.2514/6.2013-5173.

[25] Nuno Filipe and Panagiotis Tsiotras. "Adaptive Position and Attitude-Tracking Controller for Satellite Proximity Operations Using Dual Quaternions". In: *Journal of Guidance, Control, and Dynamics* 38.4 (2015), pp. 566–577. DOI: 10.2514/1.G000054. eprint: https://doi.org/10.2514/1.G000054. URL: https://doi.org/10.2514/1.G000054.

[26] Alfredo Valverde and Panagiotis Tsiotras. "Spacecraft Robot Kinematics Using Dual Quaternions". In: *Robotics* 7.4 (2018). ISSN: 2218-6581. DOI: 10.3390/robotics7040064. URL: https://www.mdpi.com/2218-6581/7/4/64.

[27] Alfredo Valverde and Panagiotis Tsiotras. "Dual Quaternion Framework for Modeling of Spacecraft-Mounted Multibody Robotic Systems". In: *Frontiers in Robotics and AI* 5 (2018), p. 128. ISSN: 2296-9144. DOI: 10.3389/frobt.2018.00128. URL: https://www.frontiersin.org/article/10.3389/frobt.2018.00128.

[28] Angel Flores-Abad et al. "A review of space robotics technologies for on-orbit servicing". In: *Progress in Aerospace Sciences* 68 (2014), pp. 1 –26. ISSN: 0376-0421. DOI: https://doi.org/10.1016/j.paerosci.2014.03.002. URL: http://www.sciencedirect.com/science/article/pii/S0376042114000347.

[29] Z. Vafa and S. Dubowsky. "On the dynamics of manipulators in space using the virtual manipulator approach". In: *Proceedings. 1987 IEEE International Conference on Robotics and Automation*. Vol. 4. 1987, pp. 579–585.

[30] Bin Liang, Yangsheng Xu, and M. Bergerman. "Dynamically equivalent manipulator for space manipulator system. 1". In: *Proceedings of International Conference on Robotics and Automation*. Vol. 4. 1997, 2765–2770 vol.4.

[31] Osman Parlaktuna and Metin Ozkan. "Adaptive control of free-floating space manipulators using dynamically equivalent manipulator model". In: *Robotics and Autonomous Systems* 46.3 (2004), pp. 185 –193. ISSN: 0921-8890. DOI: https://doi.org/10.1016/j.robot.2003.11.007. URL: http://www.sciencedirect.com/science/article/pii/S0921889003001957.

[32] Yoji Umetani and Kazuya Yoshida. "Continuous path control of space manipulators mounted on OMV". In: *Acta Astronautica* 15.12 (Jan. 1987), pp. 981–986. DOI: 10.1016/0094-5765(87)90022-1.

[33] E. Papadopoulos and S. Dubowsky. "Dynamic Singularities in Free-Floating Space Manipulators". In: *Journal of Dynamic Systems, Measurement, and Control* 115.1 (Mar. 1993), pp. 44–52. ISSN: 0022-0434. DOI: 10.1115/1.2897406. eprint: https://asmedigitalcollection.asme.org/dynamicsystems/article-pdf/115/1/44/5652516/44_1.pdf. URL: https://doi.org/10.1115/1.2897406.

[34] S. Dubowsky and E. Papadopoulos. "The kinematics, dynamics, and control of free-flying and free-floating space robotic systems". In: *IEEE Transactions on Robotics and Automation* 9.5 (1993), pp. 531–543.

[35] Eric Stoneking. "Newton-Euler Dynamic Equations of Motion for a Multi-Body Spacecraft". In: *AIAA Guidance, Navigation and Control Conference and Exhibit*. DOI: 10.2514/6.2007-6441. eprint: https://arc.aiaa.org/doi/pdf/10.2514/6.2007-6441. URL: https://arc.aiaa.org/doi/abs/10.2514/6.2007-6441.

[36] Andrea Antonello, Alfredo Valverde, and Panagiotis Tsiotras. "Dynamics and Control of Spacecraft Manipulators with Thrusters and Momentum Exchange Devices". In: *Journal of Guidance, Control, and Dynamics* 42.1 (2019), pp. 15–29. DOI: 10.2514/1.G003601. eprint: https://doi.org/10.2514/1.G003601. URL: https://doi.org/10.2514/1.G003601.

[37] American National Standard for Industrial Robots and Robot Systems. *ANSI/RIA R15.06-1999*. Ann Arbor, Michigan: Robotic Industries Association, 1999.

[38] Yoshihiko Nakamura and Hideo Hanafusa. "Inverse Kinematic Solutions With Singularity Robustness for Robot Manipulator Control". In: *Journal of Dynamic Systems, Measurement,*

and Control 108.3 (Sept. 1986), pp. 163–171. ISSN: 0022-0434. DOI: 10.1115/1.3143764. eprint: https://asmedigitalcollection.asme.org/dynamicsystems/article-pdf/108/3/163/5482965/163_1.pdf. URL: https://doi.org/10.1115/1.3143764.

[39] S. Vadali. "Feedback control and steering laws for spacecraft using single gimbal control moment gyros". In: *Guidance, Navigation and Control Conference*. DOI: 10.2514/6.1989-3475. eprint: https://arc.aiaa.org/doi/pdf/10.2514/6.1989-3475. URL: https://arc.aiaa.org/doi/abs/10.2514/6.1989-3475.

[40] Dongwon Jung and Panagiotis Tsiotras. "An Experimental Comparison of CMG Steering Control Laws". In: *AIAA/AAS Astrodynamics Specialist Conference and Exhibit*. DOI: 10.2514/6.2004-5294. eprint: https://arc.aiaa.org/doi/pdf/10.2514/6.2004-5294. URL: https://arc.aiaa.org/doi/abs/10.2514/6.2004-5294.

[41] Jon Kieffer. "Manipulator Inverse Kinematics for Untimed End-Effector Trajectories With Ordinary Singularities". In: *The International Journal of Robotics Research* 11.3 (1992), pp. 225–237. DOI: 10.1177/027836499201100305. eprint: https://doi.org/10.1177/027836499201100305. URL: https://doi.org/10.1177/027836499201100305.

[42] D. N. Nenchev. "Tracking manipulator trajectories with ordinary singularities: a null-space based approach". In: *1994 International Conference on Control - Control '94.* Vol. 2. 1994, 1145–1147 vol.2.

[43] M. Nagumo. "Über die Lage der Integralkurven gewöhnlicher Differentialgleichungen". In: *Proceedings of the Physico-Mathematical Society of Japan. 3rd Series* 24 (1942), pp. 551–559. DOI: 10.11429/ppmsj1919.24.0_551.

[44] Haim Brezis. “On a characterization of flow-invariant sets”. In: *Communications on Pure and Applied Mathematics* 23.2 (1970), pp. 261–263. DOI: 10.1002/cpa.3160230211. eprint: https://onlinelibrary.wiley.com/doi/pdf/10.1002/cpa.3160230211. URL: https://onlinelibrary.wiley.com/doi/abs/10.1002/cpa.3160230211.

[45] Stephen Prajna and Ali Jadbabaie. “Safety Verification of Hybrid Systems Using Barrier Certificates”. In: *Hybrid Systems: Computation and Control*. Ed. by Rajeev Alur and George J. Pappas. Berlin, Heidelberg: Springer Berlin Heidelberg, 2004, pp. 477–492. ISBN: 978-3-540-24743-2.

[46] Peter Wieland and Frank Allgöwer. “Constructive Safety Using Control Barrier Functions”. In: *IFAC Proceedings Volumes* 40.12 (2007). 7th IFAC Symposium on Nonlinear Control Systems, pp. 462 –467. ISSN: 1474-6670. DOI: https://doi.org/10.3182/20070822-3-ZA-2920.00076. URL: http://www.sciencedirect.com/science/article/pii/S1474667016355690.

[47] A. D. Ames, J. W. Grizzle, and P. Tabuada. “Control barrier function based quadratic programs with application to adaptive cruise control”. In: *53rd IEEE Conference on Decision and Control*. 2014, pp. 6271–6278.

[48] A. D. Ames et al. “Control Barrier Function Based Quadratic Programs for Safety Critical Systems”. In: *IEEE Transactions on Automatic Control* 62.8 (2017), pp. 3861–3876.

[49] A. D. Ames et al. “Control Barrier Functions: Theory and Applications”. In: *2019 18th European Control Conference (ECC)*. 2019, pp. 3420–3431.

[50] Luiz Radavelli et al. “Points, Lines, Screws and Planes in Dual Quaternions Kinematics”. In: June 2014, pp. 285–293. ISBN: 978-3-319-06697-4. DOI: 10.1007/978-3-319-06698-1_30.

[51] N. Filipe and P. Tsiotras. "Simultaneous position and attitude control without linear and angular velocity feedback using dual quaternions". In: *2013 American Control Conference*. 2013, pp. 4808–4813.

[52] Hassan K Khalil. *Nonlinear systems; 3rd ed.* The book can be consulted by contacting: PH-AID: Wallet, Lionel. Upper Saddle River, NJ: Prentice-Hall, 2002. URL: https://cds.cern.ch/record/1173048.

[53] Dae-Min Cho, Dongwon Jung, and Panagiotis Tsiotras. "A 5-dof Experimental Platform for Spacecraft Rendezvous and Docking". In: *AIAA Infotech@Aerospace Conference*. DOI: 10.2514/6.2009-1869. eprint: https://arc.aiaa.org/doi/pdf/10.2514/6.2009-1869. URL: https://arc.aiaa.org/doi/abs/10.2514/6.2009-1869.

[54] A. M. Lyapunov. "The general problem of the stability of motion". In: *International Journal of Control* 55.3 (1992), pp. 531–534. DOI: 10.1080/00207179208934253. eprint: https://doi.org/10.1080/00207179208934253. URL: https://doi.org/10.1080/00207179208934253.

[55] Kevin M. Lynch and Frank C. Park. *Modern Robotics: Mechanics, Planning, and Control*. 1st. USA: Cambridge University Press, 2017. ISBN: 1107156300.

[56] S. Hsu, X. Xu, and A. D. Ames. "Control barrier function based quadratic programs with application to bipedal robotic walking". In: *2015 American Control Conference (ACC)*. 2015, pp. 4542–4548.

[57] Matthias Weyrer, Mathias Brandstötter, and Manfred Husty. "Singularity Avoidance Control of a Non-Holonomic Mobile Manipulator for Intuitive Hand Guidance". In: *Robotics* 8 (Feb. 2019), p. 14. DOI: 10.3390/robotics8010014.

[58] Universal Robots. *Parameters for calculations of kinematics and dynamics*. 2020. URL: https://www.universal-robots.com/articles/ur-articles/parameters-for-calculations-of-kinematics-and-dynamics/.

[59] Kevin Ford and Christopher Hall. "Singular direction avoidance steering for control moment gyros". In: *AIAA/AAS Astrodynamics Specialist Conference and Exhibit*. DOI: 10.2514/6.1998-4470. eprint: https://arc.aiaa.org/doi/pdf/10.2514/6.1998-4470. URL: https://arc.aiaa.org/doi/abs/10.2514/6.1998-4470.

[60] Nazareth S. Bedrossian et al. "Steering law design for redundant single-gimbal control moment gyroscopes". In: *Journal of Guidance, Control, and Dynamics* 13.6 (1990), pp. 1083–1089. DOI: 10.2514/3.20582. eprint: https://doi.org/10.2514/3.20582. URL: https://doi.org/10.2514/3.20582.

[61] G. Zielke. "Horn, R. A.; Johnson, C. R., Matrix Analysis. Cambridge etc., Cambridge University Press 1985. XIII, 561 S., £ 35.00. ISBN 0-521-30586-1". In: *ZAMM - Journal of Applied Mathematics and Mechanics / Zeitschrift für Angewandte Mathematik und Mechanik* 67.3 (1987), pp. 212–212. DOI: 10.1002/zamm.19870670330. eprint: https://onlinelibrary.wiley.com/doi/pdf/10.1002/zamm.19870670330. URL: https://onlinelibrary.wiley.com/doi/abs/10.1002/zamm.19870670330.

[62] MathWorks® Help Center. *quadprog - Quadratic programming*. 2020. URL: https://it.mathworks.com/help/optim/quadratic-programming.html?s_tid=CRUX_lftnav.

[63] "Terminology for model credibility". In: *SIMULATION* 32.3 (1979), pp. 103–104. DOI: 10.1177/003754977903200304. eprint: https://doi.org/10.1177/003754977903200304. URL: https://doi.org/10.1177/003754977903200304.

[64] J. Funda and R. P. Paul. “A computational analysis of screw transformations in robotics”. In: *IEEE Transactions on Robotics and Automation* 6.3 (1990), pp. 348–356.